Aus dem

Institut für Kardiovaskuläre Physiologie und Pathophysiologie im Walter-Brendel-Zentrum für Experimentelle Medizin

Institut der Universität München

Spatio-temporal dynamics and molecular principles of macropinocytosis in immune cells

Dissertation
zum Erwerb des Doctor of Philosophy (Ph.D.)
an der Medizinischen Fakultät der
Ludwig-Maximilians-Universität München

vorgelegt von
Malte Benjamin Braun

aus
Herford

Jahr
2024

Mit Genehmigung der Medizinischen Fakultät der
Ludwig-Maximilians-Universität München

Erstes Gutachten:	Prof. Dr. Jörg Renkawitz
Zweites Gutachten:	Prof. Dr. Annette Müller-Taubenberger
Drittes Gutachten:	Prof. Dr. Heiko Adler
Viertes Gutachten:	Prof. Dr. Thomas Korn

Dekan: Prof. Dr. med. Thomas Gudermann

Tag der mündlichen Prüfung: 13.06.2024

TABLE OF CONTENTS

ABSTRACT

Macropinocytosis is an endocytotic pathway that allows cells to engulf large amounts of extracellular fluid from their environment. It plays an important role in the immune system when antigen presenting cells, such as dendritic cells and macrophages, sample their environment for pathogens. At the same time, macropinocytosis can be abused by pathogens to cross the cell membrane barrier and by cancer cells to acquire nutrients from the environment.

Although it is well known that macropinocytosis is regulated by activation of actin polymerisation via the Ras-Rac axis and that phosphoinositides and Rab GTPases play a role in regulating and guiding the process, the precise mechanisms regulating macropinocytosis are still unknown. We performed a genome-wide CRISPR knockout screen to identify novel genes involved in macropinocytosis. Thereby, we identified Lrch2, Pilra and Adgre1 as potential novel regulators of macropinocytosis. While loss of Pilra and Adgre1 increases extracellular fluid uptake by macropinocytosis, making them potential negative regulators, loss of Lrch2 decreases macropinocytosis, making it a potential positive regulator.

In vivo, cells typically encounter a 3D environment in which they experience a variety of interactions with their local environment, ranging from cell-cell contacts and the exchange of signalling molecules to physical cues. Traditional 2D assay systems used in research laboratories miss many of these features, while overemphasising others such as substrate stiffness and cell adhesion. 3D hydrogels represent a more physiological environment with lower adhesion and the ability for cells to navigate in a 3D environment. Thus, we wondered how the local microenvironment regulates macropinocytosis.

To answer this question, we used 3D hydrogels, surface modifications and micropatterning to precisely alter microenvironmental parameters. Our results demonstrate that macrophages, dendritic cells and the breast cancer cell line 4T1 perform more macropinocytosis inside 3D hydrogels. Furthermore, we discovered that this increased rate of macropinocytosis in macrophages is not the result of spatial confinement but of lower cell adhesion in hydrogels. This reduced adhesion is accompanied by a switch from formin-mediated actin polymerisation in 2D to Arp2/3-mediated actin polymerisation in 3D, leading to an overall increase in actin activity which in turn increases membrane tension.

In conclusion, we found mechanistic differences in macropinocytosis between cells adhering to less physiological 2D surfaces and cells in more physiological 3D hydrogels. These differences lead to higher macropinocytosis rates in 3D environments. Our findings show that macropinocytosis is regulated by the microenvironment. In addition, our results suggest a mechanistic basis of how immune cells can efficiently sample their environment *in vivo* in low adhesion situations, such as in the intestine or in the lymph nodes.

ZUSAMMENFASSUNG

Makropinozytose ist ein endozytotischer Weg, der es Zellen ermöglicht, große Mengen extrazellulärer Flüssigkeit aufzunehmen. Dieser Vorgang spielt eine wichtige Rolle im Immunsystem. Antigenpräsentierende Zellen wie dendritische Zellen und Makrophagen nutzen ihn, um ihre Umgebung nach Krankheitserregern abzusuchen. Gleichzeitig kann der Prozess von Krankheitserregern missbraucht werden, um die Zellmembranbarriere zu überwinden, und von Krebszellen, um sich aus ihrer Umgebung mit Nährstoffen zu versorgen.

Obwohl bereits bekannt ist, dass die Aktinpolymerisation für Makropinozytose über die Ras-Rac-Achse aktiviert wird und Phosphatidylinositole und Rab GTPasen eine wichtige Rolle bei der Regulation des Prozesses spielen, ist der genaue Mechanismus noch unbekannt. Daher haben wir einen genomweiten CRISPR Knockout Screen durchgeführt, um bisher unbekannte Gene zu identifizieren, die mit Makropinozytose assoziiert sind. Wir haben drei potentielle Kandidaten identifiziert, Lrch2, Pilra und Adgre1. Während der Verlust von Pilra und Adgre1 die Flüssigkeitsaufnahme über Makropinozytose erhöht, was sie zu potentiellen Kandidaten als negative Regulatoren von Makropinozytose macht, reduziert Lrch2 die Aufnahme. Daher ist Lrch2 ein möglicher positiver Regulator von Makropinozytose.

In ihrer physiologischen Umgebung können sich Zellen dreidimensional ausbreiten und eine Vielzahl von Interaktionen mit ihrer Umgebung eingehen. Diese Interaktionen reichen von Zell-Zell-Kontakten über den Austausch von Botenstoffen bis hin zu mechanischen Reizen durch die Umgebung. Traditionell werden im Labor zweidimensionale Testsysteme verwendet, die viele dieser Eigenschaften nicht besitzen, dafür aber anderen Eigenschaften wie Substratsteifigkeit und Adhäsion eine zu große Bedeutung beimessen. Im Gegensatz dazu bieten dreidimensionale Hydrogele eine physiologischere Umgebung mit geringer Adhäsion und der Möglichkeit, sich dreidimensional auszubreiten. Wir haben uns daher gefragt, welche Unterschiede zwischen Makropinozytose in diesen Umgebungen bestehen.

Um diese Frage zu beantworten, haben wir dreidimensionale Hydrogele, Oberflächenmodifikationen und Oberflächen mit Mikrostrukturen verwendet. Unsere Ergebnisse zeigen, dass Makrophagen, dendritische Zellen und die Brustkrebszelllinie 4T1 in dreidimensionalen Umgebungen mehr Makropinozytose betreiben als auf zweidimensionalen Oberflächen. Darüber hinaus konnten wir für Makrophagen zeigen, dass die Zunahme der Makropinozytose nicht durch die räumliche Beschränkung, sondern durch eine verringerte Adhäsion in den Hydrogelen hervorgerufen wird. Diese Adhäsionsreduktion geht mit einer Veränderung der Aktinpolymerisation einher. In zweidimensionalen Umgebungen ist die Aktinpolymerisation Formin-abhängig, während sie in dreidimensionalen

Umgebungen Arp2/3-abhängig ist. Diese Veränderung führt zu einer Erhöhung der allgemeinen Aktinaktivität. Dies wiederum führt zu einer Erhöhung der Membranspannung.

Zusammenfassend haben wir festgestellt, dass es mechanistische Unterschiede in der Makropinozytose zwischen Zellen, die an weniger physiologischen zweidimensionalen Oberflächen adhärieren, und Zellen in dreidimensionalen Hydrogelen gibt. Diese Unterschiede führen zu einer höheren Makropinozytose in dreidimensionalen Umgebungen und anderen Situationen mit geringerer Adhäsion. Daher zeigen die Ergebnisse, dass es wichtig ist, die Umgebung, in der sich die Zellen befinden, zu berücksichtigen, wenn Makropinozytose untersucht wird. Darüber hinaus könnte dies eine Erklärung dafür liefern, wie Immunzellen *in vivo* ihre Umgebung effizient nach Pathogenen absuchen können, wenn sie sich in Situationen mit geringer Adhäsion befinden, wie zum Beispiel im Darm oder in den Lymphknoten.

LIST OF FIGURES

LIST OF TABLES

GLOSSARY

AAV adeno-associated viruses. 28

BM bone marrow. 43, 56, 59, 74, 76, 85, 98
BMC Biomedical Center Munich. 37, 48, 59, 136
BME 2-Mercaptoethanol. 31, 35–37
BSA bovine serum albumin. 32, 36, 52, 53, 82, 84

CAR chimeric antigen receptor. 29
CaSR calcium-sensing receptor. 19, 22, 97

DC dendritic cell. 3, 13, 17–19, 24, 34, 36, 43, 44, 50–52, 54, 56, 59, 65, 74–76, 98, 100, 106, 107, 110, 111
DMEM Dulbecco's modified eagle medium. 31, 35, 43, 45–47, 50
DMSO dimethyl sulfoxide. 32, 35, 53, 54, 74, 90, 94
DNA deoxyribonucleic acid. 27, 28, 44–46, 48, 49, 59, 63, 97, 98

EDTA ethylenediaminetetraacetic acid. 36, 37, 47, 48, 50–54, 71, 72, 82
EGFR epidermal growth factor receptor. 20, 22
EIPA ethylisopropyl amiloride. 21, 31, 54, 56, 59, 71, 72, 74–76, 87, 94, 95, 100, 105, 106, 108, 109
EtOH ethanol. 48, 49

FACS fluorescence activated cell sorting. 28, 36, 43, 47, 48, 50–53, 55, 56, 59, 63, 65, 68, 71, 74, 75, 82–85, 88, 90, 97, 100, 136
FcRn neonatal Fc receptor. 18
FCS fetal calf serum. 31, 35–37, 47, 52, 53
FITC fluorescein isothiocyanate. 48–53, 55, 57, 59, 63, 65, 68, 71, 72, 74, 82, 84, 87, 89, 90, 97, 105, 106
FLIM fluorescence lifetime imaging. 54
FWD forward. 38–41, 45, 47

GEF guanine nucleotide exchange factor. 99
GFP green fluorescent protein. 52

KO knock out. 9, 27–29, 38, 40, 43, 46, 49, 50, 53, 55, 57–59, 65–69, 85, 86, 92, 93, 97, 100, 104, 106, 107, 110, 136

LB lysogeny broth. 44, 47
LPS lipopolysaccharide. 44, 98, 105–107

MC macrophage. 3, 13, 16–19, 24, 34, 36, 42, 43, 47–54, 56–60, 63, 68–72, 74, 75, 77–101, 103, 105–107, 110, 111, 136
mβCD methyl-β-cyclodextrin. 31, 96

MEM minimum essential medium. 52
MHC major histocompatibility complex. 14, 15, 17
MOI multiplicity of infection. 28, 47, 48, 59

NF1 neurofibromin 1. 17, 18, 57, 59, 97
NGS next-generation sequencing. 28, 40, 49, 59, 60, 63, 136
NHE sodium proton exchanger. 21, 56, 100, 104, 108
NHEJ non-homologous end joining. 27, 66–68

PAA poly(acrylic acid). 3, 23, 32, 50, 51, 70, 71, 75, 76
PBS phosphate-buffered saline. 31, 36, 37, 42–44, 46–48, 50–53
PCR polymerase chain reaction. 28, 40, 44–49, 59, 67
PDGFR platelet-derived growth factor receptor. 20, 22
PDMS polydimethylsiloxane. 23, 24, 106
PEG polyethylene glycol. 23, 78, 82, 84, 136
PEI polyethylenimine. 32, 36, 46
PI phosphoinositide. 20–22, 24, 26, 30, 98, 99, 105
PI3K phosphoinositide-3-kinase. 19, 20
PIK3 phosphatidylinositol-4-phosphate-3-kinase. 98, 99
PLL poly-L-lysine. 23, 82, 84

REV reverse. 38–42, 45, 49
RNP ribonucleoprotein. 85
roi region of interest. 54, 94
RT room temperature. 45–49

SCR scrambled. 38, 49, 57, 59, 66, 68, 69
sgRNA single guide RNA. 26–29, 38, 45–47, 49, 57, 59, 60, 63–66, 68, 69, 97, 98, 100

WT wild-type. 24, 43, 57, 59, 67, 68, 74, 85–88, 90–93, 95–97, 100, 105, 107

1 INTRODUCTION

1.1 ENDOCYTOTIC PROCESSES

In order to function properly, cells must constantly exchange informations, signals, and substances with their environment. At the same time it is essential for life to maintain an intact cell membrane that separates the inside of the cell from the outside. To overcome these two conflicting requirements, cells have developed a variety of endocytotic processes during the evolution of life. These processes allow the transfer of membrane-impermeable substances across the cell membrane barrier. The most important endocytotic processes are phagocytosis, clathrin-mediated endocytosis, caveolin-mediated endocytosis and macropinocytosis (see Figure 1).

Phagocytosis was first described in 1883 by Ilya Metchnikoff [238]. Under the microscope, Metchnikoff observed phagocytes in a starfish larva surrounding and engulfing particles that he had inserted into the larva [238]. He therefore named the process phagocytosis, derived from the Greek words "phagos", meaning "to eat", and "cyte", which is the cell [238].

From an evolutionary perspective, phagocytosis is one of the oldest endocytotic processes. The oldest fossil records date back to the late Ediacaran and early Cambrian, when algae developed mineralised skeletons to protect themselves from phagocytotic predators [192]. Phagocytosis also played a crucial role in the development of eukaryotic cells, as the uptake of indigestible endosymbionts resulted in the formation of cell organelles such as mitochondria [161, 209] and chloroplasts [159].

Phagocytosis is a receptor-dependent endocytotic process. The process begins with the interaction of a substrate with the receptor [70], which triggers the polymerization and branching of actin and the formation of finger-like membrane extensions. These structures surround the object with a lipid bilayer membrane, resulting in the engulfment of the particle into the cell and the formation of a phagosome. [127, 163] Inside the cell, the newly formed phagosome can fuse with the lysosome, resulting in the formation of a phagolysosome, and the digestion of the internalised substrate. This digestion is facilitated by lysosomal peptidases and lipases, which are activated by the low pH inside the lysosome. [24, 63].

Thereby, phagocytosis represents an important pathway for predatory eukaryotes, such as the amoeba *Dictyostelium discoideum* [23]. But it also plays a vital role in multicellular organisms. One important area where phagocytosis is essential in multicellular organisms is the immune system. Professional phagocytes, such as macrophages (MCs), dendritic cells (DCs) and neutrophils, use receptor-mediated phagocytosis to detect and eliminate pathogen infections [82, 111]. In addition, the

digestion of pathogens following phagocytotic uptake plays an essential role in the activation of the adaptive immune system through major histocompatibility complex (MHC)-mediated antigen presentation [111, 158].

Phagocytosis is also critical for embryonic development and the maintenance of physiological homeostasis. During embryonic development, not only many new cells are generated, but some of these cells also undergo programmed cell death (apoptosis) to ensure correct organ development. Phagocytotic active cells, such as macrophages and epithelial cells, are responsible for clearing the debris of these apoptotic cells [91]. In addition, macrophages can also engulf still-living cells using phagocytosis, actively inducing apoptosis in these cells, and shape the developing tissue microenvironment, as observed in the development of the fetal brain [156].

Two additional major endocytotic pathways are clathrin-mediated endocytosis and caveolin-mediated endocytosis, which share many mechanistic features. Both pathways require the enrichment of specific coating proteins on the inner side of the plasma membrane for their formation. In the case of clathrin-mediated endocytosis, after binding of the ligand, clathrin is recruited to the receptors on the cell surface by specific adapter proteins. [113]. Conversely, in caveolin-mediated endocytosis, caveolin is enriched in cholesterol-rich lipid raft effector domains together with cell surface receptors, and cavins are recruited to the membrane to stabilise the complex [29, 182]. This protein recruitment causes the membrane to bend inwards, facilitating the formation of membrane invaginations called caveolae. Another common feature of both endocytotic processes is their dependence on dynamin to tie off endosomes [88, 193].

Clathrin-mediated endocytosis is the most abundant form of endocytototic uptake, accounting for 95% of all endosomes [21]. It has a wide variety of different cargos and plays an important role in the internalisation of plasma membrane receptors, which is necessary to maintain cellular homeostasis, control of growth, cell differentiation, and signal transduction, for example at the synaptic cleft [166]. Clathrin-mediated endocytosis is found in all known eukaryotic cells [166]. The process starts with the recruitment of clathrin from the cytosolic pool to the inner membrane side of a receptor [114]. This recruitment leads to the invagination of the plasma membrane [114]. Finally, a vesicle is tied off and released from the membrane, stripped of from clathrin and fused with the endosomal system [114].

As clathrin-mediated endocytosis results in the uptake of receptors, all receptor-bound cargos accumulate in the newly formed vesicles and are transported into the cell. This process can also be exploited by viruses that bind to receptors at the cell surface and abuse clathrin-mediated endocytosis to enter the cell [11,22,49,53].

Caveolin-mediated endocytosis is a clathrin-independent endocytotic pathway. It generally describes the uptake of substances by the formation of caveolae called invaginations into the plasma membrane. These invaginations are formed by the interaction of caveolin-1 with cholesterol-rich lipid raft domains in the plasma membrane [189] and are sealed by dynamin activity [88]. Another important

factor in caveolae formation are cavins, which are also required for proper vesicle formation [90, 188].

Caveolin-mediated endocytosis plays a role in lipid uptake and homeostasis [16, 197], Ca_2^+ signalling [99, 217] and transcellular transport [212]. The fact that caveolae can flatten in response to mechanical stretching also suggests that they may act as mechanosensors [188]. Similar to clathrin-mediated endocytosis, calveolin-mediated endocytosis can also lead to the uptake of cell surface receptors and their cargo, allowing this process to be hijacked by viruses [66, 226, 258, 265].

In addition to caveolin mediated endocytosis, other clathrin-independent endocytotic pathways exist, which are classified according to the involvement of different small GTPases such as CDC42, RhoA or ARF6 [164]. While RhoA-regulated endocytosis depends on dynamin, like clathrin- and caveolin-mediated endocytosis, CDC42- and ARF6-regulated endocytosis are dynamin independent [164]. All three processes are important for the engulfment of different cargoes. While RhoA-regulated endocytosis is important for the uptake of interleukin receptors and cytokine receptors, CDC42-regulated endocytosis plays a role in the uptake of various toxins and ARF6-regulated endocytosis of adhesion proteins and MHC [164].

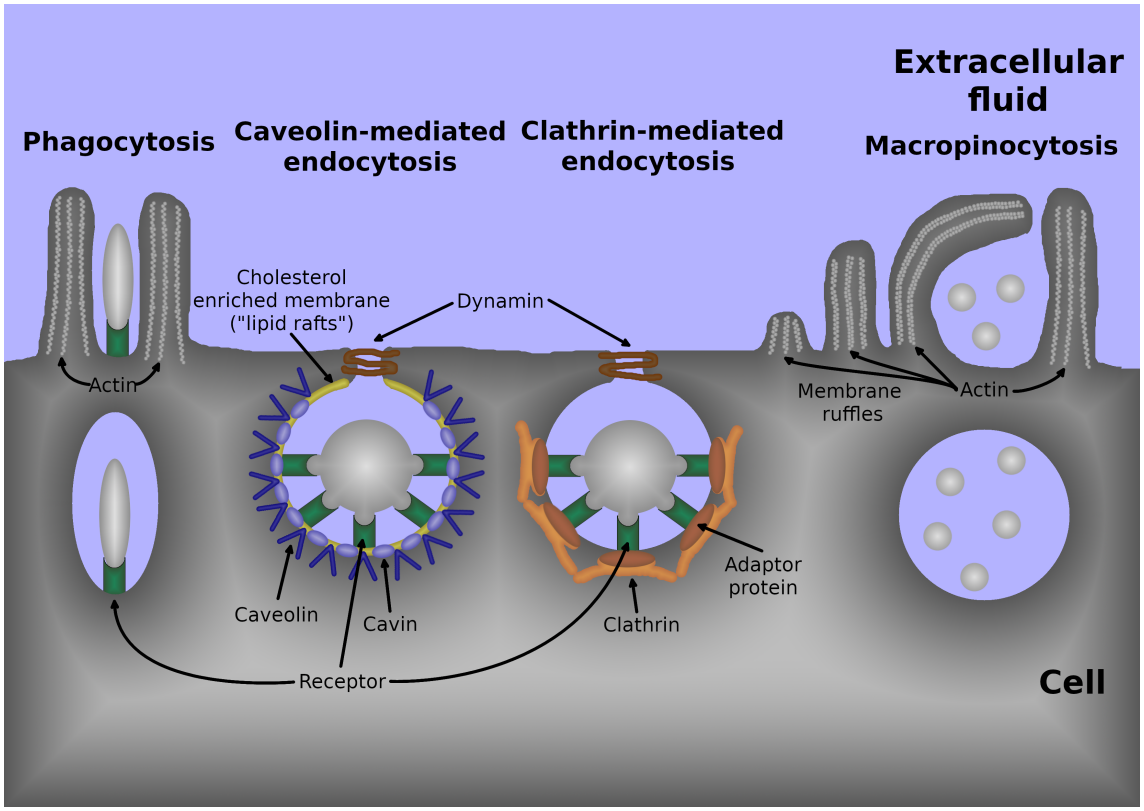

Figure 1: Summary of major endocytotic pathways and associated proteins: Phagocytosis, caveolin-mediated endocytosis and clathrin-mediated endocytosis are receptor-dependent processes. The endocytotic pits in caveolin- and clathrin-mediated endocytosis are additionally covered with caveolin and clathrin, the proteins that give them their names. In contrast, macropinocytosis can be constitutively induced in a receptor-independent manner. Furthermore, membrane ruffling for macropinocytosis can be induced by spatially separated receptors (induced macropinocytosis). See main text for further details. Adapted from [2, 3, 164].

1.2 MACROPINOCYTOSIS

In the 1930s, Warren Lewis was the first to describe another important endocytotic process [139, 140]. He observed under the microscope that macrophages (MCs) and malignant cells formed large fluid-filled vesicles. He named this process pinocytosis (cell drinking) [139, 140]. Due to the large size of the fluid-filled vesicles, ranging from 0.2 µm to 5 µm [144], the process was later renamed to macropinocytosis [236]. As macropinocytosis results in the uptake of large volumes of extracellular fluid, macropinosomes can be labelled using large cell-impermeable molecules coupled to a fluorescent marker. Typically, dextran with a molecular weight of 70 kDa and larger is used, as this is selectively internalised via macropinocytosis, whereas smaller dextran molecules would also be internalised via other endocytotic pathways like clathrin- or caveolin-mediated endocytosis. [141].

1.2.1 *Functional roles of macropinocytosis*

Macropinocytosis played a similar role as phagocytosis during the evolution of life. It evolved as a feeding mechanism for lower life forms. Choanoflagellates, sponges and amoebae can use macropinocytosis to acquire nutrients from their environment by engulfing extracellular fluid containing nutrients, peptides, or whole organisms [135]. The amoeba *Dictyostelium discoideum* has become an important model organism for macropinocytosis, as prolonged cultivation in the laboratory and isolation of desired clones has led to the development of laboratory strains that have altered their feeding behaviour. This strain uses macropinocytosis instead of phagocytosis to feed on bacteria [23, 251]. This adaptation allows the strain to grow in simple nutrient medium rather than being fed with bacterial cultures [23, 251]. The strain is therefore called an axenic laboratory strain [23, 251]. The switch in feeding behavior is a result of a mutation in the Ras GTPase activating protein neurofibromin 1 (NF1). NF1 loss modifies Ras activity leading to more macropinocytosis [23, 251].

Macropinocytosis not only plays a role as a feeding mechanism but also as sampling mechanism in the immune system. Immature dendritic cells (DCs) and MCs play an important role at the crossroads of innate and adaptive immunity. As part of the innate immune system, their task is to engulf invading pathogens and prevent their dissemination within the organism. At the same time, the digestion of engulfed pathogens leads to antigen presentation of pathogen peptides via major histocompatibility complex (MHC)-II, thereby activating T and B cells. One way by which immature DCs and MCs engulf pathogens for antigen presentation is through macropinocytosis. Immature DCs and MCs constantly perform macropinocytosis to sample their local environment for pathogen threats. MCs in particular have a very high macropinocytotic capacity, exchanging their entire cell surface area every 33 min [227]. After internalisation by macropinocytosis, pathogens or pathogen particles are transported to the lysosome for degradation. The peptides that are generated by lysosomal degradation are presented via MHC-II [210, 244] or bind to intracellular Toll-like receptors and induce cytokine responses [246].

Interestingly, it is also possible that pathogen particles are presented via MHC-I, when they are taken up by macropinocytosis [184]. Normally, antigen presentation via MHC-I and MHC-II are strictly separated. Extracellular peptides, taken up by the cell are usually presented via MHC-II, while MHC-I is reserved for the presentation of intracellular peptides [201]. Therefore, MHC-II presentation is usually associated with defence against foreign threats, such as bacterial infections, whereas MHC-I presentation is important for recognition of malignant cells and defence against intracellular pathogens and viruses [201]. As an exception to this rule, in the case of macropinocytosis, internalised peptides can be presented via both pathways [184]. This process is referred to as cross-presentation [31].

Macropinocytosis also plays an important role in mediating peripheral tolerance [151, 254]. In the absence of external pathogen threats, DCs take up large amounts

of self-antigens [151, 254]. By presenting these self-antigens, DCs stimulate the regulatory T cell response and induce peripheral tolerance [151, 254].

Macropinocytosis plays not only a role in homeostasis, but also in pathological changes. Mutations similar to those that allow axenic *Dictyostelium* strains to grow in nutrient-rich media have been shown to be a hallmark of tumour progression. Loss of NF1 leads to increased macropinocytosis in human cancer cells [25,79] and is therefore associated with more aggressive cancer growth and reduced patient survival. In cancer cells, loss of NF1 leads to an increased phosphorylation of PKCδ-P47, which in turn increases the production of reactive oxygen by NADPH oxidase 2, which increases membrane ruffling [79]. In addition, other mutations can occur in cancer to promote macropinocytosis. For example, the loss of PTEN, a known tumour suppressor gene, can increase the amount of macropinocytosis in prostate cancer [121]. Activating KRAS mutations are another known type of mutation that increases macropinocytosis. These mutations are frequent in pancreatic ductal adenocarcinoma and are almost universally fatal [33].

In general, cancer cells abuse macropinocytosis to meet their increased nutrient demands by engulfing large amounts of extracellular fluid and particles contained in the fluid [50, 56]. Albumin plays a special role as a nutrient source. As the most abundant protein in the blood [56], macropinocytotically active cells take up large amounts of albumin. Normally, albumin is rapidly recycled from the endosomes to the cell surface via the neonatal Fc receptor (FcRn) [43]. In KRAS-mutated cancer cells, this recycling can be prevented and albumin is instead transferred to the lysosome, where it is degraded to supply additional amino acids to the cancer cells [50, 56].

By ingesting necrotic cell debris, cancer cells acquire not only amino acids but also lipids and sugars. This uptake protects them against chemotherapeutic drugs that target anabolic pathways, rendering cancer cells treatment resistant [104]. In addition, the uptake of necrotic cell debris by macropinocytosis increases the risk of cancer relapse by providing additional nutrients in the cancer niche, which is overflowing with necrotic cell debris after chemotherapy [104].

While cancer cells exploit macropinocytosis for their proliferation, this feature of cancer can also be used against them as a treatment strategy. Several approaches have been developed to conjugate peptides that can be taken up by macropinocytosis or that directly induce macropinocytosis, coupled to toxins for targeted delivery into cancer cells with higher macropinocytotic activity [67, 147, 183, 233]. This results in the targeted elimination of cancer cells. At the same time, this treatment strategy could endanger other cells with high macropinocytosis rates, such as immature DCs and MCs.

Similarly, macropinocytosis-inducing peptides can be used as a tool to deliver peptides, drugs and genetic material into cells that are difficult to transfect [13, 14, 233, 256].

While macropinocytosis is generally used by the immune system to fight infections, it also provides an easy way to cross the cell membrane barrier, which represents a first line of defence against cellular infection. Therefore,

some pathogens developed mechanisms to actively induce macropinocytosis to be engulfed by the target cell. Bacteria such as *Mycobacterium* [78], *Neisseria gonorrhoeae* [262] and *Hemophilus influenzae* [119] directly induce macropinocytosis and use this ability to infect cells. In addition, *Salmonella* and *Shigella* bacteria induce macropinocytosis not only for their uptake. *Salmonella* uses infection-associated macropinosomes to shape its pathogenic niche inside the cell as it pursues its vacuolar lifestyle [228]. *Shigella* on the other hand, requires these additional macropinosomes for vacuole rupture and release into the cytoplasm [40, 41].

Similarly, certain viruses such as SARS-CoV-2 [263], reavirus [15] and adenovirus [168] can actively induce macropinocytosis to cross the cell membrane barrier. This viruses trigger release from the vesicle after acidification of maturing macropiosomes [206].

In conclusion, macropinocytosis is an important pathway for immune cells such as immature DCs and MCs to sample their environment for pathogen threats, but can be hijacked by pathogens to invade the cell and by cancer cells to acquire nutrients.

1.2.2 *Formation and maturation of macropinosomes*

The process of macropinocytosis can be divided into four distinct phases. In the first phase, actin polymerisation leads to the formation and extension of membrane ruffles. These ruffles form the macropinocytotic cup, which engulfs large amounts of extracellular fluid and its contents as it closes. After closure, early macropiosomes are transported along microtubules to the centre of the cell [252]. They mature into late macropiosomes, which subsequently fuse with lysosomes for digestion of the ingested material.

Conceptually, macropinocytosis has therefore similarities to phagocytosis. The main difference is that macropinocytosis does not require direct receptor interaction but instead can be constitutively active in certain cell types. Typically, macropinocytosis is initiated by Ras activation (see Figure 2.1). Ras proteins are a group of proteins that act as molecular switches [255]. In their inactive form they bind GDP, but during activation the GDP is exchanged for GTP [255]. This activation of Ras leads to further activation of downstream signalling pathways using Rac, CDC42, Pak and phosphoinositide-3-kinase (PI3K) [198].

Constitutive macropinocytosis is based on constant activation of Ras. This constant activation can be the result of oncogenic Ras mutations [33]. Alternatively, Ras can be constitutively activated by constant signalling from the calcium-sensing receptor (CaSR), which is activated by the presence of extracellular Ca^{2+}. This pathway is particularly important for the activation of constitutive macropinocytosis in immune cells [37].

In addition to the constitutive activation of macropinocytosis, macropinocytosis can also be actively induced by plasma membrane receptors. The important difference between receptor-mediated activation of macropinocytosis and other

receptor-mediated processes is that macropinocytosis can be activated by spatially distant cell surface receptors. For example, whereas in classical phagocytosis receptor activation leads to local induction of actin polymerisation to facilitat the uptake of the receptor and cargo, in macropinocytosis the binding of receptor ligands can induce membrane ruffling at some distance from the receptor or even in the entire cell [234]. In particular, growth factor receptors such as epidermal growth factor receptor (EGFR) [32] and platelet-derived growth factor receptor (PDGFR) [57] are known to induce macropinocytosis in a variety of cell types by activating Ras (see Figure 2.1).

Phosphoinositides (PIs) play an important role in the formation and maturation of macropinosomes. During the membrane ruffling phase (see Figure 2.2), PI is initially phosphorylated to PI(4)P [235, 248]. This phosphorylation is one of the activation steps in early ruffle formation. PI(4)P is further phosphorylated to $PI(4,5)P_2$ [235, 248]. Ras-mediated activation of PI3K leads to phosphorylation of $PI(4,5)P_2$ to $PI(3,4,5)P_3$, which is a signal for closure of the macropinocytic cup [235, 248]. After cup closure, $PI(3,4,5)P_3$ is converted to $PI(3,4)P_2$ by the P5 phosphatase SHIP, followed by its conversion to PI(3)P by the P4 phosphatase INNP4 [235, 248]. Early macropinosomes are therefore PI(3)P positive (see Figure 2.3) [235, 248]. During macropinosome maturation, PIKfyve phosphorylates PI(3)P to $PI(3,5)P_2$ (see Figure 2.4) [128].

PI is therefore a versatile marker for studying macropinosome maturation. As a fluorescently tagged version, 2xFYVE can be used to visualise later macropinosomes by interacting with PI(3)P, while Phafin2 can be used to visualise newly formed macropinosomes by interacting with PI(3,4,5)P3 and PI(3,4)P2 [211].

In addition to altering PI phosphorylation, Ras activation also affects Rac1 activity. Activated Rac1 together with Cdc42 leads to Pak1 activation, which in turn also activates actin polymerisation. Actin polymerisation can be induced by two different nucleators. On the one hand, nucleation by formins facilitate the formation of linear actin filaments. On the other hand, nucleation by Arp2/3 leads to the formation of branched actin networks. Arp2/3 can be recruited by two different membrane complexes, the SCAR/WAVE complex [172] and the WASP complex [222]. Both formin- and Arp2/3-mediated actin polymerisation have been shown to play a role in macropinocytosis [110, 116, 214].

Junemann et al. showed that the *Diaphanous*-related formin G plays a role in macropinocytosis and phagocytosis in *Dictyostelium* by synergising with Arp2/3 in the process of actin polymerisation [110]. Insall et al. showed that Arp2/3 is initially recruited to newly forming macropinocytosis cups in *Dictyostelium* and subsequently covers the entire macropinosome [98]. Shortly after macropinosome closure, the entire macropinosome is striped from Arp2/3 [98].

Suetsugu et al. showed that Arp2/3 recruitment in macropinocytosis depends on Wave2, as loss of Wave2 impaired macropinocytosis in mouse embryonic fibroblasts [231]. When Veltman et al. studied the colocalisation of Wasp and SCAR with $PI(3,4,5)P_3$ patches that are associated with membrane ruffling and macropinocytosis in *Dictyostelium*, they observed the formation of SCAR rings

around the patches [241]. Wasp also showed a ring formation around the patches, but was much weaker and less coherent, indicating that SCAR/WAVE is more important for the recruitment of Arp2/3 in *Dictyostelium* [241].

Several additional markers of macropinosome maturation exist. One important group are the Rab proteins, which are small GTPases belonging to the Ras superfamily. During and after cup closure (see Figure 2.2), macropinosomes are Rab5 positive [162]. Recruitment of Rab5 is an important step in macropinosome closure. It leads to the recruitment of PI-5-phosphatases via APPL1, and loss of Rab5 recruitment prevents macropinosome closure [162].

As macropinsomes mature, they change their decoration by Rab proteins, from Rab5 to Rab21 (see Figure 2.3) and then to Rab7 (see Figure 2.4) [64]. Upon fusion with the lysosome, macropinsomes also become Lamp1 positive (see Figure 2.5) [64].

As macropinocytosis is mechanistically very similar to phagocytosis, it is difficult to selectively inhibit only one of both processes. Commonly used inhibitors of actin polymerisation and depolymerisation, such as latrunculin and jasplakinolide, affect global actin polymerisation irrespective of macropinocytosis or phagocytosis [100]. Therefore, amilorides such as ethylisopropyl amiloride (EIPA) have been used to specifically block macropinocytosis. These drugs block sodium proton exchanger (NHE), leading to an increase in the intracellular pH, which blocks the Rac1/Cdc42 pathway [125]. Therefore, amilorides are supposed to selectively block only macropinocytosis without affecting other endocytotic pathways [243, 250]. This feature makes amilorides in general and EIPA in particular the most widely used drugs to inhibit macropinocytosis. However, there are also several repords showing that amilorides are not as selective as desired and may also affect other cell functions and endocytotic pathways [89, 101, 104, 249]. For example, amilorides can affect clathrin-mediated endocytosis and K-ATP channel activity [26].

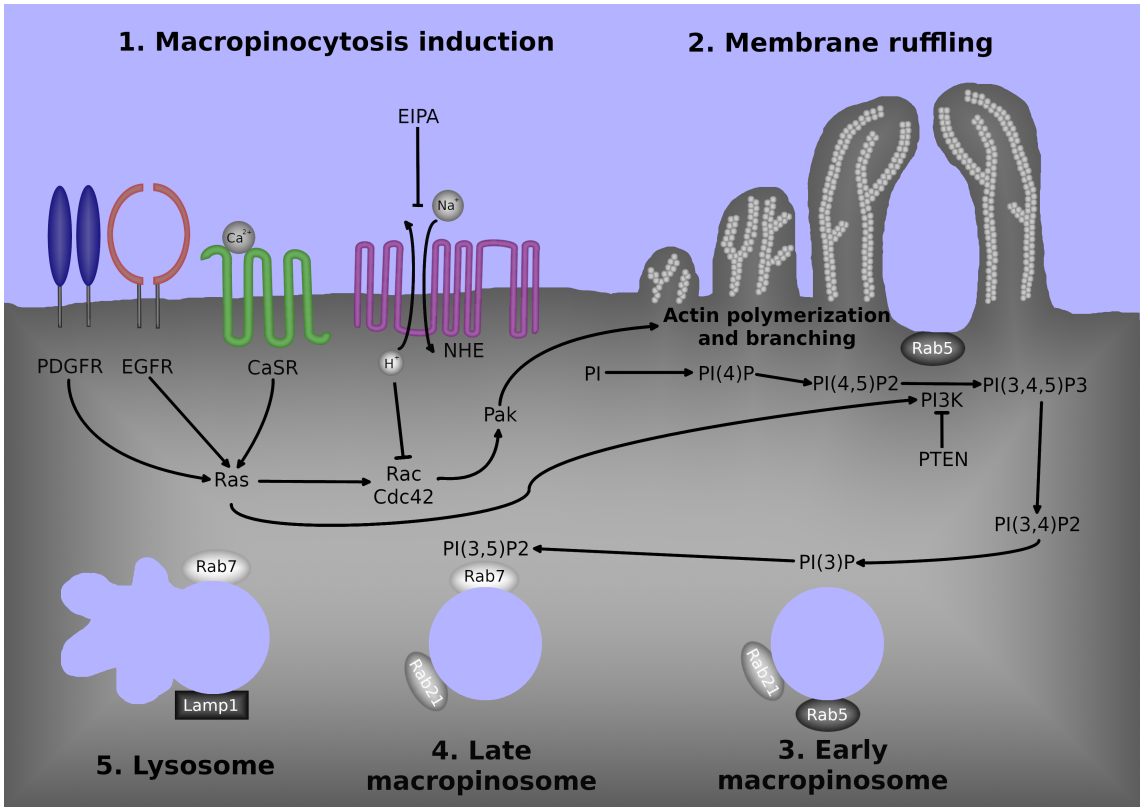

Figure 2: Regulation of macropinocytosis: Receptor signalling by receptors like platelet-derived growth factor receptor (PDGFR), epidermal growth factor receptor (EGFR) or calcium-sensing receptor (CaSR) induces Ras activation, which in turn triggers actin polymerisation and branching through Rac, Cdc42 and Pak. In addition, actin polymerisation is activated by phosphoinositide (PI) phosphorylation. PI_3 kinase (PI3K) activity also plays a role in macropiosome closure. Early macropinosomes are Rab5 and Rab21 positive whereas late macropinosomes become Rab7 positive before ultimately fusing with the lysosome. Adapted from [64, 65, 198].

1.2.3 *Influences of the environment on macropinocytosis*

When studying cellular processes *in vitro*, researchers typically use simplified systems that ignore many physiological aspects, such as the role of the microenvironment on cellular processes. *In vivo*, cells are usually surrounded by other cells and tissues with specific properties such as stiffness, rigidity, adhesiveness, and porosity. These properties influence cellular behaviours such as cell migration [42]. In addition, cells are constantly exchanging signals with their local microenvironment, either directly through cell-cell interactions or indirectly via signalling molecules.

Several approaches have been developed to study cellular behaviour in more physiological environments than clasical cell culture dishes. The simplest three-dimensional matrix is based on collagen hydrogels [129]. Cells can be embedded in three-dimensional networks of collagen [129]. By changing the collagen content, the density and porosity of the network can be easily modified [129]. As collagen is a natural component of the extracellular matrix, these hydrogels represent a

physiological environment encountered by cells *in vivo* [129]. However, collagen-based hydrogels have the disadvantage that the extraction of cells is difficult and time-consuming.

Another option to mimic physiological matrices are carbomer-bases hydrogels. Carbomer is an alternative name for long-chain poly(acrylic acid) (PAA). These Hydrogels can be generated by mixing PAA with a liquid medium. This hydrogel generation uses a specific feature of PAA. In a low pH environment, PAA is in a tightly packed coiled conformation that takes up less space. As PAA itself acts as an acid, solutions of PAA generally start at a low pH. When the pH is subsequently adjusted to neutral, PAA changes its conformation to a linear chain [120]. This linear chain occupies more space, resulting in the formation of a hydrogel. Similar to collagen, the density of PAA hydrogels can be easily modified by changing the PAA concentration. An advantage of PAA hydrogels is the ability to dissolve them to extract cells. As there is no cross-linking of the fibres, PAA hydrogels can be easily dissolved by diluting them with more volume. However, as a synthetic polymer, PAA does not mimic the physiological environment as closely as collagen. For example, PAA is non-adhesive and therefore only allows ameboid cell migration [52, 160].

Not only the 3D structure of the environment can influence cell functions, but also cell adhesion to the substrate. While normal plastic dishes are highly adherent to cells, in the physiological environment cells experience much lower cell adhesion [133]. To modulate cell adhesion to surfaces, surfaces can be modified by their coating with peptides or other chemicals. One simple way to increase cell adhesion to surfaces is coating with poly-L-lysine (PLL), fibronectin or fibrinogen. Cell adhesion can also be reduced with substances such as polyethylene glycol (PEG) that are inert for cells. It is also possible to use micropatterning with surface coatings to generate surfaces with a wide variety of different shapes for cell adhesion. This can be done either by stamping specific patterns onto the passivated surface [167] or by using a photomask to remove specific regions with photosensitive chemicals [157].

For some questions it is also important to rebuild structures found *in vivo* with synthetic materials *in vitro*. One material commonly used to generate customised environments is polydimethylsiloxane (PDMS). PDMS polymers can be generated by mixing two liquid components. Polymerization is initiated by mixing PDMS with a curing agent. The mixture can be casted into specific shapes using custom moulds. These PDMS devices can be used to study cell migration or the effects of spatial confinement of cells [129].

To date, most research on macropinocytosis has focused solely on the effects of growth factors or other soluble molecules, while other environmental influences like physiological properties have been largely neglected. Yet, there are a few examples of how the microenvironment influences macropinocytosis.

Honda et al. showed that the topography of microfabricated surfaces influences macropinocytosis in *Dictyostelium* [92]. When the authors placed amoeba cells on top of microridges, they observed that more cells form macropinocytotic actin

patches compared to cells on flat surfaces [92]. They also observed that actin patches on the cell migrated alongside the microridges, following the direction of cell migration [92].

In addition, cell shape has been shown to influence the propagation of $PI(3,4,5)P_3$ waves, which are important for the formation of macropinosomes [93].

Also in *Dictyostelium*, it has been observed that both myosin A/B and myosin B/C double knockouts have a macropinocytosis defect, when the cells were grown in suspension culture, but perform similar amounts of macropinocytosis to wild-type (WT) cells when the cells were grown as adherent cultures [185]. However, macropinocytosis of adherent *Dictyostelium* is also much lower than in suspension [185].

Zeng et al. showed that the stiffness of the cellular substrate influence the formation of circular dorsal ruffles, which are an important step in the macropinosome formation [261]. They observed longer lasting circular dorsal ruffles in NIH 3T3 fibroblast cells adhering to substrates with higher stiffness [261].

The same effect was observed by Freeman et al. [74]. When they seeded cancer cells on substrate matrices of different stiffness, they observed an increase in macropinocytosis [74]. They were able to link this increase in macropinocytosis to the activity of the tension-sensitive Ca^{2+} channel Piezo1 [74].

Taken together, these publications indicate that macropinocytosis can be influenced by the topography, adhesion to the substrate and stiffness of the substrate.

Another area where macropinocytosis and the environment are interconnected is in the cellular exploration of the environment. In migrating dendritic cells (DCs), macropinocytosis plays a role in regulating cell exploratory behaviour [175]. While immature DCs show a highly exploratory phenotype, ignoring hydraulic resistance and thereby also exploring dead ends, mature DCs loose this ability [175]. Moreau et al. showed that this difference in cell behavior is due to differences in the macropinocytotic activity [175]. When macropinocytosis was inhibited, immature DCs lost their exploratory ability and instead developed sensitivity to hydraulic resistance [175].

The environment can also influence the pathway of actin polymerisation [239]. While both formin- and Arp2/3-mediated actin polymerisation are generally associated with macropinocytosis [110, 116, 214], Vargas et al. observed higher macropinocytosis in immature DCs by knocking out the formin mDia1 and using the formin inhibitor Smifh2 inside straight PDMS microchannels [239]. At the same time, Arp2/3 impairment reduced macropinocytosis [239]. This shows that macropinocytosis in 3D microchannels depends on Arp2/3-mediated actin polymerisation, but not on formins.

Davidson and Wood showed that macrophages (MCs) in *Drosophila* embryos switch their actin regulators during phagocytosis of necrotic cell debris [55]. When MCs are not confined, they mainly use Arp2/3 mediated actin branching to engulf larger particles of necrotic cell debris. However, when MCs are highly spatially confined, they switch to formin-mediated actin polymerisation to form long linear actin filaments [55].

Taken together, these results indicate a link between the spatial environment and endocytotic processes However, the principles and mechanisms of how the microenvironment regulates macropinocytosis remain still largely unexplored.

1.3 DYNAMICS AND TENSION OF THE CELL MEMBRANE

The cell membrane is highly dynamic and subjected to constant forces from both inside and outside the cell. These forces can lead to both local and global changes in the membrane tension [58]. Intracellular forces are mainly generated by the membrane cortex, consisting of two parts [220]. The outer part is composed of the plasma membrane, which consists of a lipid bilayer and integrated membrane proteins [220]. Beneath the membrane lies inner part called the actomyosin cortex, which consists of actin filaments myosin and microtubules [220]. Actin generates force by controlled polymerisation and depolymerisation [174], while the motor protein myosin generates force by moving alongside actin filaments [203]. Actin filaments are either directly attached to membrane proteins or indirectly connected to the membrane by membrane-to-cortex attachment proteins [220]. This connection allows force to be transmitted directly from the actomyosin cortex to the cell membrane. The interconnected network of cell membrane, membrane proteins and actomyosin cortex is an important factor in cell motility, membrane dynamics and influences the tension of the membrane [58, 220].

There are several approaches to measure and modulate membrane tension. The most common approach is the use of optical tweezers [220, 223]. In this assay, microspheres are connected to the membrane-cytoskeleton complex. This leads to the formation of a thin membrane tether that connects the cell to the microshere. Membrane tension can be calculated by measuring the changes in the length of the tether Δx [223]. At the same time, the same setup can be used to modify membrane tension. The microspheres can be optically caged. By moving this cage, the microsheres can be moved away from the cell, resulting in the transfer of force from the microsphere via the tether to the cell membrane, thereby increasing membrane tension. Using this approach, De Belly et al. were able to show that actin- and mysosin-based protrusions produce global changes in membrane tension, whereas tether-based pulling only leads to local changes in tension [58].

A simple way of modifying membrane tension is the application of osmotic pressure. By using media with a low solute concentration, creating a hypotonic solution, cells begin to swell, increasing membrane tension and eventually leading to cell rupture. At the same time, cells are able to increase membrane surface area to some extent by using intracellular lipid reservoirs to prevent osmotic rupture [83]. The use of a hypertonic solution with a higher solute concentration leads to cell shrinkage, thereby reducing membrane tension [204].

More recently a new approach has been developed to measure membrane tension using fluorescence lifetime changes of a fluorescent probe. The Flipper-TR dye intercalates into lipid membranes [204]. The dye consists of two fluorophore domains connected by a linker [204]. This linker allows the molecule to change its

conformation depending on membrane tension: in a low-tension environment, the molecule is twisted around the linker region, while in higher-tension environment, the molecule adopts a planar conformation [204]. This conformational change results in little change in fluorescence intensity and a small shift in the excitation and emission profile, but causes an increase in fluorescence lifetime [204]. The fluorescence lifetime is defined as the time it takes for a fluorophore to return from the excited state to the lower energy state after excitation. This reduction is accompanied by the emission of photons with a wavelength longer than the excitation wavelength.

A disadvantage of the Flipper-TR probe is that the lifetime is not only dependent on the membrane tension, but can also be affected by membrane composition. Therefore, changes in the lipid composition or protein content can also affect the lifetime of the probe [204].

Macropinocytosis is highly dependent on membrane dynamics, but to date there has been little research into the relationship between macropinocytosis, membrane tension and membrane dynamics. Shemesh et al. showed with a computational model that increased membrane tension leads to a more stationary lamellipodium while lower membrane tension leads to advancing lamellipodia [218]. When Pontes et al. investigated the lamellipodium in migrating cells in relation to membrane tension they also observed a correlation between membrane tension, protrusion formation and cell adhesion [191]. They concluded, that membrane tension controls adhesion of the migrating cell front [191].

In line with this Delanoe et al. observed the accumulation of cadherins, a group of proteins associated with cell adhesion, when membrane tension was increased [59].

Membrane tension can also influence macropinocytosis. For example, it has been shown in myoblasts that decreasing membrane tension with hypertonic solution leads to the formation of more F-actin and $PI(4,5)P_2$, which in turn increases the amount of macropinocytosis [152]. On the other hand, Lin and Liu report that treatment of myotubes with hypotonic buffer and mechanical stretch can also actively induce macropinocytosis by activating the mTOR pathway [146]. Lutton et al. generated a data-driven model of macropinosome closure in *Dictyostelium*. In this model, higher membrane tension was required for cup closure [155].

Thus, although there is evidence for a link between macropinocytosis and membrane tension, the interplay is still not fully understood.

1.4 CRISPR/CAS9 SCREENING

Since its discovery in 2012 by Jennifer Doudna and Emmanuelle Charpentier [108], genetic engineering by CRISPR has rapidly become a powerful tool to investigate gene functions and modify gene activity. The principle behind the tool is simple: a single guide RNA (sgRNA) forms a complex with a endonuclease enzyme like Cas9. This complex is directed by the sgRNA sequence to a complementary

region, where the endonuclease cleaves the deoxyribonucleic acid (DNA) double-strand, generating a double strand break. This DNA double strand break can be repaired by non-homologous end joining (NHEJ) or homology-derived repair. The process of NHEJ is the most prominent replair mechanism, but at the same time it is also error prone with an accuracy of only 75% [224]. These errors can result in the deletion or insertion of amino acids, leading to frame-shift mutations that can render the affected gene non-functional [103].

This tool, known as CRISPRko, has been further developed to not only allow gene inactivation but also inhibition (CRISPRi) or activation (CRISPRa). CRISPRi uses a version of the endonuclease that is unable to cleave the double strand and therefore blocks gene transcription by steric hindrance. In CRISPRa, the endonuclease is also inactive but is fused to a transcription-activating domain [44].

Because CRISPR is a simple tool for modifying gene activity, it is well suited to analyse gene functions. While only one sgRNA is usually used to generate knock outs (KOs), it is also possible to combine several sgRNAs in a sgRNA library. When cells are transfected with this sgRNA pool in such a way that each cell carries only one sgRNA, a pool of cells is generated in which each cell either carries only one of the KOs or no genetic alterations [109]. Screening this pool of cells for specific phenotypes allows the identification of candidates involved in the process of interest [109].

Two types of sgRNA libraries have been used in the literature, namely genome-wide libraries and sub-libraries. A genome-wide library contains multiple sgRNAs for each gene of the entire genome of the target species. In addition, some sgRNA libraries also contain guides for microRNAs in the genome to also take their effects into account. One of the first of such libraries was the GeCKO library for CRISPR screening in human cells [216].Meanwhile additional genome-wide libraries have been generated, such as the one developed by the Kerschsteiner lab that was used for the screen in this thesis [117]. On the other hand, there are sub-libraries that consist only of a limited number of sgRNAs. This can be either a thematic library for a specific gene family or a smaller library of candidate genes identified with a genome-wide screen.

Here I will focus on genome-wide libraries as we have used a genome-wide screen in this work, but most of the considerations apply to sub-libraries as well. The first detail to consider is the library design. For each gene of interest, three to four sgRNAs should be used to account for off-target effects, in which the sgRNA binds a similar DNA sequence of another non-target genomic location and may thereby alter the function of another gene. The use of several guides per target also protects against the failure of single guides with low efficiency to induce KOs. At the same time, too many guides per target are a disadvantage, as this would inflates the size of the library, leading to coverage problems, which I will discuss later. Each library should also contain a number of non-targeting sgRNAs as controls.

The next detail to consider is the delivery system for the guides. Since lipofection, other chemical transfection methods and electroporation have low trans-

fection efficiencies, viral transfections are usually used to reach high delivery efficiency. Either lentiviruses or adeno-associated viruses (AAV) can be used. While AAV have the advantage of being considered as biosafety level 1, they are limited in the size of their cargo to <5 kb [257]. Lentiviruses, on the other hand, can deliver larger cargoes, but are classified as biosafety level 2, and therefore require more careful handling. In addition, lentiviruses integrate their cargo randomly into the genome, which carries the risk of producing undesired mutations [35].

To amplify the library for virus production, the library is cloned into a plasmid backbone and amplified in *E. coli*. It is very important to maintain similar levels of all sgRNAs during library amplification, virus production and target cell infection. Therefore, it can be beneficial to split the library into several sub-libraries. The plasmids are then used to produce the viral delivery system. This virus can be used to transform the cells of interest. For the infection, it is again important to achieve a high coverage of the library. For full genome size libraries, a coverage of at least 100 cells per guide is usually desired, which means that for each sgRNA in the library, 100 cells should be infected with the lentivirus. At the same time, the multiplicity of infection (MOI) should be around 0.3 to ensure that each cell carries only one KO.

Using a lentiviral library of 10^5 sgRNAs as an example, 3.3×10^7 cells would need to be infected to obtain 10^7 cells carrying only one sgRNA each after selection with a coverage of 100 cells per guide. Selection can be achieved either by using fluorescent markers in the viral vector and fluorescence activated cell sorting (FACS), or by using antibiotic resistance genes such as puromycin.

The next detail to consider is the read out of the gene activity. The simplest and most direct approach is a lethal screen, where cells die if they lack an essential gene. Thus, cells with the corresponding sgRNA are removed from the cell pool. An alternative is to use the uptake or binding of a fluorescent substrate as a readout. This allows to separate cells with higher and lower fluorescence by FACS.

The next step is to isolate genomic DNA from the cells, amplify the sgRNA using polymerase chain reaction (PCR) and sequence them using next-generation sequencing (NGS). When isolating and amplifying DNA, it is again important to avoid any errors that could lead to generate a bias towards certain sgRNAs.

A variety of software solutions have been established to analyse the NGS data from genome-wide screens [105, 142, 225]. In general, all these tools use the same principle: They extract the number of reads for each sgRNA and compare the abundance of the sgRNAs in the desired experimental condition with the abundance in control cells that have simply been infected with the library. They use the non-targeting sgRNAs as a baseline, as they should have no effect and therefore be similarly abundant in both sets of data. At the end, the software returns a list of the sgRNAs and corresponding genes with their enrichment or depletion and a p-value for the probability that this change in abundance is significant. This list can be used to identify interesting candidates that need to be

further validated by generating single KOs of these genes as well as using other sgRNAs to exclude off-target effects.

As genome-wide screens tend to be very noisy in their results, it is also possible to use a genome-wide screen in a first step to generate a smaller subset of interesting candidate genes and then in a second step to generate a smaller library specifically for these candidates with more sgRNAs per guide and repeat the screen with this sub-library [62].

Recently, also new CRISPR cassettes have been generated that allow the combination of several sgRNAs in one backbone [187]. This approach allows the multiplexing of KOs and the investigation of gene interactions. However, it is very important to consider, that the use of these multiplexed sgRNAs significantly increases the number of cells that need to be infected to achieve acceptable coverage in a library screen.

While most CRISPR screens to this date have been performed *in vitro*, there are also *in vivo* approaches. For example, *in vivo* CRISPR screens have been used to investigate mediators of immune evasion in cancer [28] and factors that render cancer immune to chimeric antigen receptor (CAR) T-cell therapy [195]. Another *in vivo* approach investigated genetic factors involved in the infiltration of auto-regulatory T cells into the central nervous system in a multiple sclerosis model [117].

2

OBJECTIVES

Although some key factors in macropinocytosis have been identified, such as Ras, Rac, Cdc42, PI3-kinase and F-actin, our understanding of the regulation and initiation of macropinocytosis is still limited.

Therefore, the first aim of this PhD project was to develop a deeper understanding of the regulation of macropinocytosis in immune cells and to identify unknown genes involved in this process as positive or negative regulators.

In addition, cells in their physiological environment are constantly exposed to chemical and mechanical signals from surrounding cells and tissues. While the influence of growth factors and other receptor ligands has already been extensively studied, the effects of mechanical cues in general, the three-dimensional environment, and cell adhesion on macropinocytosis have not been investigated. Given that three-dimensional environments and cell adhesion influence cell behaviours such as migration and phagocytosis, we hypothesised that the microenvironment might also influence macropinocytosis. Therefore, our second aim was to investigate how three-dimensional environments and cell adhesion may regulate the principles and mechanisms of macropinocytosis.

To achieve these aims, we used two different approaches. First, we performed a genome-wide CRISPR/Cas9 knockout screen to identify novel regulators of macropinocytosis, using a lentiviral sgRNA library. By sorting the knockout cells based on their ability to take up fluorescence-labelled 70 kDa dextran as a fluid marker for macropinocytosis, we identified potential candidates of positive and negative regulators of macropinocytosis. In this screen, decreased dextran uptake indicates that a candidate gene is either directly involved in macropinocytosis or positively influences the process. On the other hand, increased uptake indicates that the candidate gene down-regulates or blocks macropinocytosis.

Secondly, we have developed a wide variety of assays that allow us to precisely modify the cellular microenvironment. Using more physiological three-dimensional hydrogels, we investigated how three-dimensional environments affect macropinocytosis and compared the behaviour with cells adhering to less physiological planar surfaces (2D assay). We also used different inhibitors and genetic knockouts to investigate how actin polymerisation is organised in these different environments. Using micropattern assays and different surface modifications, we investigated how macropinocytosis is influenced by the adhesiveness of macrophages, a relevant immune cell type known to perform high amounts of macropinocytosis. Finally, we investigated the relationship between macropinocytosis and membrane tension in low and high adhesion environments using the Flipper-TR probe and fluorescence lifetime imaging.

3

MATERIAL AND METHODS

3.1 MATERIALS

3.1.1 *Chemicals*

Table 1 shows all inhibitors and used concentrations. Table 2 lists all additional chemicals, while Table 3 lists all the kits used in this thesis.

Inhibitor	**Supplier**	**Catalog number**	**Used concentration**
EIPA	Sigma-Aldrich	A3085	55 µM
Jasplakinolide	TOCRIS	2792	8 µM
CK-666	Sigma-Aldrich	SML0006	60 µM
CK-689	Sigma-Aldrich	182517	60 µM
Smifh2	Sigma-Aldrich	S4826	60 µM
Pyrrophenone	Sigma-Aldrich	530538	1 µM , 5 µM, 10 µM
mβCD	Sigma-Aldrich	332615	6 mM
Nystatin	Sigma-Aldrich	N6261	10 µM
Chlorpromazine hydrochloride	Sigma-Aldrich	C8138	10 µM

Table 1: List of inhibitors

Chemical	**Supplier**	**Catalog number**
Sodium hydroxide	AppliChem	A6829
Ethylenediaminetetraacetic acid	Sigma-Aldrich	EDS-500G
PBS	Apotheke Klinikum der Universität München	L20201215-01C
RPMI 1640 medium	Invitrogen	21875034
FCS	Gibco	10437-028
BME (50 mM)	Gibco	31350-010
Penicillin-streptomycin (10,000 units penicillin and 10 mg mL^{-1} streptomycin)	Sigma-Aldrich	P0781
β-estradiol	Sigma-Aldrich	E2758-1G
DMEM	Invitrogen	31885-023

DMSO	Acros Organics	327182500
$CaCl_2 \cdot 2\,H_2O$	Sigma-Aldrich	C3306
PEI MAX	Polyscience	24765-1
Glycerol	Sigma-Aldrich	G5516
Albumin (BSA) fraction V	AppliChem	A1391
PAA average Mv $4,000,000$	Sigma-Aldrich	30631
Nutragen	Advenced Biomatrix	5010
DNase/RNase-free distilled water	Invitrogen	10977035
Ethanol absolute $99.8 + \%$	Fisher Scientific	E/0650DF/17
Formaldehyde solution 37%	Sigma-Aldrich	8.18708
Isopropanol	Fisher Scientific	P/7500/15
Lennox L broth base	Invitrogen	12780052
LB-Agar	Invitrogen	22700025
Ampicillin sodium salt	Sigma-Aldrich	A0166
Trypsin 0.25%/EDTA 0.02% in DPBS	PAN-Biotech	P10-020100
Dextran, fluorescein, $70,000$ MW	Invitrogen	D1822
Dextran, TexasRed, $70,000$ MW	Invitrogen	D1864
Bovine serum albumin (BSA), FITC conjugate	Invitrogen	A23015
Flipper-TR	Spirochrome	SC020
Puromycine	Gibco	A1113803
TAE buffer	Thermo Fisher scientific	B49
Loading dye	New England Biolabs	B7024A
BbsI-HF restriction enzyme	New England Biolabs	R3539
Polynucleotide kinase	New England Biolabs	M02021
Adenosine 5′-triphosphate	New England Biolabs	P0756

Table 2: Other chemicals

3.1.2 *Kits*

Kit	**Supplier**	**Catalog number**
GeneJET Plasmid-Miniprep-Kit	Thermo Fisher	K0503
PureLink Expi Endotoxin-Free Maxi Plasmid Purification Kit	Thermo Fisher	A31231
Phire Tissue Direct PCR Master Mix	Thermo Fisher	F170L
Monarch PCR & DNA Cleanup Kit	New England Biolabs	T1030L
Monarch DNA Gel Extraction Kit	New England Biolabs	T1020L
DNA 1000 Kit	Agilent	5067-1504
DNeasy Blood & Tissue Kit	Qiagen	69504
AMPure XP SPRI Reagent	Beckman Coulter	A63881
Qick Ligation Kit	New England Biolabs	M2200

Table 3: List of kits used

3.1.3 *Antibodies*

Table 4 contains all antibodies, cellular models, and concentrations used for antibody staining.

Antibody	**Fluorophore**	**Supplier**	**Catalog number**	**Cellular model**	**Used dilution**
Anti-Mo CD16/CD32	-	Invitrogen	14-0161-86	blocking antibody	1:100
Anti- Mo MHC Class II	eFluor450	Invitrogen	48-5321-82	dendritic cell (DC)	1:300
Anti-Mo CD11c	APC	Invitrogen	17-0114-82	DC	1:300
Anti-mouse CX3CR1 Antibody	Alexa Fluor 647	Biolegend	149004	macrophage (MC)	1:500
Anti-mouse CD68 Antibody	PE	Biolegend	137014	MC	1:100
Anti-mouse/human CD11b Antibody	Pacific Blue	Biolegend	101224	MC	1:100

Table 4: List of antibodies

3.1.4 *Plasmids*

All plasmids used in this thesis can be found in Table 5.

Plasmid	**Generated by:**	**Addgene number:**
pKLV2-U6gRNA5(BbsI)-PGKpuro2ABFP-W	Kosuke Yusa	# 67974
psPAX2	Didier Trono	# 12260
pMD2.G	Didier Trono	# 12259
Plasmids with KO library based on pKLV2-U6gRNA5(BbsI)-PGKpuro2ABFP-W	Arek Kendirli	-

Table 5: Plasmids

3.1.5 *Media and buffer*

Table 6 shows the composition of all medias and buffers used.

Basis medium:
500 mL RPMI-1640
50 mL fetal calf serum (FCS)
500 mL Penicillin/Streptomycin
550 µL 2-Mercaptoethanol (BME) (50 mM)
Freezing medium:
45 mL FCS
5 mL dimethyl sulfoxide (DMSO)
Hoxb8 medium:
500 mL RPMI-1640
50 mL FCS
500 mL Penicillin/Streptomycin
550 µL BME (50 mM)
22.5 mL Supernatant of Flt3l expressing cell line
58 µL Estradiol (10 mM in Ethanol)
Dulbecco's modified eagle medium (DMEM) medium:
500 mL DMEM
50 mL FCS
500 mL Penicillin/Streptomycin
550 µL BME (50 mM)

MC medium: 500 mL RPMI-1640 50 mL FCS 500 mL Penicillin/Streptomycin 550 µL BME (50 mM) 25 mL Supernatant of Flt3l expressing cell line 100 mL Supernatant of M-CSF expressing cell line
10% DC medium: 500 mL RPMI-1640 50 mL FCS 500 mL Penicillin/Streptomycin 550 µL BME (50 mM) 61 mL Supernatant of GM-CSF expressing cell line
20% DC medium: 500 mL RPMI-1640 50 mL FCS 500 mL Penicillin/Streptomycin 550 µL BME (50 mM) 122 mL Supernatant of GM-CSF expressing cell line
$CaCl_2$ medium: 500 mL Milli-q water 7.3 g $CaCl_2 \cdot 2\,H_2O$ filter through 0.2 µm sterile filter
$CaCl_2$ medium with 15% glycerol: 51 mL $CaCl_2$ medium 9 mL glycerol
Polyethylenimine (PEI) transfection solution: 50 mg 50 mL milli-q water adjust pH to 7,1
Fluorescence activated cell sorting (FACS) buffer: 500 mL phosphate-buffered saline (PBS) 5 g bovine serum albumin (BSA) 293 mg ethylenediaminetetraacetic acid (EDTA) (2 mM)

EDTA solution:
500 mL PBS
1.5 g EDTA (10 mM)
adjust to pH 7,2
Medium with reduced FCS content:
49 mL RPMI-1640
500 µL FCS
500 mL Penicillin/Streptomycin
50 µL BME (50 mM)

Table 6: Media and buffer

3.1.6 *Mice*

All mice used were breed and kept in the core facility animal models at the Biomedical Center Munich (BMC) in accordance with German animal welfare legislation. The used mice strain was C57Bl6/J.

3.1.7 *Cell lines and bacterial strains*

Cell line:	**Origin:**
Hoxb8:	
WT	Sixt lab (IST austria)
mTmG	Sixt lab (IST austria)
Hem1 KO	Sixt lab (IST austria)
Wasp KO	Sixt lab (IST austria)
Kindlin-3 (+/-)	Moser lab (TranslaTUM munich)
Kindlin-3 (neo/neo)	Moser lab (TranslaTUM munich)
Kindlin-3 (neo/-)	Moser lab (TranslaTUM munich)
Kindlin-3 (-/-)	Moser lab (TranslaTUM munich)
Cas9 homo	Schmidt-Supprian lab (TranslaTUM munich)
LX293	Sixt lab (IST austria)
4T1	Sixt lab (IST austria)
3T3	Sixt lab (IST austria)
HT1080	Sixt lab (IST austria)
NEB Stable Competent *E.coli*	New england Biolabs (C3040H)

Table 7: Cell lines and bacteria strains

3.1.8 *Oligonucleotides*

Oligonucleotides for CRISPR-based knock out (KO) generation were generated using the CRISPick tool from the Broad institute (https://portals.broadinstitute.org/gppx/crispick/public). To be able to clone these oligos into the pKLV2-U6gRNA5(BbsI)-PGKpuro2ABFP-W backbone, complementary overhangs were added to the single guide RNA (sgRNA) sequence. For the forward (FWD) oligos, "CACCG" was added in front of the guide sequence. For the reverse (REV) oligos, "AAAC" was added in the front and one "C" in the end. These overhangs were complementary to the overhangs generated by BbsI digestion of pKLV2-U6gRNA5(BbsI)-PGKpuro2ABFP-W. Additionally, one "G" was added at the start of every sgRNA sequence. Scrambled (SCR) sequences were generated using Sequence Scramble from GeneScript (https://www.genscript.com/tools/create-scrambled-sequence) with mouse reference genome. All oligonucleotides were ordered from eurofins.

Name:	**Sequence:**
NF1 KO1 oligo FWD	CACCGGGAAACGTGGCATGTCTCGG
NF1 KO1 oligo REV	AAACCCGAGACATGCCACGTTTCCC
NF1 KO2 oligo FWD	CACCGACTCTAACCATTGCAAACCA
NF1 KO2 oligo REV	AAACTGGTTTGCAATGGTTAGAGTC
NF1 KO3 oligo FWD	CACCGTGTGTAACCACGAGAAAGTG
NF1 KO3 oligo REV	AAACCACTTTCTCGTGGTTACACAC
Rac1 SCR control oligo FWD	CACCGACATGCCGCGACCAGTTCCT
Rac1 SCR control oligo REV	AAACAGGAACTGGTCGCGGCATGTC
CaSR SCR control oligo FWD	CACCGGGTGCTGCGTTAACGGTGGA
CaSR SCR control oligo REV	AAACTCCACCGTTAACGCAGCACCC
NF1 SCR control oligo FWD	CACCGATGCGATGGCGTATGGCGAC
NF1 SCR control oligo REV	AAACGTCGCCATACGCCATCGCATC
Adgre1 KO3 oligo FWD	CACCGTATTACTGCACCTGTAAACG
Adgre1 KO3 oligo REV	AAACCGTTTACAGGTGCAGTAATAC
Temem2301 KO3 oligo FWD	CACCGGCCTTATAAGGGATCTTAGG
Temem2301 KO3 oligo REV	AAACCCTAAGATCCCTTATAAGGCC
Arhgap11a KO4 oligo FWD	CACCGAGTCATCAGTAACAAATACG
Arhgap11a KO4 oligo REV	AAACCGTATTTGTTACTGATGACTC
Pilra KO3 oligo FWD	CACCGAGTTGTAGATGAATTCCCCA
Pilra KO3 oligo REV	AAACTGGGGAATTCATCTACAACTC

Atp6v1e1 KO1 oligo FWD	CACCGCCAACTTGATGAATCAAGCA
Atp6v1e1 KO1 oligo REV	AAACTGCTTGATTCATCAAGTTGGC
Mark3 KO3 oligo FWD	CACCGCAGCTACTTACTTGCTACTG
Mark3 KO3 oligo REV	AAACCAGTAGCAAGTAAGTAGCTGC
Sphk2 KO2 oligo FWD	CACCGAGAGAGACTAGACCATCTCG
Sphk2 KO2 oligo REV	AAACCGAGATGGTCTAGTCTCTCTC
Nprl3 KO4 oligo FWD	CACCGGCAACCAAATCTGAAATGTG
Nprl3 KO4 oligo REV	AAACCACATTTCAGATTTGGTTGCC
Dnah3 KO4 oligo FWD	CACCGAGCCGACTAAAGTCCAGACA
Dnah3 KO4 oligo REV	AAACTGTCTGGACTTTAGTCGGCTC
Lrch2 KO4 oligo FWD	CACCGTAATCTATACCTAGACCAGG
Lrch2 KO4 oligo REV	AAACCCTGGTCTAGGTATAGATTAC
Mospd2 KO4 oligo FWD	CACCGGTGAATCCTCTATTCCAAGA
Mospd2 KO4 oligo REV	AAACTCTTGGAATAGAGGATTCACC
Lrch2 KO5 oligo FWD	CACCGTGTTAACATACCTTAACATC
Lrch2 KO5 oligo REV	AAACGATGTTAAGGTATGTTAACAC
Lrch2 KO6 oligo FWD	CACCGCACTTCCGATTCCAGAGTCA
Lrch2 KO6 oligo REV	AAACTGACTCTGGAATCGGAAGTGC
Lrch2 KO7 oligo FWD	CACCGCAGGTCCTTCCTCAACAAAT
Lrch2 KO7 oligo REV	AAACATTTGTTGAGGAAGGACCTGC
Pilra KO5 oligo FWD	CACCGGATCCTTGGCCAACTTCCAG
Pilra KO5 oligo REV	AAACCTGGAAGTTGGCCAAGGATCG
Pilra KO6 oligo FWD	CACCGCCACTCACCAGCATGCAGAC
Pilra KO6 oligo REV	AAACGTCTGCATGCTGGTGAGTGGG
Pilra KO7 oligo FWD	CACCGCTCCAGAGCAGCTTTCAGGT
Pilra KO7 oligo REV	AAACACCTGAAAGCTGCTCTGGAGG
Adgre1 KO5 oligo FWD	CACCGTCCAACTGCTCTAACTCTGT
Adgre1 KO5 oligo REV	AAACACAGAGTTAGAGCAGTTGGAG
Adgre1 KO6 oligo FWD	CACCGCACAGTGCCACCAACAACAC
Adgre1 KO6 oligo REV	AAACGTGTTGTTGGTGGCACTGTGG
Adgre1 KO7 oligo FWD	CACCGATTGCTGTATCTGCTCACTT
Adgre1 KO7 oligo REV	AAACAAGTGAGCAGATACAGCAATG

Table 8: Oligonucleotides

3.1.9 *Primers*

U6 FWD primer was used to validate correct insertion of oligos into the pKLV2-U6gRNA5(BbsI)-PGKpuro2ABFP-W backbone. polymerase chain reaction (PCR) primers were used to check Hoxb8 cells for CRISPR KO efficiency and for sequencing of KO cells after singel cell dilution. This primers were generated using the benchling primer designer (https://www.benchling.com/). The borders for optimization were set to 150 bd up- and down-stream of the guide sequence. The optimal amplicon length was set to 500 bp.

Next-generation sequencing (NGS) primers were designed with an adapter sequence for binding to the NGS chip. For the FWD primer this sequence was "AATGATACGGCGACCACCGAGA" and for the REV it was "CAAGCAGAAGACGGCATACGAGAT". In the REV primer the adapter sequence was followed by a 8 bp barcoding sequence, allowing separate samples to be run on the same sequencing chip. Both FWD and REV primers included a region where the primer for NGS can bind (FWD: "TCTACACTCTTTCCCTACACGACGCTCTTCCGATCT", REV: "GTGACTGGAGTTCAGACGTGTGCTCTTCCGATCT"). In the FWD primer, this sequence was followed by 4 to 6 random bases to increase heterogeneity, which increases reliability for NGS. Finally, both primers carried one sequence, which is complementary to the region of interest on the pKLV2-U6gRNA5(BbsI)-PGKpuro2ABFP-W plasmid that carries the CRISPR guide (FWD: "TCTTGTGGAAAGGACGAAACACC", REV: "CCGACTCGGTGCCACTTTTTCAA"). All primers were ordered from eurofins.

Name	**Sequence**
U6 FWD	GAGGGCCTATTTCCCATGATTCC
NF1 KO1 PCR FWD	GCAGATGCTTACAGTGGCCC
NF1 KO1 PCR REV	TGAGCCACCCTTCCCACCCA
NF1 KO2 PCR FWD	TAGCTAACATGGCGTGGGGG
NF1 KO2 PCR REV	CCCTTGCCCTTAACAGTGGC
NF1 KO3 PCR FWD	ACTGGCTTCCTTTGTGCCCT
NF1 KO3 PCR REV	TCCAGGCATACCCACAGGCC
Lrch2 KO5 PCR FWD	GGTGGAGAGGTTAGGTGTGG
Lrch2 KO5 PCR REV	TGGATCCCCGAAACTGGTCT
Lrch2 KO6 PCR FWD	GCCTGGCCTGCAATCACCCT
Lrch2 KO6 PCR REV	AAGTCCCCCATACCCTCCCC
Lrch2 KO7 PCR FWD	GCAATTTGGCCATGTGCTCA
Lrch2 KO7 PCR REV	CCTGTGCCGGTGGTACTTGC

Pilra KO5 PCR FWD	TGCAGAGGGAGCCCAACCCA
Pilra KO5 PCR REV	CACCAAAGGCAGGGCTGGGA
Pilra KO6 PCR FWD	TGGAGAGGTCCTGCCCCAAC
Pilra KO6 PCR REV	GCACAGGCAGGGCTGAGACA
Pilra KO7 PCR FWD	TGCAGAGGGAGCCCAACCCA
Pilra KO7 PCR REV	CACCAAAGGCAGGGCTGGGA
Adgre1 KO5 PCR FWD	TGGGGAGAGCCAAGTGCAGC
Adgre1 KO5 PCR REV	TGATGTGCCATGGTGGGGTG
Adgre1 KO6 PCR FWD	TCCAACCCTGCCTCAACTGA
Adgre1 KO6 PCR REV	AAGGCACACAGCATCTCTCT
Adgre1 KO7 PCR FWD	TGCGTCCCGTCTCACTCCCT
Adgre1 KO7 PCR REV	ATGCTCCAGTGGATGCCCCA
NGS PCR FWD +4	AATGATACGGCGACCACCGAGATCTACA CTCTTTCCCTACACGACGCTCTTCCGAT CTATCAGGCTTTATATATCTTGTGGAAAGG ACGAAACACC
NGS PCR FWD +5	AATGATACGGCGACCACCGAGATCTACA CTCTTTCCCTACACGACGCTCTTCCGAT CTGATGCGGCTTTATATATCTTGTGGAAAG GACGAAACACC
NGS PCR FWD +6	AATGATACGGCGACCACCGAGATCTACA CTCTTTCCCTACACGACGCTCTTCCGAT CTTAAGTAGGCTTTATATATCTTGTGGAAA GGACGAAACACC
NGS PCR REV 1	CAAGCAGAAGACGGCATACGAGATTCG CCTGTGACTGGAGTTCAGACGTGTGCTC TTCCGATCTCCGACTCGGTGCCACTTTT TCAA
NGS PCR REV 2	CAAGCAGAAGACGGCATACGAGATATA GCGGTGACTGGAGTTCAGACGTGTGCTC TTCCGATCTCCGACTCGGTGCCACTTTT TCAA
NGS PCR REV 3	CAAGCAGAAGACGGCATACGAGATTCT AGGGTGACTGGAGTTCAGACGTGTGCTC TTCCGATCTCCGACTCGGTGCCACTTTT TCAA

NGS PCR REV 4	CAAGCAGAAGACGGCATACGAGATTTA CCAGTGACTGGAGTTCAGACGTGTGCTC TTCCGATCTCCGACTCGGTGCCACTTTT TCAA
NGS PCR REV 5	CAAGCAGAAGACGGCATACGAGATCTG ATGGTGACTGGAGTTCAGACGTGTGCTC TTCCGATCTCCGACTCGGTGCCACTTTT TCAA
NGS PCR REV 6	CAAGCAGAAGACGGCATACGAGATTTA CGCGTGACTGGAGTTCAGACGTGTGCTC TTCCGATCTCCGACTCGGTGCCACTTTT TCAA
NGS PCR REV 7	CAAGCAGAAGACGGCATACGAGATGAA TAGGTGACTGGAGTTCAGACGTGTGCTC TTCCGATCTCCGACTCGGTGCCACTTTT TCAA
NGS PCR REV 8	CAAGCAGAAGACGGCATACGAGATGTCT GAGTGACTGGAGTTCAGACGTGTGCTC TTCCGATCTCCGACTCGGTGCCACTTTT TCAA
NGS PCR REV 9	CAAGCAGAAGACGGCATACGAGATGCC TTGGTGACTGGAGTTCAGACGTGTGCTC TTCCGATCTCCGACTCGGTGCCACTTTT TCAA

Table 9: Primer

3.2 METHODS

3.2.1 *Isolation of murine bone marrow*

To isolate precursor cells from the bone marrow, C57Bl6/J mice aged 2 to 3 months were euthanized via cervical dislocation in accordance with German animal protective legislation. Femur and tibia were isolated from the hind legs of the mice and stored in phosphate-buffered saline (PBS). The bones were cut open on both sides and flushed with basis medium using a syringe to extract the bone marrow. The extracted bone marrow was centrifuged at 300 g for 5 min. Isolated bone marrow was either used directly for differentiation into macrophages (MCs)

or frozen in freezing medium at −80 °C and stored in liquid nitrogen for later use.

3.2.2 *Basic cell culture*

All cell lines were cultured in a cell culture incubator at 37 °C, 5% CO_2 with saturated humidity, and they were passaged every 2-3 days.

One system which we used extensively is the Hoxb8 cell system. In this system bone marrow (BM) cells are infected with a virus which leads to the expression of the Hoxb8 gene under the control of a estradiol promotor [199]. This leads to expression of Hoxb8 as long as estradiol is supplemented into the medium. Hoxb8 expression prevents presursor cells from differentiating further into different cell types [199]. This allows long term cultivation of the precursor cells as they are kept in a immature state. Removal of estradiol in combination with the addition of colony stimulating factors like M-CSF, GM-CSF and G-CSF allows differentiation of the cells into immune cells like MCs, dendritic cells (DCs) and neutrophils [199].

Hoxb8 cells were cultured in 75 cm^2 suspension cell culture flasks with Hoxb8 medium. 3T3 cells, HT1080 and LX293 were cultured in cell culture-treated 75 cm^2 flasks for adherent cells in Dulbecco's modified eagle medium (DMEM) medium. 4T1 cells were cultured in cell culture-treated 75 cm^2 flasks for adherent cells with basis medium.

3.2.3 *Macrophage differentiation*

To start the differentiation of Hoxb8 cells into MCs, cells were harvested by centrifugation at 300 g for 5 min, washed twice with 20 mL PBS, and taken up in 5 mL MC medium. 2×10^5 cells were seeded in each well of a 6-well plate in 5 mL MC medium. Cells were differentiated for a total of 5 days. On day 3, the entire volume of old medium was removed, and adherent cells were washed once with 1 mL PBS and 5 mL of fresh MC medium were added. On Day 5, cells were fully differentiated as determined by high expression of CX3CR1 and CD68, measured by fluorescence activated cell sorting (FACS), and then used in different assays.

For the differentiation of MCs from frozen bone marrow, 1×10^6 cells were seeded per well.

When differentiating MCs with an adhesion defect like kindlin-3 knock out (KO) and their respective wild-type (WT) controls, on day 3, only 4 mL of old medium were removed, and 5 mL of fresh medium were added without the PBS washing step. This was repeated on day 5 and the cells were used on day 7.

3.2.4 *Dendritic cell differentiation*

DCs differentiation is based on the protocol from Leithner et al [137]. To differentiate Hoxb8 cells into immature DCs, cells were harvested by centrifugation at 300 g for 5 min, washed twice with 20 mL PBS, and taken up in 5 mL 10% DC medium. Cells were counted, and 1×10^5 cells were seeded per 10 cm dish in untreated bacteria petri dishes with 10 mL DC medium. Cells were differentiated for 7 days to mostly acquire immature DCs. On day 3, 10 mL of fresh 20% DC medium were added on top, and on day 5, 10 mL of old medium were removed from the top, and 10 mL of fresh 20% DC medium added.

To obtain mature DCs, 10 mL fresh 20% DC medium were added on top on day 3, and on day 6, 10 mL of old medium were removed from the top, and 10 mL of fresh 20% DC medium were added. On day 8, cells were either harvested, frozen in freezing medium at $-80\,^{\circ}\mathrm{C}$, and stored in liquid nitrogen for later use, or they were directly used in experiments. To obtain fully mature DCs, cells were seeded in 10 mL 10% DC medium inside cell culture-treated 10 cm dishes and stimulated with $200\,\mathrm{ng\,mL^{-1}}$ lipopolysaccharide (LPS). On day 9, DCs were fully mature determined by expression of CD11c and MHC-II. Cells expressing CD11c but not MHC-II were classified as immature DCs.

3.2.5 *Generating competent E. coli*

To generate competent *E. coli* for transformation with plasmids, 1 mL lysogeny broth (LB)-medium was inoculated with *E coli* (NEB Stable Competent *E. coli*) and incubated over night at 37 °C while shaking with 200 rpm. On the next day, 99 mL of LB-medium were inoculated with the entire overnight culture and further cultivated for 4 h. The bacteria were then centrifuged at 4 °C with 4000 g for 10 min. The supernatant was removed, and the bacteria were resuspended in 20 mL $CaCl_2$ medium and incubated for 30 min on ice. Afterwards, the bacteria were again centrifuged at 4 °C with 4000 g for 10 min, resuspended in 2.5 mL $CaCl_2$ medium with 15% glycerol and stored at $-80\,^{\circ}\mathrm{C}$ in 50 µL aliquots.

3.2.6 *Cloning of sgRNAs into plasmid backbones*

The pKLV2-U6gRNA5(BbsI)-PGKpuro2ABFP-W plasmid was amplified in *E.coli* and isolated using a PureLink Expi Endotoxin-Free Maxi Plasmid Purification Kit according to manufacturer's instructions. For the digestion, 1.2 µg of the plasmid were mixed with 1 µL BbsI-HF restriction enzyme, 5 µL CutSmart buffer, and filled up to 50 µL with polymerase chain reaction (PCR)-grade water. The mixture was incubated for 3 h at 37 °C. To purify the digested deoxyribonucleic acid (DNA), a 1 % agarose gel was prepared by mixing 1 g agarose with 100 mL TAE buffer. This mixture was quickly cooked in the microwave. The entire volume of the restriction digestion was mixed with 10 µL of loading dye and loaded into the agarose gel chambers. To achieve separation of DNA-fragments with different

length, the gel was run for 1h at 120 V. After separation, the DNA band with a length of 8600 bp was cut out and purified using a gel extraction kit according to manufacturer's instructions.

Before the ligation process, oligonucleotides were phosphorylated using polynucleotide kinase protein. For this phosphorylation, 1 µL of the forward (FWD) strand and 1 µL of the reverse (REV) strand with a concentration of 100 µM were mixed with 5 µL ATP (10 mM), 5 µL of T_4 Polynucleotide Kinase buffer, 1 µL T_4 Polynucleotide Kinase (10 000 units/mL) and 37 µL PCR-grade water. The mixture was incubated for 1 h at 37 °C.

For the ligation, the previously prepared phosphorylated oligonucleotides were diluted 1:20 with water. 50 ng of the digested plasmid were mixed with 1 µL of diluted oligonucleotides, 10 µL ligase buffer and filled up to 20 µL with PCR-grade water. Afterwards, 1 µL of Quick ligase was added and the entire volume was mixed by pipetting up and down. The mixture was incubated for 5 min at room temperature (RT) and then directly transformed into competent *E. coli*.

To transform the *E. coli* with the recombinant plasmid, 50 µL of competent *E. coli* were thawed and mixed with 5 µL of the freshly ligated plasmid. The bacteria were thoroughly mixed with the plasmid and chilled for 30 min on ice. Then the bacteria were heat shocked at 42 °C for 30 sec, chilled on ice for 5 min, mixed with 950 µL fresh LB Medium and further cultivated for 1 h at 37 °C. The bacteria were centrifuged at 14 000 rpm for 5 min and resuspended in 50 µL medium. The entire volume was plated on bacterial agar plates with 100 µg mL^{-1} ampicillin and incubated over night at 37 °C.

To check for the correct insertion of the desired single guide RNAs (sgRNAs), single colonies were picked and grown over night in 3 mL of LB Medium with 100 µg mL^{-1} ampicillin. 2 mL of the culture were used to perform a plasmid mini prep according to the manufacturer's instructions. The rest of the culture was stored at 4 °C until the plasmid was sequenced. When the plasmid contained the desired sgRNA, the rest of the culture was mixed with 100 mL of fresh LB Medium with 100 µg mL^{-1} ampicillin and cultivated over night at 37 °C. The entire culture volume was used for plasmid isolation using PureLink Expi Endotoxin-Free Maxi Plasmid Purification Kit according to manufacturer's instructions.

3.2.7 *Virus production*

Three days before the start of the virus production, 10^7 LX293 cells were thawed and seeded in a 175 cm^2 adhesive cell culture flask with 50 mL of DMEM medium. Two days later, the cells were detached using trypsin/EDTA, and for every viral construct to be produced 6×10^6 cells were seeded in a 75 cm^2 adhesive cell culture flask with 20 mL of DMEM medium. The cells were cultured overnight, and the virus production was started on the next day. For the production of lentivirus, 217 µL of pure DMEM without supplements were mixed with 1.13 µg pMD2.G VSV-G envelope expressing plasmid, 2.27 µg psPAX2 2nd generation

lentiviral packaging plasmid, 4.53 µg of the target plasmid containing the desired sgRNA, and 65 µL polyethylenimine (PEI) transfection solution (1 mg mL^{-1}). The solution was carefully mixed by vortexing and incubated for 10 min at RT. Afterwards, 8.3 mL of DMEM medium without penicillin/streptomycin were added on top. The cells were washed once with PBS, and then the entire volume of the transfection mixture was added.

Two days after starting the virus production, the lentivirus was harvested by filtration through a sterile filter with 0.45 µm pore size. The virus was either used directly for infection or aliquoted and frozen at −80 °C.

3.2.8 *Generating knockouts via CRISPR/Cas9*

To generate cells with a specific KO using the CRISPR/Cas9 system, 10^5 Hoxb8 cells expressing Cas9 (Hoxb8 Cas9 Homo) were seeded in 5 mL of basis medium in a 6-well plate. 1.5 µL of Polybrene transfection reagent (10 mg mL^{-1}) and 100 µL of the lentivirus-containing solution were added. After three days of cultivation, 4 mL of the medium were replaced with 4 mL of fresh basis medium, and 2 µL of puromycin (10 mg mL^{-1}) were added. The cells were further cultivated for 10 days, splitting them according to their density ever second day. Thirteen days after the infection, a single-cell dilution was performed by diluting the cells to a density of 0.7 cells/100 µL. An entire 96-well plate was filled by adding 100 µL of the dilution per well. Cells were cultivated for at least one week, adding 50 µL fresh basis medium per well every second day. When cells reached near confluence, 24 wells were picked and transferred to 12-well plates and further cultivated, until reaching near confluence in a 6-well plate. 4 mL of the cells were frozen in freezing medium, and 1 mL of the cells was used to check the KO efficiency and location of the insertion or deletion using TIDE PCR.

To prepare samples for the TIDE PCR, cells were centrifuged at 300 g for 10 min. The entire medium was removed, and cells were dissolved in 40 µL dilution buffer of the Thermo Scientific Phire Tissue Direct PCR Kit and 1 µL DNA release reagent was added. The mixture was briefly vortexed and incubated for 5 min at RT. Afterwards, the sample was heated for 2 min at 98 °C. These samples were either used directly for further analysis in the TIDE PCR or stored at −20 °C.

For the TIDE PCR, 17.5 µL PCR grade water, 25 µL of 2x Phire Tissue direct PCR master mix, 5 µL of primer mixture containing the desired FWD and REV primer (5 µM of each) complementary to the target region of the gene of interest, and 2.5 µL of the sample to analyze were mixed. PCR was performed with initial denaturation at 98 °C for 5 min, followed by 40 cycles of denaturation at 98 °C (5 s), annealing (5 s) and extension at 72 °C (20 s), and final extension for 1 min at 72 °C. Annealing temperature was optimized for every primer set using thermo fishers T_m calculator. PCR products were purified using Neb PCR clean up Kit according to manufacturer's instructions. The products were sequenced by eurofins using

the FWD primer as sequencing primer. Sequencing of PCR product was analysed with the TIDE online tool (https://tide.nki.nl/).

3.2.9 *Genome wide CRISPR/Cas9 knockout screen*

For the CRISPR screen, a custom library consisting of 3 individual sub-libraries was used. Each sub-library contained of 3×10^4 guides targeting protein-coding genes and microRNAs, with four guides per target. All guides represent the four best matching sgRNAs according to the Broad Institute's CRISPick tool (https://portals.broadinstitute.org/gppx/crispick/public). Additionally, every sub-library included the same 800 non targeting control sgRNAs.

The library was supplied as glycerol stock Arek Kendirli from the Kerschenstiner lab [117]. For library amplification, 2 mL of the glycerol stock from each sub-library were added separately to 250 mL of LB medium containing 125 µL of ampicillin (100 mg mL^{-1}) and 25 µL of carbenicillin (500 mg mL^{-1}), and grown for 16 h at 30 °C. The plasmid was isolated using a PureLink Expi Endotoxin-Free Maxi Plasmid Purification Kit according to manufacturer's instructions.

For lentivirus production, 2×10^7 LX293 cells were thawed five days before starting the virus production. Two days later, the cells were passaged in four 300 cm^2 cell culture flasks for adherent cells, each containing 75 mL of DMEM medium. After two additional days, the cells were detached, counted, and seeded into eight 300 cm^2 flasks with $2,4 \times 10^7$ cells per flask. On the following day, a mixture containing 868 µL of DMEM without fetal calf serum (FCS), 4.5 µg of pMD2.G, 9.1 µg of psPAX2, 260 µL of PEI solution, and 6 µg of each sub library (reaching a combined amount of 18 µg target plasmid) was prepared. The solution was mixed well by quickly vortexing and incubated for 10 min at RT. Afterwards 33.3 mL of DMEM medium without penicillin/streptomycin were slowly added to the mixture. The same mixture was prepared for every of the eight flasks. The old medium was removed from the cells, they were once washed with PBS and the plasmid mixture was added. After two days, the supernatant was harvested and purified by sterile filtration through a filter cup with a pore size of 0.45 µm. The lentivirus was stored at −80 °C until usage.

To determine the multiplicity of infection (MOI) of the lentiviral library, two 6-well plates were seeded with 1×10^5 Hoxb8 Cas9 Homo cells per well in 5 mL of MC medium. 1.5 µL of Polybrene (10 mg mL^{-1}) and varying amounts of lentivirus (0 µL, 25 µL, 50 µL, 100 µL, 200 µL or 400 µL) were added. After three days, the medium was replaced with fresh MC medium, and in one plate, 2 µL of puromycin (10 mg mL^{-1}) were added to each well. After an additional two days, the cells were washed once with PBS. To detach the cells, 1 mL of ethylenediaminetetraacetic acid (EDTA) solution (10 mM) was added to every well. After 5 min of incubation at 37 °C, 1 mL FACS buffer was added, and cells were carefully detached, centrifuged at 300 G for 5 min, and resuspended in 500 µL FACS buffer. The number of cells was counted, and the MOI was calculated by following formula:

$$MOI = \frac{cell\ number\ with\ puromycin}{cell\ number\ without\ puromycin} \quad (1)$$

For every of the three biological replicates, fresh Hoxb8 cells expressing Cas9 (Hoxb8 Cas9 Homo) were thawed and expanded until reaching four 300 cm^2 flasks. The cells were washes twice with PBS. Twelve flasks were seeded with $18,75 \times 10^6$ cells per flask in 150 mL of MC medium without puromycin. 54 µL polybrene and 30 mL lentivirus were added to each flask to reach an MOI of 0,3. Cells were cultivated for 13 days, with medium changes on day three, five, seven, nine and eleven. After 13 d, the medium was removed, the cells were washed once with PBS, and 80 mL basis medium were added to the cells. They were pre-incubated for 1 h at 37 °C in a cell culture incubator. Afterwards, 48 mL of fluorescein isothiocyanate (FITC)-dextran in PBS with 2 mg mL^{-1} were mixed with 48 mL fresh basis medium. The old medium was removed from the cells, and 8 mL FITC-dextran mixture were added per flask. After 15 min of incubation at 37 °C, cells were washed twice with PBS, and fixed by adding 8 mL of 3,7% formaldehyde solution. Cells were incubated for 1 h at RT, washed twice with PBS, and detached with trypsin/EDTA solution for 10 min at 37 °C. The trypsin reaction was stopped by adding 4 mL FACS buffer. Cells were centrifuged and resuspended in FACS buffer for FACS sorting.

Sorting was performed by the Core Facility Flow Cytometry at the Biomedical Center Munich (BMC) using a BD FACSAriaFusion. All cells were sorted by their FITC fluorescence into one of three categories: 5% of cells with the lowest fluorescence, 90% with medium fluorescence, and 5% with highest fluorescence. Final cell numbers after sorting ranged from 10×10^6 to 14×10^6 cells. After sorting, the cells were centrifuged at 400 g for 10 min, and each population was resuspended in PBS to achieve a final concentration lower 5×10^6 cells per 200 µL portion. To each 200 µL fraction, 20 µL of Proteinkinase A and 200 µL of Lysis buffer were added and incubated over night at 56 °C. On the next day, 200 µL of ethanol (EtOH) were added, and the mixture was briefly vortexed. The entire volume was added to a DNeasy mini spin column, centrifuged once for 1 min at 8000 rpm, washed once with 500 µL washing buffer 1, and once with 500 µL washing buffer 2. To remove any remaining liquid, the column was centrifuged for 3 min at 14 000 rpm. Then, 200 µL of the elution buffer preheated to 70 °C were added on top, incubated for 1 min, and centrifuged at 8000 rpm for 1 min to elute the DNA from the column. Elution was repeated for a second time with 100 µL elution buffer. DNA concentration was measured using a nano drop.

For amplification, PCR reactions were prepared as following: 25 µL of 2x NEB high fidelity PCR master mix, 1.5 µL of primer mixture and 23.5 µL of released DNA from the step before were mixed. The primer mix contained 2.5 nmol mL^{-1} of each of the four FWD primers and 10 nmol mL^{-1} of the REV primer. For each of the three cell fractions (5% of cells with the lowest fluorescence, 90% with medium fluorescence, and 5% with highest fluorescence), a different REV primer was used, containing a specific barcode region. PCR was performed with initial

denaturation at 98 °C for 2 min, followed by 24 amplification cycles with 10 sec at 98 °C, 15 sec at 66 °C for annealing, 15 sec at 72 °C for elongation, and a final elongation step for 5 min at 72 °C

The PCR product was purified using Ampure purification beads. Therefore, each 50 µL PCR reaction was mixed with 43 µL of beads. All reactions of the same sample were pooled, vortexed, and incubated for 5 min for DNA binding. The magnetic beads were separated from the fluid using a strong magnetic field for 5 min. The supernatant was removed, and beads were washed twice with 400 µL 80% EtOH. After the second washing step, the supernatant was removed, and the beads were dried for 7 min at RT. DNA was then released with 20 µL PCR grade water for 5 min. The beads were separated again with the magnetic field and 19 µL of the supernatant were collected for further processing, leaving 1 µL of supernatant behind to avoid accidental collection of beads. Elution was repeated with another 19 µL of water. DNA concentration was roughly quantified using the nano drop. For more accurate quantification, the concentration was additionally measured using a DNA1000 Bioanalyzer chip following manufacturer's instructions.

The experiment was performed as three independent biological replicates on different days. For each replicate, different barcoded REV primers were used to allow simultaneous next-generation sequencing (NGS). NGS was carried out at the Gene Center Munich by the Blum Lab using an Illumina NextSeq 1000, with 10^7 reads per sample and a read length of 50 bp.

Screening data were processed using Cutadapt to remove 5′ adapter sequences, Trimmomatic to crop the reads to 20 bp, representing the respective sgRNA of the read, and MaGECK to extract read counts for each sgRNA. To compare sgRNA representation in the top 5% and bottom 5% with the representation in the medium 90%, various bioinformatic tools, including CRISPRCloud2, MaGECK and PinAPL-Py, were employed, and the results were compared. For final selection of the candidates, a combination of this three tools were utilized, resulting in the selection of 11 candidates for further validation. To select these candidates, we checked already existing functional annotation of the highest-ranking genes in the databases of UniProt, NCBI, and GeneCard for relations to cell membrane dynamics, actin dynamics, and vesicle transfer.

To validate the findings of the screen, a single-KO for each candidate was generated using the highest-ranking sgRNA selected from the four sgRNAs in the library. These sgRNAs were cloned into the pKLV2 backbone and produced as lentivirus as described before. For the initial follow up screening, 10^5 cells were seeded in 5 mL of MC medium with 1.5 µL of Polybrene (10 mg mL^{-1}) and 100 µL of the lentivirus. Cells were cultivated for 13 days, with medium changes on the days 3, 5, 7, 9, and 11. On day 13 macropinocytosis assay was performed as described before, measuring the uptake of 70 kDa FITC-dextran. For three candidates that showed an effective change in their macropinocytosis uptake compared to cells expressing a non-targeting scrambled (SCR) control sgRNA, three additional guides per candidate were created to exclude possible

off-target effects. For these guides, CRISPR/Cas9 KOs with single cell dilution were generated as described before.

3.2.10 *Macropinocytosis assays on two dimensional surfaces*

To analyse the fluid uptake by cells in an unconfined two-dimensional (2D) environement, day 5 MCs were preincubated with basis medium for 1 h. After preincubation, the cells were detached using 10 mM EDTA solution, centrifuged at 300 g for 5 min and added to a 6-well plate with 1000 µL of basis medium. After 1 h of cell attachment, 600 µL of medium were removed and 4 µL of FITC-dextran were added. The cells were incubated for 15 min at 37 °C in the cell culture incubator. After incubation, 3 mL of ice-cold EDTA solution were added to stop the uptake of 70 kDa dextran and detach the cells. Cells were detached using a cell scraper, washed once with ice-cold PBS and fixed with 3,7% formaldehyde solution for 1 h at 37 °C. After fixation, cells were washed twice with PBS and stained with antibodies in FACS buffer, washed again with PBS and analysed on a CytoFLEX S B75408 FACS. Cells were gated for intact cells using FSC-A and SSC-A and for fully mature cells (Cd11b-, CX3CR1+, CD68+ for MCs and CD11c+, MHC-II+ for fully mature DCs) using antibody signals. For each sample 10^4 gated cells were analysed.

3.2.11 *Generating 3D microenvironments with poly(acrylic acid)*

To produce 1,5% carbomer hydrogels, 800 mg poly(acrylic acid) (PAA) with a medium chain length of 4×10^6 MW were dissolved in 52.9 mL of basis medium for MC, DC and 4T1, or in DMEM medium for HT1080 and 3T3. The mixture was stirred for 1 h. Afterwards, the pH was adjusted to 7.2 with 10 M NaOH and briefly centrifuged at 300 g. The hydrogel was used no earlier than 24 h after preparation and was stored for up to one month at 4 °C. Dilutions to achieve lower carbomer concentrations can be found in Table 10. When carbomer concentrations <0.4% are used, no hydrogel is formed and the solution remains liquid.

Carbomer concentration	**Volume** 1,5% **carbomer** [µL]	**Volume medium** [µL]
1.1%	1100	400
0.9%	900	600
0.75%	750	750
0.6%	600	900
0.4%	400	1100

Table 10: Dilution for different carbomer concentrations

3.2.12 *Macropinocytosis assays inside poly(acrylic acid) hydrogels*

The carbomer hydrogel was diluted to 0.6% by mixing 600 µL of carbomer stock (1,5%) with 900 µL of basis medium. For experiments with inhibitors, the inhibitor was pre-diluted in the basis medium before mixing with the carbomer at a 1.7-fold concentration. Final concentrations of inhibitors used can be found in Table 1. The mixture was incubated for at least 1 h in the incubator. MC differentiation medium was removed from MCs, and the cells were washed once with PBS. Then, 5 mL of fresh basis medium were added to the cells, and they were pre-incubated for 1 h. Next, the cells were detached with 1 mL of EDTA solution from the plate, centrifuged, and resuspended in 40 µL of basis medium. The carbomer hydrogel was aliquoted in 400 µL portions. 4 µL of the cell solution were added to 400 µL of the 0.6% carbomer in 1.5 mL reaction tubes for the carbomer assays or 1000 µL basis medium in one well of 6-well plate for two dimensional assays. They were incubated for 1 h in the incubator. Afterwards, 600 µL of medium were removed from the two dimensional assay, leaving 400 µL back. Then, 4 µL of FITC-dextran (100 mg mL^{-1}) were added, and the cells were incubated for another 15 min. The uptake of labeled dextran was stopped, and cells were detached by adding 3 mL ice-cold EDTA solution. Cells were centrifuged at 300 g for 5 min, washed once with PBS, and then fixed with 3.7% formaldehyde at 37 °C for 1 h. Afterwards, the cells were washed again twice with PBS.

The same protocol was used for DCs, 4T1 breast cancer cells, and 3T3 fibroblasts with respective cell culture medium previously described in "Basic cell culture". For DCs and 4T1 5×10^5 cells were seeded per experimental condition and for 3T3 2×10^5

To analyze the cells by FACS, MCs were stained with antibodies against CX3CR1 (Alexa Fluor 647), Cd11b (Pacific blue) and CD68 (PE) to control for differentiation. DCs were stained with antibodies for CD11c (APC) and MHC-II (eFluor 450). Other cell types were not further stained. Cells were taken up in 100 µL of FACS buffer and measured on a CytoFLEX S B75408 using the FITC channel for FITC-dextran, PE for CD68, ECD for TexasRed-dextran APC for CX3CR1 or CD11c, and PB450 for Cd11b or MHC-II. Cells were gated for intact cells using FSC-A and SSC-A and fully mature cells (Cd11b-, CX3CR1+, CD68+

for MCs and CD11c+, MHC-II+ for fully mature DCs) using antibody signals. For every sample, 10^4 gated cells were analysed.

3.2.13 *Macropinocytosis assay on micropatterned surface*

To investigate the effect of cell adhesion, micropatterned surfaces were used. Micropatterns were coated one day in advance with 100 µL of 1 mg mL^{-1} FITC conjugated bovine serum albumin (BSA) and washed once with PBS on the experiment day. MCs were pre-incubated for 1 h with basis medium and then detached with EDTA. The cells were resuspended in medium with reduced FCS content (1% FCS) and seeded on micropatterns. The micropatterned surfaces carried four regions with either round adhesion spots with a 1.5 µm diameter and distances of 5 µm, 7 µm, 9.7 µm or 13.4 µm, or circles with diameters of 5 µm, 12.2 µm, 16.6 µm or 20 µm. After 1 h to allow the cells to adhere, they were incubated with 1 mg mL^{-1} TexasRed-dextran for 15 min, washed once with PBS, and fixed with formaldehyde. Images were acquired at a Leica DMi8 Inverted fluorescence microscope equipped with a 100x Objective, a DFT51010 filter cube, and a TXR filter cube. FITC was excited at 490 nm, and TexasRed-dextran at 580 nm.

For live imaging of MCs, the micropatterns were one day in advance coated with 1 mg mL^{-1} TexasRed-dextran and washed once with PBS on the experiment day. MCs expressing a green fluorescent protein (GFP) tag in the cell membrane were pre-incubated for 1 h with basis medium, detached with EDTA, seeded on the patterns, and incubated for 1 h before the start of image acquisition. Images were acquired using a Leica DMi8 Inverted fluorescence microscope equipped with a 100x objective, temperature and CO2 control. GFP was excited at 490 nm and TexasRed-dextran at 580 nm.

3.2.14 *Macropinocytosis assay using collagen hydrogels*

Collagen hydrogels are based on the ones decried by Sixt and Lämmermann [221]. To investigate the fluid uptake via macropinocytosis on top of collagen I hydrogels, a mixture of 30 µL of 10x minimum essential medium (MEM), and 15 µL of $NaHCO_3$ was prepared. 225 µL of Nutragen were added (6 mg mL^{-1} bovine collagen in HCl). Then, 200 µL of this mixture were added to 100 µL of basis medium. For each experimental condition, one well of a 12-well plate was coated with 100 µL collagen and afterwards incubated for 1 h at 37 °C in the incubator. Day 5 MCs were detached and seeded on top of the collagen gel in 400 µL basis medium. The cells were incubated for another 1 h in the incubator. Afterwards, 4 µL of 100 mg mL^{-1} FITC-dextran were added, and the cells were incubated for 15 min. Uptake was stopped by adding 3 mL of ice cold EDTA and 1 mL Trypsin-EDTA. Cells were fixed with formaldehyde, stained with antibodies, and analysed by FACS as described before.

To measure the rate of macropinocytosis by cells located inside collagen hydrogels, the incubation time had to be increased to 3 h to allow diffusion of dextran into the collagen matrix. In addition, the FITC-dextran concentration was decreased to 50 µg mL^{-1}. Collagen was prepared as described before, and for every condition, one well of a 12-well plate was pre-coated with 50 µL collagen and incubated for 1 h at 37 °C. Cells were detached and resuspended in 50 µL basis medium per condition. Collagen was prepared with cells inside basis medium and allowed to polymerize for 30 min at 37 °C in the incubator. After polymerization, 1 mL of basis medium containing inhibitors or dimethyl sulfoxide (DMSO) was added on top, and cells were incubated for another 1 h. Then, the old medium was removed and replaced with fresh medium containing the inhibitors or DMSO and 50 µg mL^{-1} FITC-dextran. The cells were incubated for 3 h with dextran. Afterwards, uptake was stopped as described before, cells were fixed, stained and analysed by FACS.

3.2.15 *Combined macropinocytosis and phagocytosis quantification*

To analyse the relationship between macropinocytosis and phagocytosis, a combined assay was performed using fluorescently labelled *E. coli* and fluorescently labelled 70 kDa dextran as a fluid phase marker. Day 5 macrophages were washed once with PBS and then for 1 h pre-incubated with basis medium. Carbomer and collagen hydrogels were prepared as described before. The cells were detached using EDTA solution centrifuged once for 5 min at 300 G and resuspended in 40 µL basis medium. 4 µL of cell solution were added to the carbomer, or in medium on top of collagen I. After 1 h of cell adhesion 4 µL of FITC labeled dextran (100 mg mL^{-1}) and 4 µL of TexasRed labeled *E. coli* (100 mg mL^{-1}) were added. Uptake was stopped after 15 min by addition of ice cold EDTA solution. The cells were fixed, stained with antibodies, and analysed at the FACS. Uptake of FITC labeled dextran was quantified using FITC channel, while phagocytosis of *E. coli* was quantified using the ECD channel.

When working with kindlin-3 KOs, MCs were used on day 7.

3.2.16 *Membrane tension measurements using FLIM*

To analyse the relationship between membrane tension and macropinocytosis, membrane tension was measured using FLIPPER-TR membrane dye in macropinocytotic active MCs. Micropatterns were pre-coated with BSA without fluorescence tag, as described before. Day 5 MCs were detached using EDTA solution. The cells were splitted at a 1:4 ratio, seeded on the micropatterns in 1 mL medium with reduced FCS content, and mixed with 1 µL FLIPPER-TR membrane dye (1 mM). The cells were incubated for 1h with the dye. Images were acquired using an inverted Leica SP8X WLL confocal microscope. The FLIPPER-TR membrane dye was excited with a white laser at 488 nm with a 20 Hz pulse frequency, and all photons emitted in the wavelength range from 500 nm to 800 nm were

collected with a Hyd detector and analysed for fluorescence lifetime. For analysis, a region of interest (roi) was drawn, including only the cell membrane area, to exclude lifetime disturbance in the cell interior. At least 20 cells were analysed per experiment for each condition.

For the experiments with pharmacological inhibitors, MC were detached on day 4 using EDTA, splitted 1:4 and seeded in 3.5 cm microscope dishes with 3 mL MC medium. One day after seeding, cells were incubated for 1 h with DMSO, ethylisopropyl amiloride (EIPA) or jsaplakinolide in basis medium with 1:1000 FLIPPER-TR membrane dye. After incubation, lifetime was acquired as described before.

3.2.17 *Statistics*

Most experiments were performed with at least three independent biological replicates. The number of biological replicates is indicated in every figure legend as n=. If not explicitly stated otherwise, experiments were performed in a paired manner, meaning that either 1.) the same cell lines, Hoxb8-derived DCs or Hoxb8-derived MCs were processed in parallel at the same time and treated in the same way, with only a single parameter (drug treatment, environment, staining) being changed or 2.) different Hoxb8 cell lines were differentiated in parallel into MCs and processed in parallel. Experiments were repeated on different days to generate different biological replicates. As the experiments were designed and performed in a paired manner, the use of paired tests is scientifically necessary.

Points in graphs represent the median value of a single biological replicate, and the error bars represent the standard error across all biological replicates. For the micropattern assays, 10 images were taken at random locations on the pattern, and all single cells in these pictures were analyzed. In case of the membrane tension measurement using fluorescence lifetime imaging (FLIM), 20-25 cells were randomly imaged for every experimental condition.

4

RESULTS

4.1 IDENTIFYING NEW GENES RELATED TO MACROPINOCYTOSIS USING A GENOME WIDE CRISPR-CAS9 SCREEN

In the first part of the project, we aimed to identify new genes related to macropinocytosis. To identify these genes, we performed a genome-wide CRISPR/Cas9 knock out (KO) screen. To be able to perform a genome-wide screen, we first established a high-throughput compatible macropinocytosis screen that allowed us to separate cells with higher and lower macropinocytosis ability. We also selected a cell model that was suitable for the screen.

4.1.1 *Generating a high throughput compatible assay to quantify macropinocytosis*

Most studies analysing macropinocytosis use imaging-based methods to quantify macropinocytosis by measuring the uptake of fluorescently labelled dextran with a size larger than 70 kDa (for example [37, 77, 121, 130]), which is selectively engulfed by macropinocytosis. While small molecules can easily be taken up by other endocytotic processes in addition to macropinocytosis, dextran molecules larger than 70 kDa are too large for other endocytotic pathways and are therefore selectively taken up by macropinocytosis [141]. The most commonly used image-based systems have the disadvantage that they are not compatible with high throughput at a scale required for a genome-wide screen. In addition, it is difficult to isolate cells based on image-based analysis.

We decided to use fluorescence activated cell sorting (FACS) as our preferred screening system. FACS allows high-throughput analysis of fluorescence signals of cells, while at the same time cells can be sorted according to their fluorescence signal. Similar to the other studies using imaging-based quantification, we used 70 kDa fluorescein isothiocyanate (FITC)-dextran as a marker for macropinocytosis.

Macropinocytosis is a highly dynamic and rapid process in which macropinosomes can be formed and mature within minutes. Therefore, fast sample handling and samples fixation to freeze the process are important. In addition, incubation times should be short to ensure that no macropinosomes are recycled back to the cell surface and the fluorescent marker is not damaged by the acidic lysosomal environment. Taking all of this into account we established a protocol in which cells were adhered to a cell culture treated 6-well and were incubated with 70 kDa FITC-dextran for 15 min. The cells were then fixed with formaldehyde, detached, stained with antibodies and analysed at the FACS.

The first step in the preparation of our screen was to decide which cell system would be the most suitable model. Ideally, this model should perform high levels of macropinocytosis in order to produce strong phenotypes when macropinocytosis is impaired. Two physiologically relevant cell types are known to perform high levels of macropinocytosis in a constitutive manner: macrophages (MCs) and dendritic cells (DCs) [116]. These cell types naturally use constitutive macropinocytosis to sample their environment for pathogens. In addition, these two cell types are of interest because they play an important role at the interface between innate and adaptive immunity and can be easily generated either from bone marrow (BM) or using the Hoxb8 cell system. We also tested the maropinocytosis rate of 3T3 fibroblasts asa model for mesenchymal cells. Further, we tested the macropinocytosis rate of 4T1 breast cancer cells and HT1080 fibrosarcoma cells as they represent two common cancer types.

When we analysed these cell lines with our FACS based assay using 70 kDa-dextran as a fluid marker, we observed the highest macropinocytotic capacity in MCs derived from Hoxb8 cells (see Figure 3a.). The BM-derived MCs show slightly lower rates of macropinocytosis, but are comparable. All other cell lines show lower rates of macropinocytosis. Immature and mature DCs show the lowest macropinocytosis rates, with immature DCs showing slightly higher rates then mature DCs. The 3T3 fibroblast cell line and the HT1080 fibrosarcoma cells show similar macropinocytosis rates in the mid-range of our measurements, while the 4T1 breast cancer cell line is comparable to the immature DCs. One problem we encountered with the immature DCs was that they tended to spontaneously differentiate into mature DCs. This behavior makes it difficult to define the right time point to use these cells.

As MCs showed the highest macropinocytosis ratio, we decided to continue with these cells for our screening and validation assays. The next step was to prove that the observed fluorescence signal was indeed the result of macropinocytotic uptake of extracellular fluid. To test this, we used pharmacological inhibition of various endocytotic processes and membrane dynamics (see Figure 3b.). Ethylisopropyl amiloride (EIPA) is the best known inhibitor of macropinocytosis. It inhibits the sodium proton exchanger (NHE), which leads to an increase of the intracellular pH, which in turn blocks the activity of Rac and CDC42 [125]. Jasplakinolide also affects macropinocytosis. As macropinocytosis is highly dependent on directed actin polymerisation, jasplakinolide blocks the process by forcing undirected actin polymerisation, stabilising existing actin filaments and thus preventing actin depolymerisation [34]. Chlorpromazine inhibits clathrin-mediated endocytosis by inhibiting dynamin activity, which is required for the budding of clathrin pits [54]. Nystatin is an inhibitor of caveolin-mediated endocytosis, which removes the caveolin coating from the forming pits [207].

The inhibition of macropinocytosis with EIPA shows the strongest effect together with general inhibition of active cell processes at 4 °C, almost completely abolishing the uptake of fluorescently labelled dextran as a marker for macropinocytosis. Jasplakinolide, which also affects macropinocytosis by inhibit-

ing actin depolymerisation, also showed a reduction, but this reduction was not statistically significant. On the other hand, treatment with nystatin shows no effect on the uptake of the fluid phase marker, demonstrating that caveolin-mediated endocytosis does not play a role in the uptake of 70 kDa-dextran. Interestingly, chlorpromazine, an inhibitor typically associated with clathrin-mediated endocytosis, also shows a significant reduction of fluid phase uptake, comparable to the extend of reduction with Jasplakinolide. Although chlorpromazine is normally associated with clathrin-mediated endocytosis, it is possible that it may also affect macropinocytosis through its effect on dynamin. Although macropinocytosis is usually described as dynamin-independent [85], there are also examples demonstrating a dependence of macropinocytosis on dynamin, particularly for viral uptake [170, 177]. These data suggest that the process we observed is indeed macropinocytosis, although we cannot completely exclude a minor influence of clathrin-mediated endocytosis.

To further validate the capability of our screening system, we used a known genetic alteration that affects macropinocytosis. Neurofibromin 1 (NF1) is a known negative regulator of macropinocytosis [23] and a tumor suppressor gene [25]. Therefore, genetic loss of NF1 leads to increased macropinocytosis. We infected Cas9 expressing Hoxb8 cells either with lentivirus for the expression of one single guide RNA (sgRNA) targeting NF1 to generate NF1 KOs or non targeting scrambled (SCR) controls. After differentiation of the cells into MCs for 13 d, we performed the macropinocytosis assay with FITC-dextran as marker for macropinocytosis. Consistent with the effects reported in the literature, we observed a significant increase in macropinocytosis in the NF1 KO MCs. This demonstrates the ability of our screening system to resolve the effect of genetic alterations on macropinocytosis. In addition it demonstrates our ability to infect Hoxb8 cells efficiently with lentiviral constructs for the delivery of CRISPR sgRNA and to generate KOs.

As a final step, we aimed to show that our system is capable of enriching and depleting altered cells in a pool of cells where most of the cells are unaltered. To do this, we again generated MC with either NF1 KO by viral infection or without any alterations of NF1. After performing the dextran uptake assay, we stained NF1 KO cells with a red membrane marker and mixed them in different ratios with the unaltered and membrane marker negative wild-type (WT) cells. By measuring the percentage of cells that were positive for the membrane marker in the entire population, in 5% of the cells with the lowest fluorescence signal and in the population with the highest 5% of fluorescence, we checked the enrichment or depletion of NF1 KO MCs in the respective populations.

When we used equivalent mixtures containing 50% WT cells and 50% NF1 KO cells, NF1 KO cells were enriched to 71.92% in the highest 5% and depleted to 38.48% in the lowest 5%. We observed a similar distribution when we decreased the total percentage of NF1 KO cells to 10% with enrichment to 20.61% in the highest 5% and depletion to 7.42% in the lowest 5%. When we decreased the percentage of NF1 KO cells further to 1%, we observed an enrichment of NF1

KO cells in the highest 5%, while there was little change in the lowest 5%. This demonstrates that our screen is able to enrich and deplete KO cells with changes in their macropinocytosis rate.

Thus, we have developed a high-throughput compatible screening system that is capable of separating MCs by their macropinocytotic capacity and thus enriching KO cells with alterations in extracellular fluid uptake by macropinocytosis.

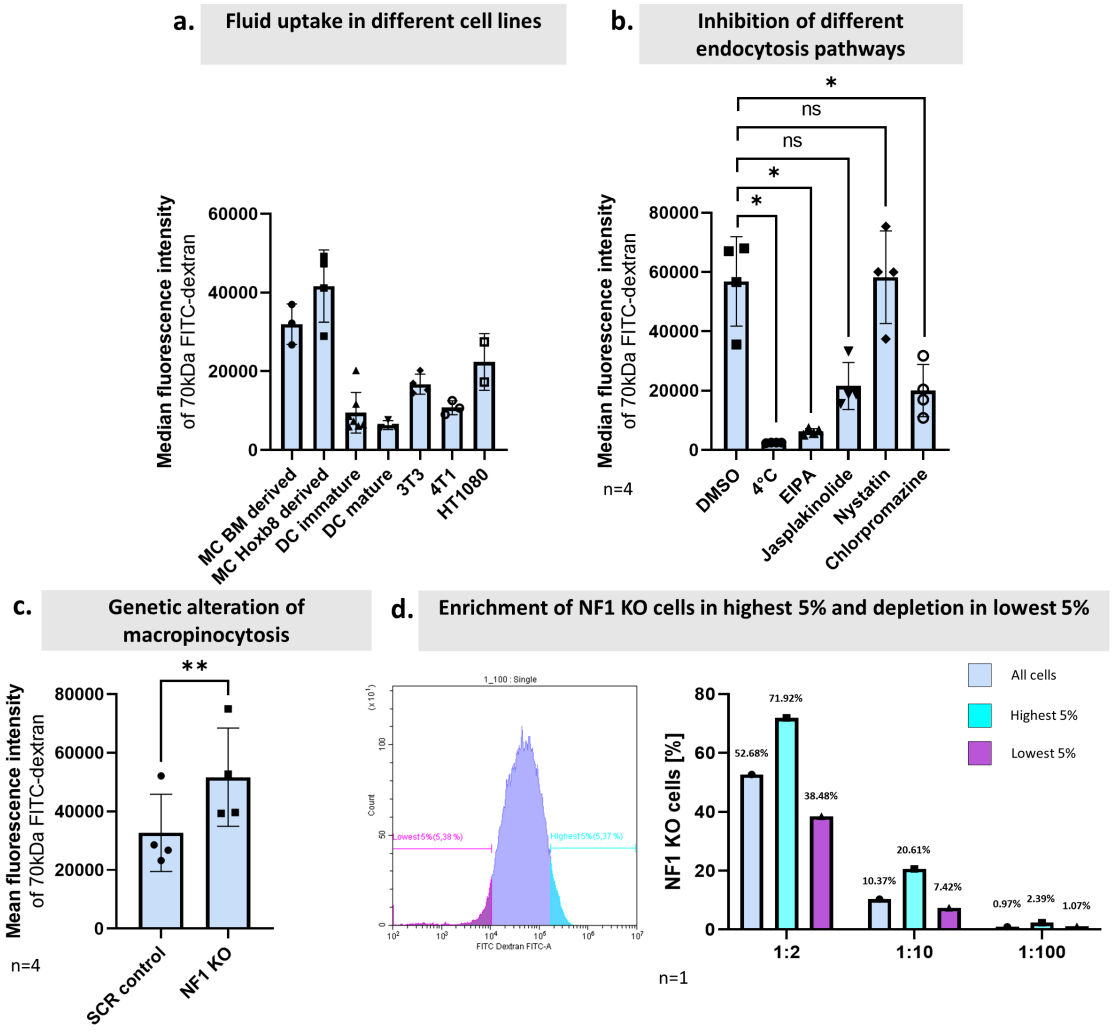

Figure 3

Figure 3: Development and validation of a high-throughput compatible macropinocytosis screen: a. Measurement of fluid uptake in immune cells (bone marrow (BM)-derived macrophages (MCs), Hoxb8 derived MCs, immature and mature dendritic cells (DCs)) and other cell types (3T3 fibroblast cell line, 4T1 human breast cancer cell line and HT1080 human fibrosarcoma cell line) by macropinocytosis using 70 kDa fluorescein isothiocyanate (FITC)-dextran as a marker, **b.** Pharmacological inhibition of different endocytotic pathways in Hoxb8-derived MCs using 55 µM ethylisopropyl amiloride (EIPA) for macropinocytosis, 10 µM chlorpromazine for clathrin-mediated endocytosis, 8 µM jasplakinolide to prevent actin-dependent membrane ruffling, 10 µM Nystatin for caveolin-mediated endocytosis or energy-dependent endocytosis incubating cells at 4 °C, **c.** Using knock out (KO) of known macropinocytosis negative regulator neurofibromin 1 (NF1) in Hoxb8-derived MCs to validate fluorescence activated cell sorting (FACS) assay and virus infection protocol, **d.** Checking enrichment of NF1 KO mixed with wild-type (WT) MCs in different ratios from 1:2 to 1:100. The blue bars represent the percentage of NF1 KO cells in the whole population, cyan in 5% of the cells with the highest FITC signal and purple in the lowest 5%. Error bars represent the standard deviation between all replicates. The number of biological replicates is indicated by n=. Significances were calculated using a paired t-test for **c.** and a paired repeated measures ANOVA for **b.** and are presented as: ns $p > 0.05$, * $p \leq 0.05$, ** $p \leq 0.01$.

4.1.2 *Perfoming a genome wide CRISPR/Cas9 KO screen to identify genes related to macropinocytosis*

We continued with the genome-wide CRISPR/Cas9 KO screen using a genome-wide library, which has been generated and provided by Arek Kendirli from the Kerschenstiner lab [117]. The library consists of three sub-libraries. Each sub-library contains 3×10^4 single guide RNAs (sgRNAs). Of these 3×10^4 sgRNAs, 800 are non-targeting scrambled (SCR) controls. The remaining 8.76×10^4 sgRNAs target protein-coding genes or microRNAs with 4 sgRNAs per target. To generate viruses that contain this genome-wide library, 3T3 cells were transfected with the library and packaging plasmids for virus production. The supernatant from this virus production was used to infect Cas9 expressing Hoxb8 cells with a multiplicity of infection (MOI) of 0.3 and differentiation into MCs was initiated by removing estradiol and adding M-CSF containing cell culture supernatant. Three days after infection, selection with puromycin was started to remove uninfected cells. To screen for macropinocytosis, we performed the dextran uptake assay 13 days after the infection by incubating cells for 15 min with FITC-dextran and fixing the cells with formaldehyde. Subsequently, the cells were sorted by Dr Lisa Richter and Pardis Khosravani of the Core Facility Flow Cytometry at the Biomedical Center Munich (BMC). All cells were sorted into three populations: 5% with the lowest fluorescence, 90% with medium fluorescence and 5% with the highest fluorescence. We isolated the deoxyribonucleic acid (DNA) and amplified the sgRNA sequences with polymerase chain reaction (PCR) using next-generation sequencing (NGS) adapters. These samples were sequenced by Dr Stefan Krebs from the Blum lab. The schematic of the screen is shown in Figure 4a.

We performed the screen three times on different days as independent biological replicates. The sequencing worked with high reliability (see Figure 4b.) as

almost all reads could be aligned to unique sgRNAs. Unfortunately, the screening results show a high variability between the different biological replicates (see Figure 4c.). Ideally, one would expect a high correlation between different replicates from the same group (low with low, medium with medium, high with high). For the medium fluorescence population we see a relatively good correlation index ranging from 0.59 to 0.69. At the same time, the correlation index for the low samples ranges from 0.37 to 0.47 and for the high samples from 0.36 to 0.52. The correlation indices between the different samples are in a similar range.

To test whether we nevertheless can detect genes that alter macropinocytosis, we analysed the NGS data from our experiments using three different established bioinformatics software tools. These tools were MaGeCK [143], PinAPL-PY [225] and CRISPRCloud2 [105]. With MaGeCK, we found 3098 genes significantly altered in cells with the lowest macropinocytosis activity and 2974 genes altered in the cell with the highest macropinocytosis activity. CRISPRCloud2 found 3018 in the lowest and 3302 in the highest and PinAPL-PY found 184 in the lowest and 124 in the highest. This shows that PinAPL-PY is much stricter in judging the significance of changes than the other two tools.

When we compared the significantly altered genes according to the different software tools, we found little overlap. Only two genes were significantly altered in the cells with the highest macropinocytosis activity according to all three tools. These genes were Adgre1 and Cypt3. Adgre1 is known to express the cell surface marker F4/80, which is a typical marker for monocytes and monocyte-derived cells. This makes Adgre1 an interesting candidate as a regulator of macropinocytosis. Cypt3 encodes the cysteine-rich perinuclear theca 3 protein. The function of this protein is not yet known. Since the perinuclear theca is part of the cytoskeleton of the nucleus in spermatozoa, an association with macropinocytosis in MCs seems unlikely [122].

On the other hand, six genes are significantly altered according to all three tools in the cells with the lowest macropinocytosis activity. These genes are Il1f8, Suv420h1, Olfr1211, Olfr1046, Myh3 and Klhl18. In addition, the group of non-target controls was also significantly altered in the lowest population according to all tools. As there are so many olfactory receptors, the two Olfr are most likely false positive results, as a relationship between olfactory receptors and macropinocytosis in MCs seems unlikely. Il1f8 is an extracellular interleukin important in T cells [264]. Suv420h1 encodes the histone methyltransferase gene KMT5B, which is associated with neurodevelopmental disorders [46]. Klhl18 encodes a ubiquitin ligase that is reported to be expressed specifically in the retina, but not in other tissues, where it plays a role in light-dark adaptation [45]. At the same time, others report a correlation between lower Klhl18 and worse outcome in lung cancer [107]. So it is rather unlikely that most of these candidates are related to macropinocytosis.

Only Myh3 appears to be a more likely hit. So far only myosin IIb has been associated with macropinocytosis [106], but a general relationship between myosin

and macropinocytosis seems likely due to its impact on the organisation of the actomyosin cortex [220].

Another aspect is that most significant hits found with PinAPL-PY are also significant when analysing the data with MaGeCK, with an overlap of 152 genes in the population of cells with low macropinocytosis and 101 in the population with high macropinocytosis. On the other hand, there is hardly any overlap between PinAPL-PY and CRISPRCloud2.

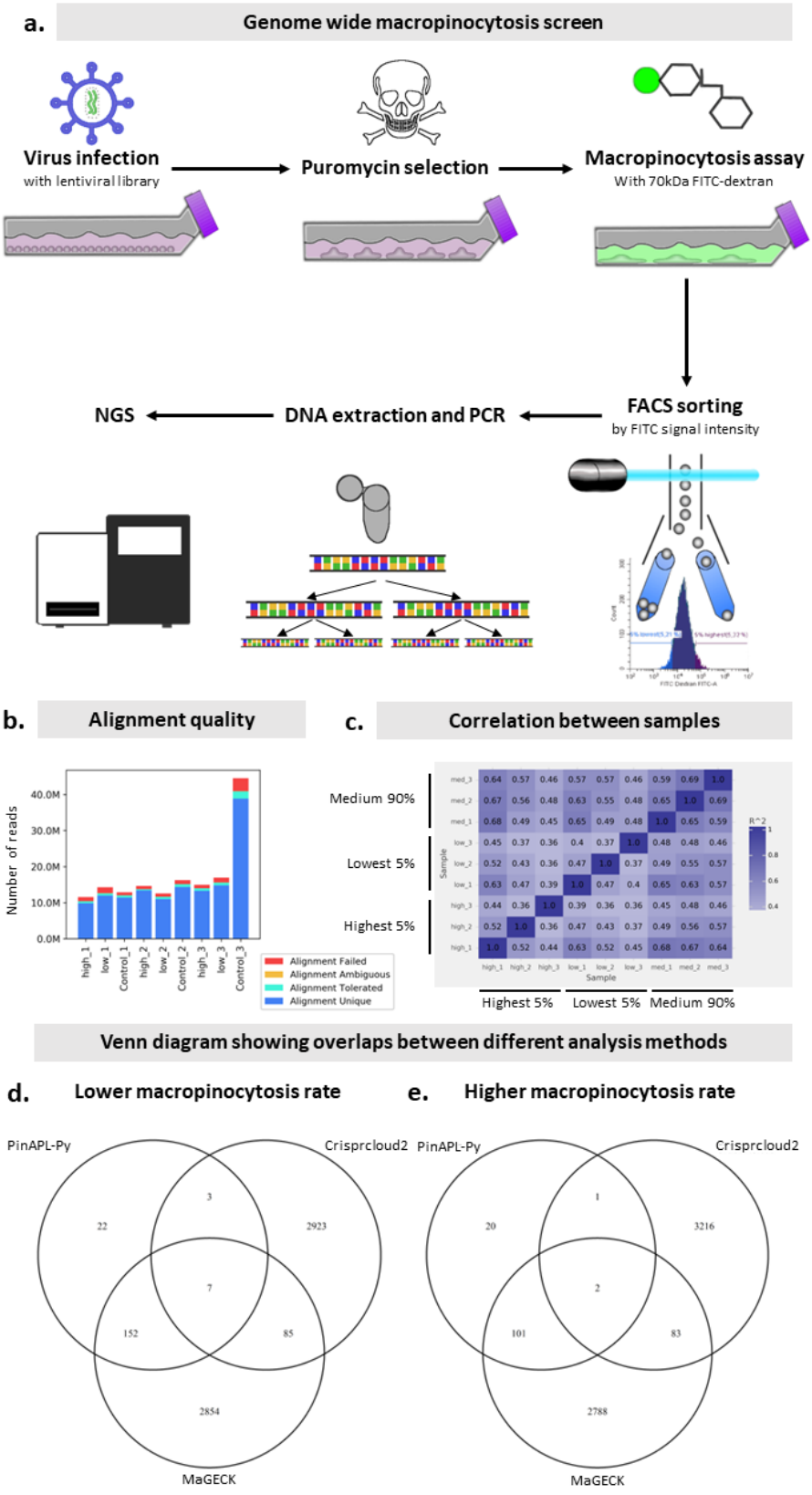
a.
Genome wide macropinocytosis screen
Virus infection
with lentiviral library
Puromycin selection
Macropinocytosis assay
With 70kDa FITC-dextran
FACS sorting
by FITC signal intensity
DNA extraction and PCR
NGS
b.
Alignment quality
Number of reads
40.0M
30.0M
20.0M
10.0M
0.0M
high_1
low_1
Control_1
high_2
low_2
Control_2
high_3
low_3
Control_3
Alignment Failed
Alignment Ambiguous
Alignment Tolerated
Alignment Unique
c.
Correlation between samples
Medium 90%
Lowest 5%
Highest 5%
Sample
R^2
Highest 5%
Lowest 5%
Medium 90%
Venn diagram showing overlaps between different analysis methods
d.
Lower macropinocytosis rate
PinAPL-Py
Crisprcloud2
MaGECK
22
3
2923
7
152
85
2854
e.
Higher macropinocytosis rate
PinAPL-Py
Crisprcloud2
MaGECK
20
1
3216
2
101
83
2788

Figure 4

Figure 4: Performing a genome-wide CRISPR/Cas9 KO screen to identify genes related to macropinocytosis: a. Flowchart of the genome-wide macropinocytosis screen. Hoxb8 cells were differentiated into macrophages (MCs) and infected with the lentiviral library during differentiation. Cells were selected with puromycin to remove uninfected cells. To quantify macropinocytosis, cells were incubated with 70 kDa fluorescein isothiocyanate (FITC)-dextran. Cells were sorted by FITC signal into the lowest 5%, medium 90% and highest 5% using fluorescence activated cell sorting (FACS). Deoxyribonucleic acid (DNA) was isolated, amplified and sequenced using next-generation sequencing (NGS). **b.** Number of reads that could be aligned to the guides in the library and the quality of the alignment, determined using PinAPL-Py. **c.** Correlation between the different samples, determined using PinAPL-Py. **d.+e.** Diagram showing the differences and overlaps between the different software tools used to analyse the NGS data generated with R. **d.** The results of comparing the lowest 5% with the medium 90%. **e.** The results of comparing the highest 5% with the medium 90%.

To give a better visual representation of how the results of the different software tools look, we created vulcano plots representing the results of the different tools. Figure 5 shows these volcano plots for the analysis that is based on the bioinformatic tools MaGeCK, PinAPL-PY and CRISPRCloud2. On the x-axis, these plots show the fold change in the abundance of single guide RNAs (sgRNAs) in the sample compared to our control population of 90% with medium fluorescence, while on the y-axis they show the probability that these changes are statistically significant. Therefore, more relevant hits can be found in the upper right corner. In these plots, the four sgRNAs for Lrch2, Adgre1 and Pilra are highlighted, as we later focused on these three candidates. In addition, the non-targeting guides are highlighted in orange as they represent guides that should have no effect. Therefore, the software tools are supposed to use these guides as a baseline, representing no change in enrichment as well as no significance. All tools show a good ability to set the non-target sgRNAs as a baseline. Only CRISPRCloud2 shows some non-targeting sgRNAs with increased fold change.

For Lrch2, MaGeCK shows one guide as one of the top candidates with high fold change and high probability. At the same time, all other guides are either unchanged or even depleted. Using PinAPL-PY, two Lrch2 guides are significantly enriched, but neither of them is one of the top hits. CRISPRCloud2 shows no significant changes in any Lrch2 guides.

Looking at the other two candidates, Adgre1 and Pilra, we see one significantly enriched guide for Adgre1 with MaGeCK, but not for Pilra. With PinAPL-PY there is one significantly enriched guide for each of them and with CRISPRCloud2 there is also only one significantly enriched guide for each of them. These differences between the results indicate that all software tools use different criteria to evaluate the significance and fold change of the guides.

Taken together, this demonstrates that there are significant differences between the different software tools. In addition, there is a high variability in the screening data between biological replicates and sgRNAs for the same gene.

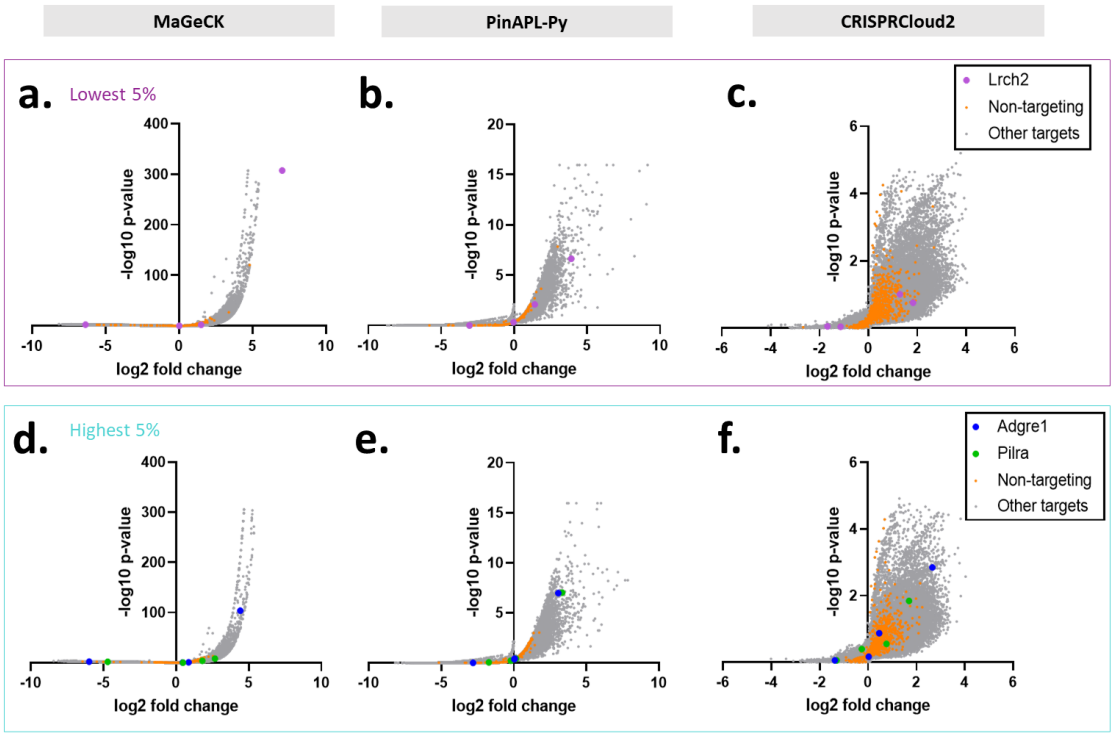

Figure 5: Vulcano plots of macropinocytosis screening results with different softwares: Vulcano plots for the results comparing the highest 5% with the medium 90% **a.+b.+c.** and the lowest 5% with the medium 90% **d.+e.+f.** with MaGeck (**a.+d.**), PinAPL-PY (**b.+e.**) and CRISPRCloud2 (**c.+f.**). The four single guide RNAs (sgRNAs) for the three most promising candidates, Lrch2, Adgre1 and Pilra, are highlighted in the respective plots.

As the bioinformatic analysis alone was not sufficient to select interesting candidates, we further filtered the results by generating a combined p-value from all three tools. In this list, we annotated the highest ranking candidates with the existing gene databases from UniProt, GeneCards and NCBI searching for annotations related to actin, cytoskeleton, membrane dynamics, vesicle dynamics and cancer. These annotations led to the manual selection of the following candidates:

Gene	**Full name:**	**Enriched in:**	**Annotations:**
Adgre1	Adhesion G protein-coupled receptor E1	highest 5%	Cell adhesion and cell-cell interaction in immune system [5]
Tmem230	Transmembrane protein 230	highest 5%	synaptic vesicle trafficing and recycling [61]
Arhgap11a	Rho GTPase activating protein 11A	highest 5%	Increases migration when expressed in cancer [112]

Pilra	Paired immunoglobulin-like type 2 receptor alpha	highest 5%	inhibitory cell surface receptor in dendritic cells (DCs) and other myeloid cells [72]
Atp6v1e1	ATPase, H+ transporting, lysosomal V1 subunit E1	lowest 5%	part of V-atpase [1]
Mark3	MAP/microtubule affinity regulating kinase 3	lowest 5%	signaling function downstream of mutated Ras [4]
Sphk2	Sphingosine Kinase 2	highest 5%	cell migration in breast cancer [219]
Nprl3	Nitrogen permease regulator-like 3	highest 5%	part of mTORC1 pathway and response to amino acid starvation [180]
Dnah3	Dynein Axonemal Heavy Chain 3	lowest 5%	force generation at minus end of microtubules [6]
Lrch2	Leucine Rich Repeats And Calponin Homology Domain Containing 2	lowest 5%	consists of LRR domain for protein-protein interaction and calponin homology domain for interaction with actin [202]
Mospd2	Motile Sperm Domain Containing 2	lowest 5%	monocyte migration [169]

Table 11: Candidates selected from the genome wide CRISPR Cas9 screen

4.1.3 *Identifying Lrch2, Pilra and Adgre1 as possible regulators of macropinocytosis*

To validate the selected candidates, we generated single knock outs (KOs) for each of the candidate genes. To do this, we again infected Cas9 expressing Hoxb8 cells with lentiviruses carrying the respective sgRNAs. To decide which sgRNA to use in this validation screen, we compared the results for all sgRNAs from our candidates for all three software tools and used the one that ranked highest across all software tools. Again, we started differentiation on the day of lentiviral infection, started puromycin selection three days after infection and performed the macropinocytosis assay using the fluorescence activated cell sorting (FACS) and 70 kDa fluorescein isothiocyanate (FITC)-dextran as a marker

for macropinocytosis 13 d post infection. As a control, cells were infected with non-targeting scrambled (SCR) sgRNAs.

We compared the dextran uptake of these KOs with the SCR controls in two independent sets of experiments. In the first set, we compared the potential positive regulators Mark3 and Atp6v1e1 and the potential negative regulators Tmem230, Pilra, Adgre1 and Arhgap11a with a SCR control (see Figure 6a.). The positive regulator candidates Mark3 and Atp6v1e1 showed little change in their uptake of the fluorescent dextran. It is therefore unlikely that these candidates are really involved in macropinocytosis. At the same time, it is also possible that KO with the selected sgRNAs was not efficient, so the cells showed no phenotype because there were no genetic alterations.

On the other hand, all positive regulator candidates in this experimental set showed an increase in their macropinocytotic uptake. However, only the effect for Pilra is statistically significant. At the same time, Adgre1 and Arhgap11a also show increased uptake in all three replicates, although this effect is not statistically significant. We therefore decided to further investigate Pilra and Adgre1. Pilra is known as an inhibitory cell surface receptor that modulates immune cell function [72] while Adgre1 is important for cell adhesion and cell-cell interaction [5].

In a second set of experiments, we compared the positive regulator candidates Lrch2, Mospd2, Dnah3 and the negative regulator candidates Sphk2 and Nprl3 (see Figure 6b.). This time we used three different SCR sgRNAs to ensure that no unspecific off-target effects of the SCR sgRNA alter macropinocytosis. All three SCR controls show a comparable rate of macropinocytosis, demonstrating that there are no unspecific off-target effects of the used SCR sgRNA controls on macropinocytosis. At the same time, all KOs tested also show the same rate of macropinocytosis. But while all the other KOs fluctuate in a similar range to the SCR controls, Lrch2 stands out. In one replicate it has a much higher rate of macropinocytosis than the SCR control, while in the other two replicates the rate of macropinocytosis is lower. We therefore decided to further investigate Lrch2 as a potential positive regulator of macropinocytosis. Lrch2 belongs to a family of proteins whose function has not yet been identified [202]. They are classified by their calponin homology domain, which is known for its ability to interact with actin, and by their leucine-rich repeats, which are important for protein-protein interactions [202].

The three most promising candidates, Lrch2, Pilra and Adgre1, were selected for further experimental investigation. For each of these candidates, three new sgRNAs were generated that were not part of the library to rule out off-target effects of the sgRNA. We infected Hoxb8 cells with lentiviruses carrying the sgRNA to generate stable cell lines with the desired KO. Since non-homologous end joining (NHEJ) leads to random insertions and deletions [224], each cell can carry different mutations. To generate a cell line that carries only one homozygous mutation that results in functional loss of the gene, we performed a single cell dilution.

We analysed the clones that we generated with the single cell dilution using a TIDE assay. For the TIDE assay, a polymerase chain reaction (PCR) is performed to amplify the genetic region where the KO occurs [30]. The sequence is then sequenced using standard Sanger sequencing. A software tool compares the peaks, which represent the sequence of bases and the probability of each nucleotide being at that specific position, with the sequence of wild-type (WT) cells that carry no mutations [30]. If the CRISPR-induced NHEJ generates insertions or deletions, there will be shifts in the base patterns that the software tool can detect. Based on this comparison, the software tool shows how many bases are lost or inserted [30]. The tool has also been specifically designed to analyse pools of cells with different insertions and deletions, as is the case before single cell dilution, showing the frequency of certain deletions or insertions [30].

The following table shows the results of our TIDE assay for some of the KO lines we have generated:

Clone:	**KO efficiency:**	**Which alterations:**
Pilra KO 5.7	89.5%	Mixture (39.2% -15, 45.1% -12)
Pilra KO 5.11	88.1%	Mixture (48.4% -32, 32.1% +2)
Pilra KO 5.19	92.10%	Homozygous(87.3% -1)
Pilra KO 5.20	87.40%	Heterozygous (48.4% -46, 30.3% -6
Lrch2 KO 5.1	5.8%	WT
Lrch2 KO 5.4	71.5	Mixture (40.2% -10, 22% -6)
Lrch2 KO 5.5	90.4%	Homozygous (+1)
Lrch2 KO 5.9	66.1%	Mixture (48.9% -8, 7.2% +2)
Lrch2 KO 5.10	90.4%	Heterozygous (39% +1, 42.7% +3)
Lrch2 KO 5.11	75.6%	Heterozygous (35.9% +1, 33.8% +4)
Lrch2 KO 5.3.2	35%	Mixture (6, 1% -6, 7.9% -1, 4.2% +1, 5% +2)
Lrch2 KO 5.13.2	4.3%	WT
Lrch2 KO 5.21.2	84.3%	Heterozygous (34.7% -10, 40.3% -4)
Lrch2 KO 7.4	4.9%	WT
Lrch2 KO 7.5	33.6%	Mixture (WT, 33% +1)
Lrch2 KO 7.8	53.7%	Heterozygous (WT, 52.5% -8)
Lrch2 KO 7.10	51.6%	Heterozygous (WT, 49.7% +1)
Lrch2 KO 7.15	50.7%	Heterozygous (WT, 43.8% +2, 5.5% +3)

Table 12: Knockout efficiency in candidates tested for macropinocytosis. Mix means that the cell line contains a mixture of different KOs, WT that the genome is unaltered, heterozygous that there are similar percentages of two KOs, indicating that both alleles of the gene are altered in different ways, and homozygous that both alleles carry the same mutation. - in the brackets indicates that bases have been deleted and + inserted. Percentages indicate the frequency of the mutation.

When we performed the single cell dilution for Pilra, many clones died and of those that survived, only one was heterozygous. For Lrch2 KO the efficiency of sgRNA 7 (Lrch2 KO 7) was low and only heterozygous KOs were produced.

We differentiated the single cell clones into macrophage (MC) and performed our macropinocytosis assay with 70 kDa FITC-dextran as a marker of macropinocytosis. Ascontrol we employed cell lines carrying SCR sgRNAs, which went through the same single cell dilution as the KO cells. For the Pilra KO, we only tested cell lines generated with one sgRNA and performed only one biological replicate (see Figure 6c.). Of the clones tested, the two clones Pilra KO 5.7 and Pilra KO 5.11 carry a mixture of different genetic alterations, while Pilra KO 5.19 is homozygous and Pilra KO 5.20 is heterozygous. While Pilra KO 5.11 shows no effect on macropinocytosis rate, all other clones increase macropinocytosis in this single test. Further testing is required to validate the effect of Pilra in general and sgRNA 5 specifically.

For Lrch2, we tested more clones. While most of these clones were either a mixture of different mutations (Lrch2 KO 5.4, 5.9, 7.5) or heterozygous (Lrch2 KO 5.10, 5.11, 5.21.2, 7.8, 7.10, 7.15), we also had one homozygous clone with Lrch2 KO 5.5. As a control, we also analysed several clones that were infected with a lentivirus and survived puromycin selection but did not develop any mutations (Lrch2 KO 5.1, 5.13.2, 7.4). When we analysed the different clones with sgRNA 5 using our FACS-based macropinocytosis assay, we observed decreased macropinocytosis in most clones (see Figure 6d.). Only the clone Lrch2 KO 5.9 showed no change in its macropinocytosis ability. For the Lrch2 KO 5.4 and 5.5 clones, the decrease was statistically significant, while all other changes were not significant. As clones that are WT according to our TIDE assay also showed an effect, it is not clear whether the KO caused the reduction or whether this is the result of off-target effects. At the same time, the clones were still in culture for some time after the TIDE assay and could have developed genetic changes as they still carried the sgRNA and the Cas9 protein and therefore could still cut the CRISPR target and perform NHEJ.

When we analysed Lrch2 sgRNA 7, no significant changes were observed in any of the clones (see Figure 6e.). Lrch2 KO 7.4 showed a reduction in both replicates, but as this is a WT clone it seems unlikely that this effect is the result of the KO. The mixed clone Lrch2 KO 7.15 showed a reduction in macropinocytosis in two replicates, whereas in the third replicate macropinocytosis was strongly increased (similar to the observation in Figure 6b.). Lrch2 KO 7.5 also showed an increase in one replicate, but no change in the other. All other clones showed no change in dextran uptake. Whether Lrch2 plays a role in macropinocytosis in MCs is therefore still unclear.

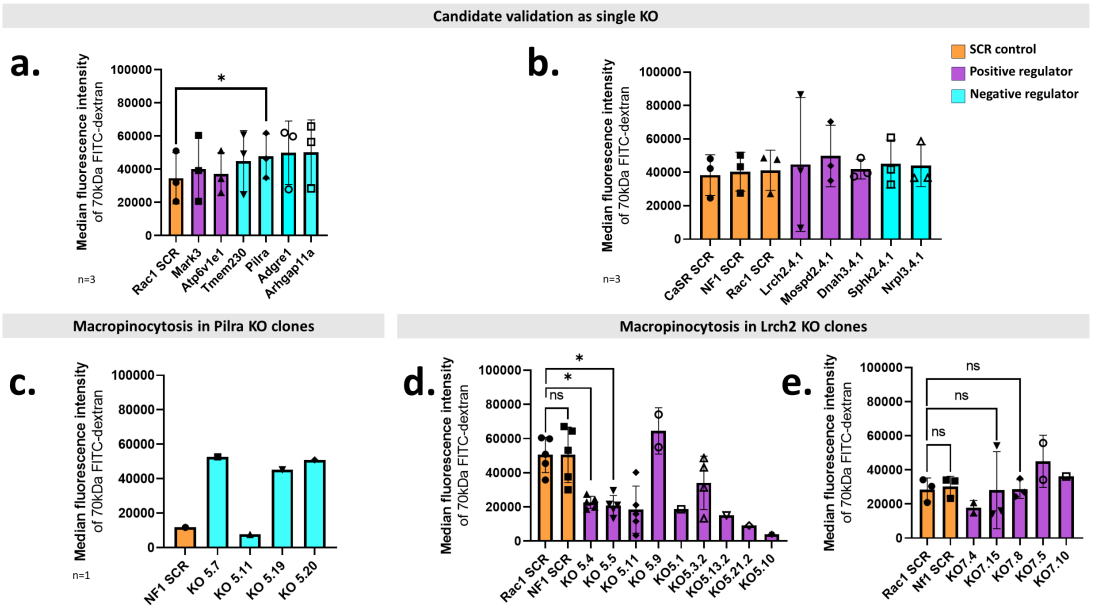

Figure 6: Candidate validation for CRISPR screen results: a.+b. The most promising candidates were tested as a single knock out (KO) within the Hoxb8-derived macrophages (MCs) with the highest ranking single guide RNA (sgRNA). Scrambled (SCR) control samples are shown in orange, positive regulator candidates enriched in the lowest 5% are shown in purple and negative regulator candidates enriched in the highest 5% are shown in cyan. **c.** Testing Pilra KO with one sgRNA inside MCs for several different Hoxb8 cell lines generated by single cell dilution. **d.+e.** Testing MCs derived from multiple clones with Lrch2 KO after single cell dilution using two different sgRNAs. **d.** CRISPR sgRNA 5. **f.** CRISPR sgRNA 7. Error bars represent the standard deviation between all replicates. The number of biological replicates is indicated by n=. Dots represent the median for each replicate. Significances were calculated using a paired repeated measures ANOVA and are presented as follows: ns $p > 0.05$, * $p \leq 0.05$.

We did not continue with the characterisation of further candidates as we focused on the micro environmental impact on macropinocytosis in the second part of our project. In summary, we have developed a high-throughput screening system for macropinocytosis. Using this approach, we performed a genome-wide CRISPR KO screen and identified several interesting candidates, including the potential negative regulators of macropinocytosis Tmem230, Arhgap11a, Pilra and Adgre1, as well as Lrch2, which may either play a direct role in macropinocytosis or be a positive regulator.

4.2 ANALYSING HOW THE MICROENVIRONMENT REGULATES MACROPINOCYTOSIS

When cells are in their physiological environment, they receive a variety of different cues from their surroundings. These cues include interactions of cells with other cells, either through direct cell-cell contact or through the exchange of signalling molecules. While the cellular stimulation of macropinocytosis has been extensively studied, the influence of physical properties of the cell environment, such as stiffness, porosity, density and mechanical cues from the environment, has received less attention. Therefore, we aimed to develop new tools to generate *in vitro* environments that more closely resemble the situation cells encounter *in vivo*, while at the same time allowing us the flexibility to modify specific parameters that influence the physical properties of the environment.

4.2.1 *Increased rates of macropinocytosis by macrophages inside 3D environments*

In a previous Master thesis project supervised by me, Rifat Ara Reza discovered that cells confined under agarose gels produce more but smaller macropinosomes (data not shown). This finding sparked our interest to understand how the physical properties of the environment affect macropinocytosis.

To answer this question, we used different assay systems to modulate the properties of the cellular microenvironment in a defined manner. We started with synthetic carbomer hydrogels based on poly(acrylic acid) (PAA). These hydrogels consist of long PAA chains that form complex networks. Their density can be easily modified by changing the PAA content of the hydrogel. In addition, it is very easy to add substances such as inhibitors, fluorescent markers or cells to the hydrogel. Further it is possible to harvest the cells from the hydrogelgel, as itl does not polymerise. PAA as a synthetic polymer is also non-adhesive. [52, 160]

Comparing the cell morphology of MCs inside the carbomer hydrogel with the morphology of cells adhering to a 2D surface, we observed some remarkable differences (see Figure 7a.). Cells adhering to 2D surfaces spread out over a large area but are flat. In comparison, MCs inside the carbomer hydrogel have a much more rounded shape. Another difference can be seen in the formation of lamellipodia and filopodia. Lamellipodia are large, flat and expanded membrane areas at the edges of the cell, which are usually in direct contact with the substrate and dynamically protrude and retract [10]. Filopodia, on the other hand, are small finger-like protrusions that extend from the cell membrane in all directions and are not in contact with the substrate [10]. Both structures are associated with high actin dynamics [10].

While cells in our 2D assays form few filopodia but extensive lamellipodia, 3D cells lack lamellipodia completely but constantly probe their environment with multiple filopodia. Live imaging of cells in different environments also revealed some differences. Although even adherent MCs show high membrane dynamics, the dynamics of cells in 3D environments are even higher. They constantly extend

and retract their finger-like protrusions. In addition, cells in 3D constantly form membrane ruffles, which is a hallmark of macropinocytosis.

When comparing the macropinosome vesicle structure in cells located on 2D surfaces or in 3D carbomer hydrogels by microscopy, only minor differences are visible. One of the problems in analysing macropinosomes under the microscope is the high heterogeneity between vesicle numbers in MCs within the same sample. Some cells form a lot of macropinosomes, while other neighbouring cells take up very little. Therefore, we decided to quantify macropinocytosis mainly by fluorescence activated cell sorting (FACS), as this allows easy analysis of higher cell numbers.

To compare the macropinocytosis rate of cells adhering to 2D surfaces with the rate in 3D environments, we again used the FACS-based macropinocytosis assay we established for the previous part of the project. This time we detached the cells before the experiment with ethylenediaminetetraacetic acid (EDTA) and seeded them either in cell culture treated plastic 6-wells as a 2D surface or in a 0.6% PAA carbomer hydrogel as a 3D environment. After 1 h of attachment we added fluorescein isothiocyanate (FITC)-dextran as a marker for macropinocytosis and incubated the cells for 15 min. We then stopped the dextran uptake and detached the cells by adding ice-cold EDTA. We fixed the cells and analysed them by FACS.

When we compared macropinocytosis rates between cells on 2D plastic surfaces and inside 3D carbomer hydrogels, we observed a significant increase in dextran uptake when we seeded cells inside the carbomer hydrogel (see Figure 7b.). To prove that this increase was indeed due to increased rates of macropinocytosis, we used the pharmacological macropinocytosis inhibitor ethylisopropyl amiloride (EIPA), the inhibitor of clathrin-mediated endocytosis chlorpromazine, and the actin polymerisation inhibitor jasplakinolide (see Figure 7c.+d.). To further investigate the combined effects of inhibition of macropinocytosis and clathrin-mediated endocytosis, we also combined both inhibitors. In 2D environments both EIPA and chlorpromazine reduced fluid uptake to comparable levels. In the 3D carbomer hydrogels, EIPA showed a stronger inhibitory effect than chlorpromazine. When both inhibitors were combined, fluid uptake was only reduced to the same level as with EIPA. This further indicates that chlorpormazine also has an inhibitory effect on macropinocytosis, as already discussed in chapter 4.1.1 through its effect on dynamin [85, 170, 177]. When we treated the cells with the actin inhibitor jasplakinolide, fluid uptake was reduced in both 2D and 3D carbomer hydrogels. In contrast to the EIPA treatment, which reduced uptake in both 2D and 3D, but not to the same extent, treatment with jasplakinolide reduced uptake to similarly levels in both environments. This proves that the increased uptake in carbomer is actin dependent.

To test whether the effect of increased macropinocytosis in the carbomer hydrogel alsooccurs in other 3D environments, we measured the levels of macropinocytosis in collagen I hydrogels. This posed two challenges. First, fluorescent dextran can only be dispersed in collagen hydrogels by diffusion, potentially creating concentration gradients within the gel. The dextran could not be added when

preparing the carbomer hydrogel either, as the cells would not experience the same force throughout the entire time as the carbomer becomes denser during polymerisation. To mitigate this problem, we extended the incubation time with dextran to 3 h instead of the usual 15 min. Another challenge we faced was harvesting the cells from the hydrogel, as macropinosomes are highly dynamic and therefore require rapid sample handling. Since fixation within the hydrogel leads to unspecific extracellular binding of the fluorescent dye, we harvested the cells by mechanically disrupting the hydrogel, which results in high cell loss. The number of cells analysed in collagen is therefore much lower than in carbomer.

We detached the cells with EDTA and seeded them in 2D cell culture treated plastic 6 -wells or in collagen I hydrogels with 3.3 g L^{-1} collagen I. After 30 min of polymerisation, we added medium on top and gave the cells another 1 h to stretch in the hydrogel. Then we added FITC dextran and incubated the cells for 3 h. We stopped the uptake with ice-cold EDTA, detached 2D cells, broke up the collagen hydrogel with a pipette tip and fixed the cells.

When we compared dextran uptake between cells adhering to 2D surfaces and inside the collagen I hydrogels, we again observed a significant increase in the hydrogels (see Figure 7e.). We treated our cells with EIPA totest whether this change in uptake was the result of increased macropinocytosis and at 4 °C to stop the energy dependent uptake (see Figure 7f.). EIPA reduced fluid uptake in both environments, although the reduction was greater in collagen I hydrogels than on 2D surfaces. Inhibition of energy dependent uptake at 4 °C also reduced fluid uptake. This proves that the increase in macropinocytosis we observed is not specific to carbomer, but a more general effect in 3D environments.

In summery, we discovered that extracellular fluid uptake by macropinocytosis in MCs is increased when cells are embedded in more physiological 3D matrices.

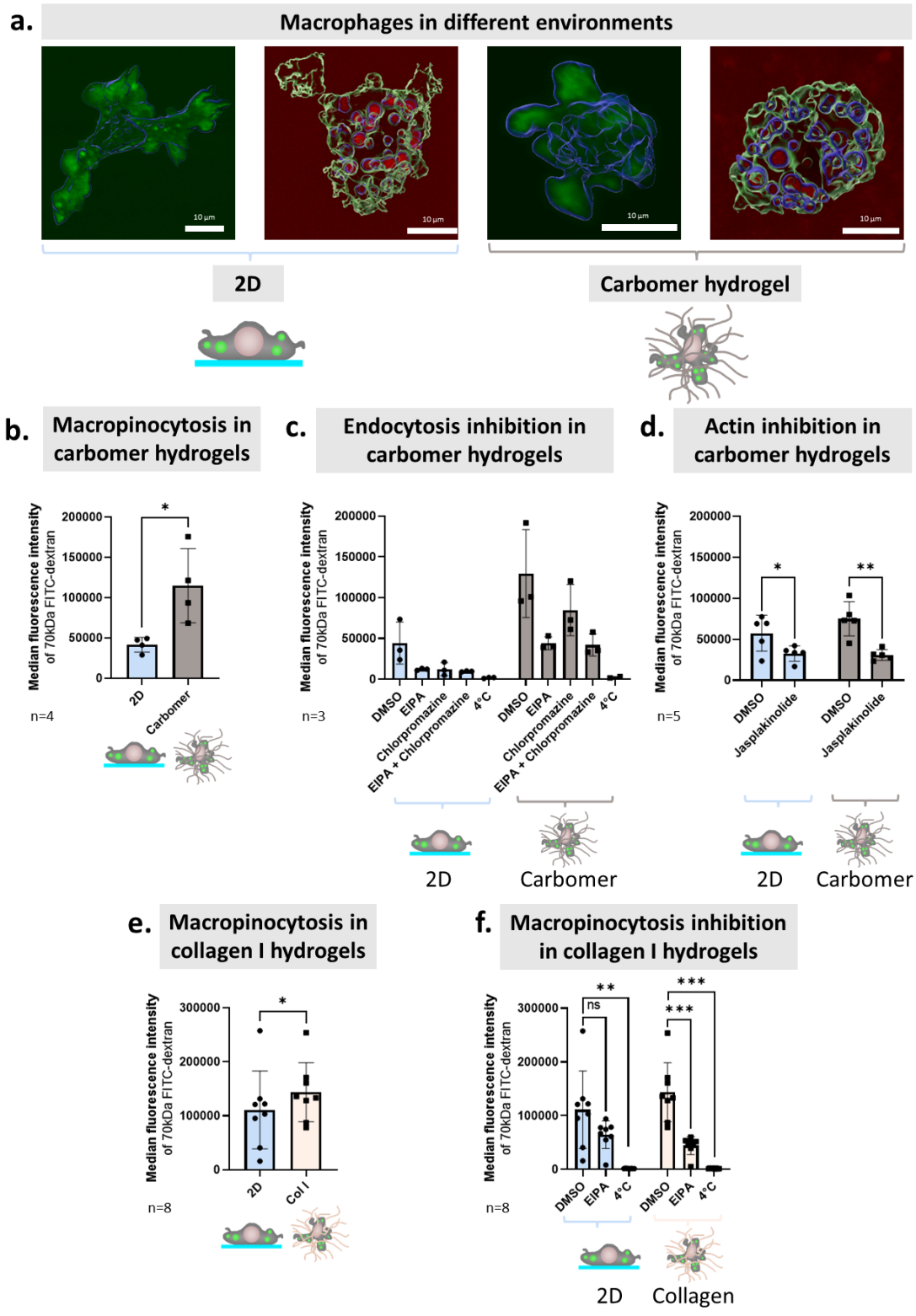
a.
Macrophages in different environments
10 µm
2D
Carbomer hydrogel
b.
Macropinocytosis in carbomer hydrogels
Median fluorescence intensity of 70kDa FITC-dextran
n=4
2D
Carbomer
c.
Endocytosis inhibition in carbomer hydrogels
n=3
DMSO
EIPA
Chlorpromazine
EIPA + Chlorpromazine
4°C
d.
Actin inhibition in carbomer hydrogels
n=5
Jasplakinolide
e.
Macropinocytosis in collagen I hydrogels
n=8
Col I
f.
Macropinocytosis inhibition in collagen I hydrogels
ns
Collagen

Figure 7

Figure 7: Macropinocytotic fluid uptake in macrophages is increased within 3D networks: **a.** Cell shape and macropinosome structure of macrophages (MCs) on a flat 2D surface and in a 3D carbomer network. Cell shape images were obtained using a lattice light-sheet microscope with lifeact-expressing MCs. Images for macropinosome visualisation were acquired by PD Dr. Petra Kameritsch using a 2-photon microscope with wild-type (WT) MCs and 70 kDa TexasRed-dextran as macropinosome marker. All images were processed for 3D rendering using Imaris. Blue lines in cell shape show 3D rendering of cell shape, green lines in macropinosomes represent rendering of cell shape and blue lines show macropinosomes **b.** Quantification of fluorescein isothiocyanate (FITC)-dextran uptake on flat 2D surface (blue) and in 3D carbomer network (grey) by fluorescence activated cell sorting (FACS). **c.** Inhibition of macropinocytosis using 55 µM ethylisopropyl amiloride (EIPA), clathrin-mediated endocytosis using 10 µM chlorpromazine or a mixture of both and inhibition of energy-dependent endocytosis at 4 °C in 2D and 3D carbomer environments. **d.** Inhibition of actin depolymerisation using 8 µM jasplakinolide in 2D and 3D environments. **e.** Quantification of FITC-dextran uptake on flat 2D surface (blue) and in 3D collagen network (pink). **f.** Inhibition of macropinocytosis using 55 µM EIPA and inhibition of energy dependent uptake at 4 °C in 2D and 3D collagen networks. Data from **e.** are also shown in **f.** as dimethyl sulfoxide (DMSO) control. All experiments were performed with Hoxb8-derived WT MCs. Error bars represent the standard deviation between all replicates. The number of biological replicates is indicated by n=. Significances were calculated using a paired t-test and are presented as follows: ns $p > 0.05$, * $p \leq 0.05$, ** $p \leq 0.01$, *** $p \leq 0.001$.

4.2.2 *Increased rates of macropinocytosis in immature dendritic cells and 4T1 breast cancer cells in 3D*

This observation led to the question of whether the effect we observed was specific to MCs or a general phenomenon of macropinocytosis in different cell types. To answer this question, we performed the FACS based macropinocytosis assay with 70 kDa FITC-dextran and cells adhering to 2D plastic surfaces or embedded in 3D carbomer hydrogels with other immune and non-immune cell types. To control whether the effects we observed were indeed macropinocytosis, we used EIPA as a specific inhibitor of macropinocytosis.

We started to confirm our results with bone marrow (BM)-derived MCs (see Figure 8a.). These cells also showed a significant increase in macropinocytosis inside carbomer hydrogels compared to when adhering to 2D surfaces. This increase was sensitive to treatment with EIPA and treatment at 4 °C, demonstrating that the increase is dependent on macropinocytosis. This shows that the effect we observed is not limited to MCs derived from Hoxb8 cells, but applies to MCs in general.

Another important immune cell type that constitutively performs high levels of macropinocytosis to sample the environment are immature dendritic cells (DCs). Thus we tested this cell type for its macropinocytosis rates in 2D and 3D environments (see Figure 8b.). Again, we observed a significant increase in macropinocytosis in 3D carbomer hydrogels that was EIPA and 4 °C sensitive. Therefore, the effect is also true for other cell types that perform constitutive macropinocytosis. As DCs mature, they switch their function from scanning their environment for pathogens to migrating to lymph nodes for antigen presentation.

Therefore, mature DCs no longer perform constitutive macropinocytosis [240]. When we tested this cell type with our macropinocytosis assay, we also observed a significant increase in fluid uptake (see Figure 8c.). However, in contrast to MCs and immature DCs, this increase was insensitive to EIPA and barely sensitive to inhibition at 4 °C. Thus, whether the increased rate of 70 kDa dextran uptake is due to macropinocytosis or other endocytotic processes remains unclear.

To test whether the increase in carbomer was also observed in other non-immune cell types, we also tested three other cell types. Dextran uptake was also increased in the 3T3 fibroblast cell line. However, this increase was insensitive to EIPA treatment but sensitive to treatment at 4 °C. The 4T1 breat cancer line also showed a significant increase in fluid uptake inside the carbomer, which was sensitive to EIPA and treatment at 4 °C. Finally, we also tested the HT1080 fibrosarcoma cell line. This cell line is the only one that did not show an increase in fluid uptake in carbomer hydrogels. Interestingly, fluid uptake was reduced by incubation at 4 °C much more in carbomer hydrogels than when adhering to 2D surfaces. In both environments EIPA shows a small reduction in fluid uptake.

Taken together, these results show that in most of the cell lines tested, fluid uptake is increased when cells are inside 3D carbomer hydrogels. For MCs, immature DCs and 4T1 breast cancer cells, we were able to demonstrate that this increase in uptake was caused by an increase in macropinocytosis, as it was sensitive to treatment with EIPA. Mature DCs and 4T1 breast cancer cells also showed an increase in their fluid uptake inside carbomer hydrogels, but this increase was insensitive to treatment with EIPA. There are two possible explanations for this phenomenon. On the one hand, it is possible that not only macropinocytosis but also other endocytotic pathways are increased in carbomer hydrogels. On the other hand, there is an ongoing debate in the field about the selectivity of EIPA and there are some opinions that certain cell types are less sensitive to it.

4.2.3 *Increased macropinocytosis is not the result of cellular squeezing in 3D environments*

The question arose as to what mechanisms are responsible for the increased rates of macropinocytosis in 3D environments. Since it is known that mechanical confinement sensed by the nucleus can control cellular processes leading to differences in cellular behaviour between 2D and 3D environments [153], we first hypothesised that mechanical confinement induces macropinocytosis in macrophages (MCs) in 3D environments. To test this hypothesis, we prepared hydrogels with densities ranging from 0.4% to 1.5% poly(acrylic acid) (PAA), whereas in previous experiments we used 0.6% PAA. Increasing the PAA content leads to a higher density of the 3D network, as PAA content and density are correlated [18]. We used Hoxb8-derived MCs in these hydrogels of different densities and performed the dextran uptake assay, followed by quantification using fluorescence activated cell sorting (FACS).

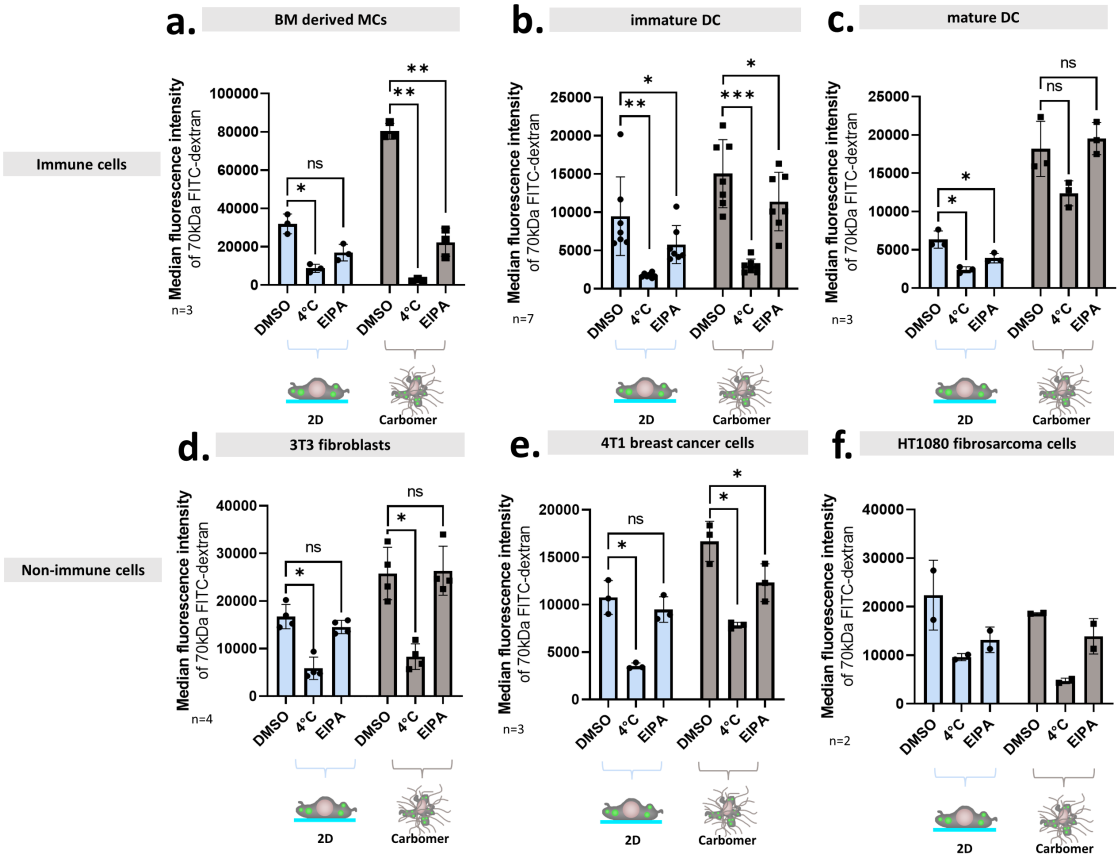

Figure 8: Fluid uptake in 2D and 3D carbomer environments in immune and non-immune cell lines: Comparison of fluid uptake in different cell lines either adhering to a 2D surface (blue) or inside carbomer hydrogels (grey). Energy dependent uptake was inhibited by incubation at 4 °C, macropinocytosis with 55 µM ethylisopropyl amiloride (EIPA). Immune cells tested were bone marrow (BM) derived macrophages (**a.**) or either immature (**b.**) or mature (**c.**) dendritic cells (DCs). Other non-immune cell types tested were 3T3 fibroblast cells (**d.**), 4T1 breast cancer cells (**e.**) and the HT1080 fribrosarcoma cell line (**f.**). Error bars represent the standard deviation between all replicates. The number of biological replicates is indicated by n=. Significances were calculated using a paired t-test and are presented as follows: ns $p > 0.05$, * $p \leq 0.05$, ** $p \leq 0.01$, *** $p \leq 0.001$.

When we used PAA concentrations of 0.4% and 0.6%, we observed a clear but not significant increase in macropinocytosis. However, when we increased the concentration further to 0.75%, macropinocytosis is still increased compared to cells on 2D surface, but lower than in 0.4% and 0.6% carbomers. Increasing the PAA concentration further to 0.9% and 1.1% further reduces the macropinocytosis to levels similar to 2D cells. At the highest concentration tested, 1.5%, we observed even less macropinocytosis than in 2D cells.

This negative correlation between the rate of macropinocytosis and the higher density of carbomer at higher PAA concentrations suggests that the increase in macropinocytosis we observe at low carbomer concentrations is not induced by increased cell confinement.

To confirm these findings from a different perspective, we used the pharmacological inhibitor pyrrophenone. It is known that the nucleus can sense mechanical

signals from the environment. The downstream signal transduction cascade of nuclear confinement sensing is based on the calcium-induced phospholipase A2α protein [153]. Phospholipase A2α activity can be inhibited pharmacologically by pyrrophenone. We performed our macropinocytosis assay on 2D surfaces and in 3D environments with pyrrophenone concentrations ranging from 1 µM to 10 µM. We did not observe any significant changes in the amount of macropinocytosis performed by MC treated with pyrrophenone in 2D. The results suggest that nuclear confinement sensing does not cause increased levels of macropinocytosis in 3D environments.

In conclusion, we have shown that increased macropinocytosis in 3D environments is unlikely to be the result of cellular confinement. In fact, too dense environments seem to hinder efficient macropinocytosis.

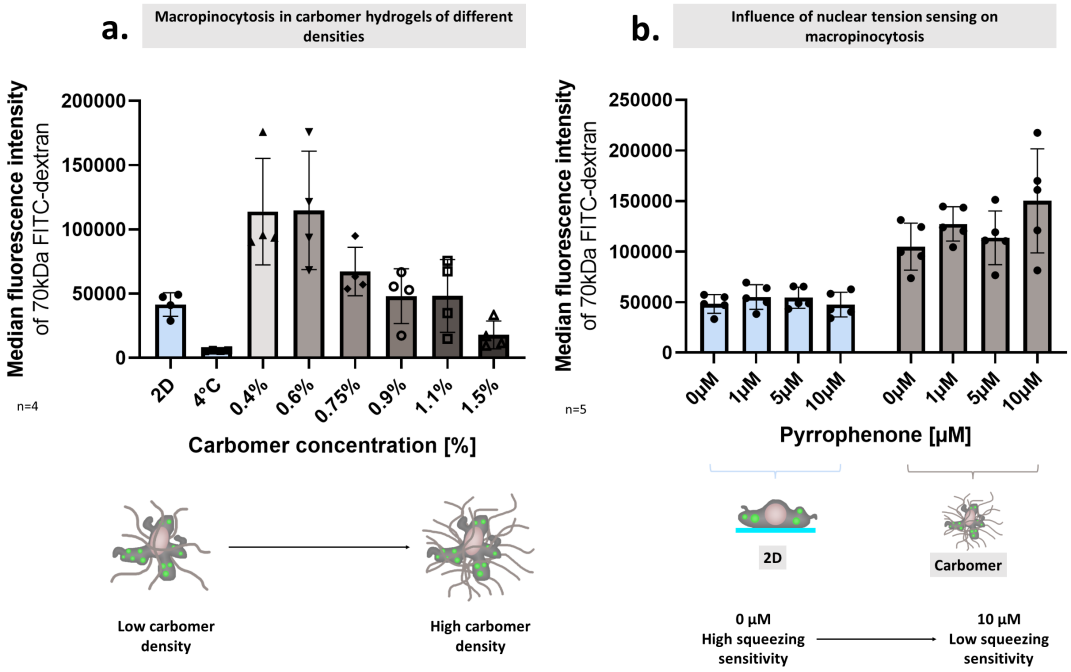

Figure 9: Influence of confinement and nuclear squeezing on macropinocytosis: a. Investigation of the influence of confinement density on macropinocytosis in Hoxb8-derived macrophages (MCs) using different carbomer densities ranging from 0.4% to 1.5%. **b.** Inhibition of nuclear squeezing sensitivity in Hoxb8-derived MCs with pyrrophenone concentrations ranging from 1 µM to 10 µM. Error bars represent the standard deviation between all replicates. The number of biological replicates is indicated by n=. Significances were calculated using a paired repeated measures ANOVA. There are no statistically significant changes.

4.2.4 *Higher cell adhesiveness decreases macropinocytosis*

Since cell confinement does not appear to be a trigger for the induction of macropinocytosis in 3D environments, we investigated other possible ways in which macropinocytosis might be influenced by the environment. Immune cells migrating within collagen networks have been shown to be less adhesive, leading

to a switch from integrin-mediated migration to non-adhesive amoeboid migration [133]. We therefore hypothesised that MCs would be less adhesive in 3D environments, making it easier for the cells to form and extend membrane ruffles and thereby engage in more macropinocytosis. To test this hypothesis, we used a variety of different assays that alter cell adhesiveness.

One of these assays were micropatterns. While MCs can freely adhere without any restrictions on untreated glass, surface coatings can be used to prevent cell adhesion. To find an intermediate between these two extremes of completely free adhesion and prevented adhesion, micropatterning can be used. Micropatterning involves the generation of patterns on surfaces where cells can adhere, while the rest of the surface is non-adhesive to the cells. This can be used to force cells into specific shapes or to limit available adhesion sites. In this project, we used the second option and restricted cell adhesion using circular micropatterns.

We collaborated with Dr Julien Polleux, who generated highly defined micropatterned surfaces. These surfaces are treated with polyethylene glycol (PEG), which prevents cells from adhering. The PEG can be removed in specific patterns using photochemistry combined with photomasks. This generates a pattern of spots where cells can adhere to.

We used two different designs of micropatterns. The first design consisted of adhesive circles with different diameters ranging from 5 µm to 20 µm (see Figure 10). As shown in the brightfield images (see Figure 10a), each cell was confined to one pattern, which limits its adhesion area. Therefore, cells become more rounded when adhering to smaller patterns. For each pattern, 20 cells were imaged and their size and fluorescence signal over the entire cell was measured after incubation with 70 kDa TexasRed-dextran as a marker for macropinocytosis. As expected, the area of cell adhesion decreased with decreasing pattern size (see Figure 10b.). At the same time, we observed an increased fluorescence signal of our macropinocytosis marker at smaller pattern sizes (see Figure 10c.). This finding indicates that there is a negative correlation between the cellular adhesion area and the rate of macropinocytosis performed by the cells. Therefore, cells with less adhesion to the microenvironment seem to perform more macropinocytosis.

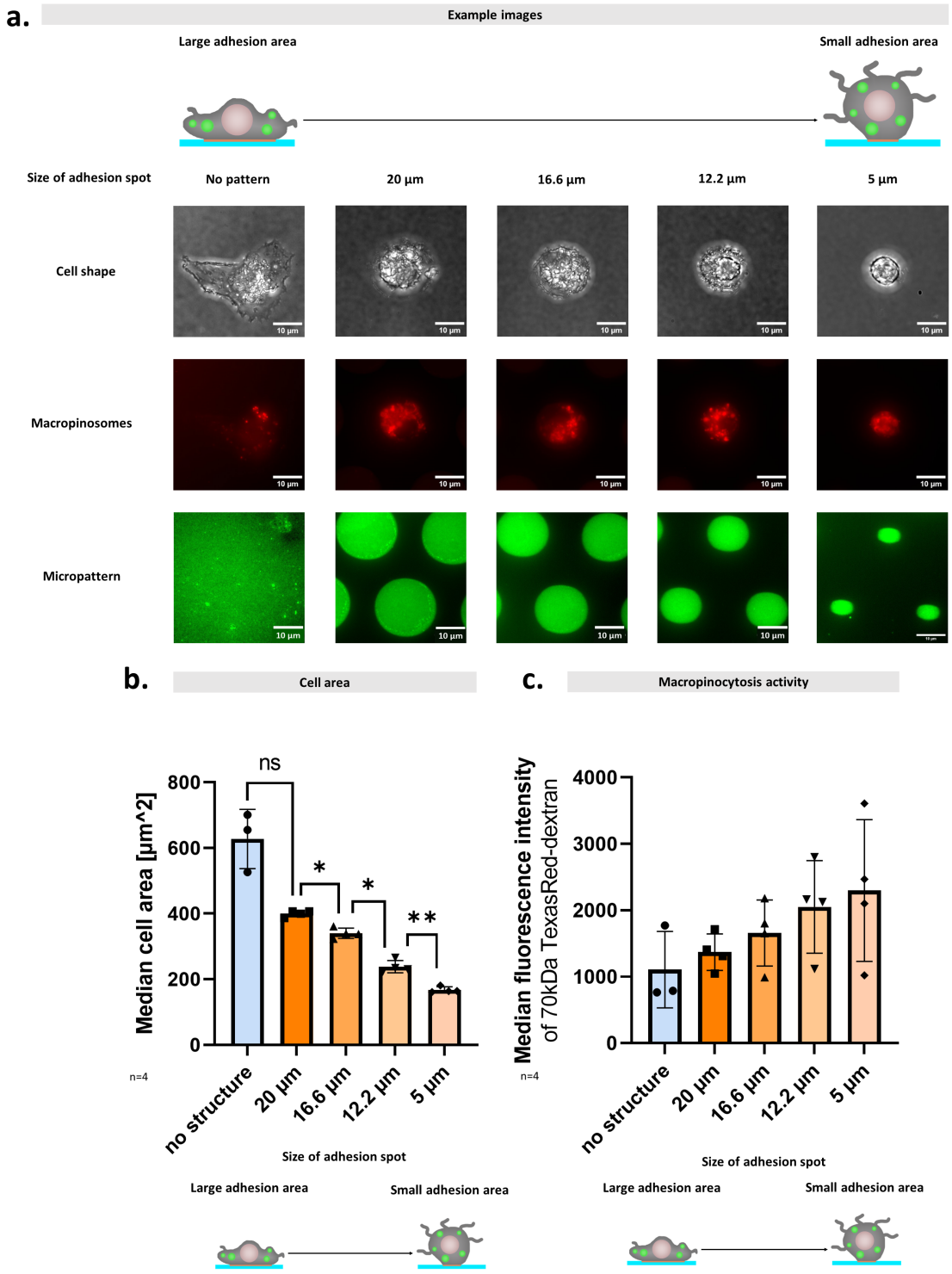

Figure 10: Investigating the influence of cell adhesion using different sized micropatterns: **a.** Images showing cell shape as a bright field image and macropinsomes stained with TexasRed-dextran as a fluorescence image. The micropattern images are not related to the cell images and are for illustrative purposes only. They were generated by adhesion of TexasRed-dextran to micropatterns. All images were taken using an epifluorescence microscope. **b.** Cell area of cells on micropatterns of different sizes. **c.** Median TexasRed fluorescence of cells on micropatterns of different sizes after background subtraction. Experiments were performed using Hoxb8-derived macrophages (MCs) with n=4 biological replicates. Error bars represent the standard deviation between all replicates. Significances were calculated using a paired repeated measures ANOVA and are presented as follows: ns $p > 0.05$, * $p \leq 0.05$, ** $p \leq 0.01$.

To further investigate whether cellular adhesion was correlated with the amount of macropinocytosis performed by MCs, we used a second micropattern design in which all micropatterns had a circular shape with the same diameter of 1.5 µm, but the spacing between the patterns varied from 5 µm to 13.4 µm. This allows cells to adhere to multiple patterns at the same time, but forces them to stretch over increasingly large non-adhesive areas to reach the next adhesive spot. The bright field images show this stretched phenotype on the patterns for 5 µm and 7 µm distances (see Figure 11a.). When the distance was increased to 9.7 µm, MCs already had problems to reach from one adhesion spot to the next, leaving them adherent to only a few spots. When the distance was further increased to 13.4 µm, most MCs were unable to reach the next adhesion spot, confining them to a single small adhesion spot and again leading to the formation of a circular morphology.

We again measured the mean fluorescence signal of the 70 kDa TexasRed-dextran as a marker of macropinocytosis over the whole cell to compare the amount of macropinocytosis performed by the MCs on patterns at different distances. In accordance to our results on micropatterns with different sizes, we also observed a gradual increase of macropinocytosis on patterns with larger distance of the adhesive spots. This increase in macropinocytosis is again correlated with a decrease in the cell surface area in contact with the substrate. At the same time it also has to be considered that the real adhesive area of cells on this patterns with larger distances between the adhesion spots is even smaller as the cells spread above large areas where they are touching the surface but are unable to adhere.

Taken together this results demonstrate that macropinocytosis is increased when there is less adhesive contact to the substrate.

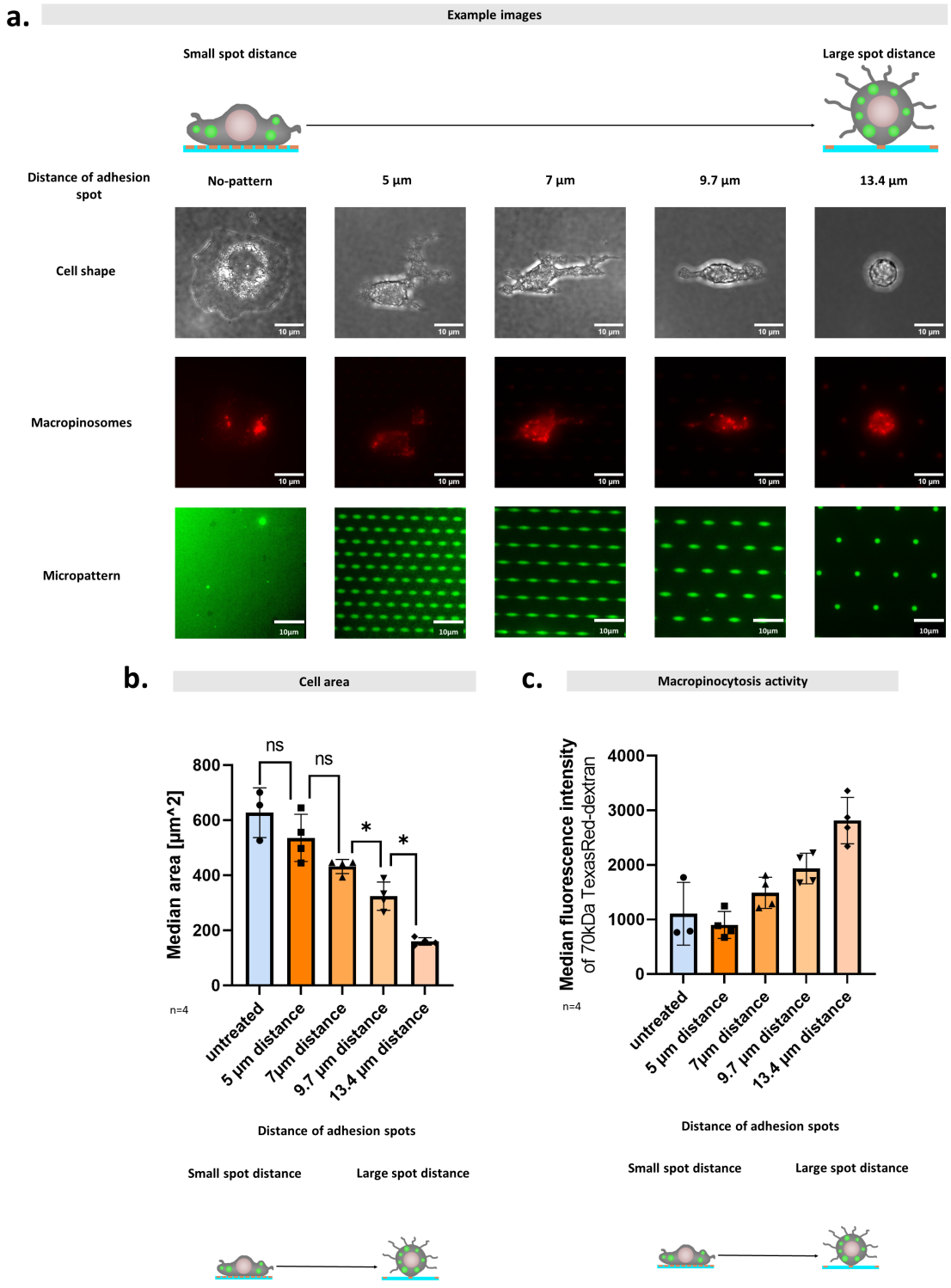

Figure 11: Investigating the influence of cell adhesion using micropatterns with different distances of adhesion spots: a. Images showing cell shape as bright field image and macropinsomes stained with TexasRed-dextran as fluorescence image. The micropattern images are not related to the cell images and are for illustrative purposes only. They were generated by adhesion of TexasRed-dextran to micropatterns. All images were taken using an epifluorescence microscope. **b.** Cell area of cells on micropatterns with different distances of adhesion spots. **c.** Median TexasRed fluorescence of cells on micropatterns with different distances of adhesion spots after background subtraction. Experiments were performed using Hoxb8-derived macrophages (MCs) with n=4 biological replicates. Error bars represent the standard deviation between all replicates. Significances were calculated using a paired repeated measures ANOVA and are presented as follows: ns $p > 0.05$, * $p \leq 0.05$.

Next, we validated these results using the fluorescence activated cell sorting (FACS) based assay and micropatterns with 1.5 µm circular spots with 7 µm distance (see Figure 12a.). We seeded MCs onto these patterns and incubated them with 70 kDa fluorescein isothiocyanate (FITC)-dextran as a marker for macropinocytosis, stopped the uptake with ice-cold ethylenediaminetetraacetic acid (EDTA), detached and fixed the cells. When we compared the uptake of the macropinocytosis marker in cells from the micropatterns with cells on unpatterned glass slides, we observed an increase in macropinocytosis on the patterned surface. However, these results were not significant and highly variable. At the same time, it should be noted that the surface was not completely covered with micropatterns and that the quality of the pattern was not consistent throughout the pattern, which probably explains the rather mild effects and the high variability. Therefore, micropatterns are not well suited for the FACS-based approach.

Surface adhesion can not only be modified by micropatterning, but also by other chemical surface modifications that enhance or suppress cell adhesion. Therefore we investigated how the modification of surfaces with proteins and other chemical substances changes the uptake of 70 kDa dextran as macropinocytosis marker. To achieve this we pre-coated glas surfaces with bovine serum albumin (BSA) and poly-L-lysine (PLL) and also used polyethylene glycol (PEG) glass slides without micropatterning, provided by Dr. Julien Polleux (see Figure 12b.). PLL increases cell adhesion by cationic interaction with the negatively charged cell membrane [96] while PEG surface coating prevents cell adhesion [76]. BSA is also described to decrease cell adhesion [115].

When we analysed dextran uptake on these differently coated surfaces and compared them with untreated surfaces, we observed a strong decrease in macropinocytosis on BSA coated surfaces and a slight decrease on PLL, whereas PEG led to a slight increase in macropinocytosis. This results do only partially match with our expectations. The decrease with PLL is in line with the higher adhesiveness of cells on this surface. Similarly the increased macropinocatosis on PEG is in line with lower adhesiveness on this surface. Only the strong decrease of macropinocytosis on less adhesive BSA is surprising. For clathrin mediated endocytosis it has been reported that clathrin recruitment is reduced on BSA micropatterns [134]. A similar effect may apply to macropinocytosis and could influence it independently of BSA effects on adhesion.

Another factor we investigated was the influence of the adhesion time after seeding the cells. Typically, we seeded cells 1 h before the experiment either on a 2D surface or inside a collagen hydrogel. In this experiment, we used different adhesion times ranging from 15 min to 3 h (see Figure 12c.). Additionally, we also analysed macropinocytosis in cells that have not been detached before the experiment. While macropinocytosis is similar in all freshly seeded cells, cells that have not been detached show much higher macropinocytosis. This suggests that either the cells need more time to fully recover from detachment, or that the cells start the adhesion process by adhering strongly and reduce their adhesion strength over time.

Koyama et. al described in their publication that macrophages do not adhere when seeded on top of collagen I [126]. Therefore, in addition to our experiment where we embedded MCs in collagen I hydrogels, we tested how MCs performed macropinocytosis when seeded on top of a collage I layer. Consistent with the results from inside collagen I, macropinocytosis was also increased on top of hydrogels (see Figure 12d.)

In a physiological environment, cells encounter not only extracellular matrix proteins but also other cells. To simulate this situation *in vitro*, we performed co-culture experiments using MCs and 3T3 fibroblast cells. When MCs were seeded on top of 3T3 cells, cell adhesion was mostly prevented and MCs squeezed in between 3T3 cells or migrated on top of them. When we performed our FACS base macropinocytosis assay using 70 kDa dextran as macropinocytosis marker with MCs which had been seeded on top of 3T3 cells and compared their dextran uptake with MCs which had been seeded alone on a 2D surface we observed a clear increase in macropinocytosis in the MCs seeded on top of 3T3 cells. As we aimed to test if this increase in macropinocytosis on top of 3T3 cells is caused by cell-cell contact or by the lower adhesiveness of MCs on 3T3 cells we also did the reverse experiment where we first seeded the MCs on the plastic surface and then let the 3T3 cells adhere on top. When we analysed macropinocytosis in this MCs we observed that it was reduced back to the same level as in MC alone. This finding suggests that the increase in macropinocytosis is caused by lower adhesiveness of MC and not by cell-cell contact.

Taken together our results from the micropatterns, the assay on top of collagen I and on top of 3T3 cells demonstrate that macropinocytosis is increased when MCs are less adhesive.

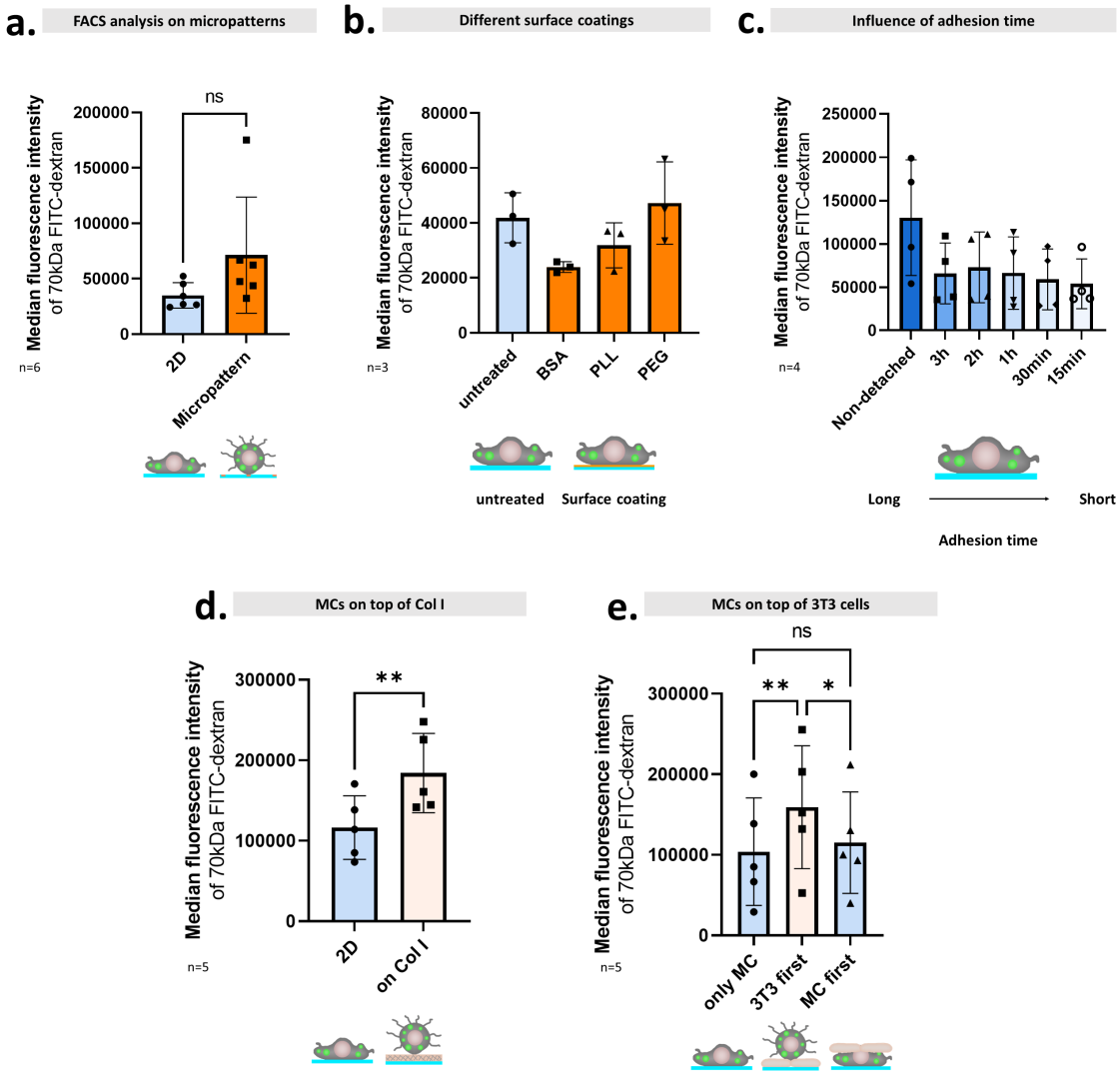

Figure 12: Surface modifications and their influence on macropinocytosis: a. Comparison of macropinocytotic uptake of 70 kDa fluorescein isothiocyanate (FITC)-dextran in Hoxb8-derived macrophages (MCs) adhering to a 2D surface without patterning or micropatterns with round spots of 1.5 µm diameter and 7 µm distance between spots using the fluorescence activated cell sorting (FACS). **b.** Surface coating using bovine serum albumin (BSA), poly-L-lysine (PLL) and polyethylene glycol (PEG) to investigate the effect of these modifications on the macropinocytotic fluid uptake of Hoxb8-derived MCs. **c.** Macropinocytosis in Hoxb8-derived MCs after different adhesion times ranging from 15 min to 3 h. Non-detached cells are MCs that were not detached prior to the experiment and therefore had 5 d to adhere to the surface. **d.** Macropinocytosis in Hoxb8-derived MCs seeded on a collagen layer. **e.** Macropinocytosis in Hoxb8-derived MCs seeded on a layer of 3T3 cells (3T3 first) and when 3T3 cells were seeded on already adherent MCs (MC first). Error bars represent the standard deviation between all replicates. The number of biological replicates is indicated by n=. Significances were calculated using a paired t-test for **a.+d.** and a repeated measures ANOVA for **b.+c.+e.** and are presented as follows: ns $p > 0.05$, * $p \leq 0.05$, ** $p \leq 0.01$.

4.2.5 *Genetic modulation of cell adhesion via genetic knockouts in the integrin adhesion pathway shows no clear impact on macropinocytosis*

Cell adhesion is mainly mediated by the interaction of integrin receptors located on the cell surface with their environment. To further investigate the effects of cell adhesion, we teamed up with Thomas Bromberger from the Moser lab. He provided us with Hoxb8 cell lines with a β2 integrin knock out (KO), KO of the integrin affinity enhancing protein talin and cells with lower expression of the integrin linker complex kindlin-3. All of these modifications should interfere with the integrin-substrate interaction and thereby reduce cell adhesion. To investigate the effects of genetic alterations in cell adhesion on macropinocytosis we performed the FACS based macropinocytosis assay with MCs derived from these Hoxb8 cell lines.

The β2 integrin KO Hoxb8 cell line was generated from the bone marrow (BM) of a KO mouse. Comparing its fluid uptake with wild-type (WT) cells adhering to a 2D surface, we observed only a slight increase in fluid uptake in β2 KO MCs (see Figure 13a.). The talin KOs was generated inside Hoxb8 cells using electroporation with ribonucleoprotein (RNP) complexes to generate the KO via CRISPR/Cas9 followed by single cell dilution. Several different clones were analysed. While two clones showed a clear reduction in the fluid uptake, the third showed no effect (see Figure 13b.). However, when we compared the two different WT clones, we also observed clear differences, indicating a high degree of clonal heterogeneity.

The expression of kindlin-3 has been altered by different genetic manipulations in mice [123]. When kindlin-3 was knocked out on one allele while the second allele was still intact (K3+/-), kindlin-3 expression was reduced to 50% of the level observed in WT cells [123]. In addition, kindlin-3 expression can be reduced by introducing a neomycin cassette into the sixth intron of the kindlin-3 gene [123]. This cassette significantly reduces kindlin-3 expression, but does not block it completely, as a KO would do. This results in only 10% of the amount of kindlin-3 being expressed as in WT cells when cells express the neomycin cassette on both alleles (K3neo/neo) [123]. Kindlin-3 expression can be further reduced to 5% of that of WT cells by KO of kindlin-3 on one allele and the other allele carrying the neomycin cassette (K3neo/-) [123]. Unlike the complete kindlin-3 KOs, which is lethal shortly after birth, K3neo mice are viable [123].

The kindlin-3 Hoxb8 cells with lower kindlin-3 expression could therefore be generated from the bone marrow of mice with the corresponding mutation. We investigated the macropinocytotic fluid uptake in MCs generated from these Hoxb8 lines using the FACS assay. While reduced kindlin-3 expression had no effect on cells on a 2D surface, a clear dose-dependent reduction in fluid uptake was observed within 3D carbomer hydrogels with lower kindlin-3 expression (see Figure 13c.). This suggests that kindlin-3 plays a role in macropinocytosis. The exact role of kindlin-3 in this context remains unknown.

It should be noted that, contrary to our expectations, neither the β2 integrin KO nor talin KO completely prevented macrophage adhesion. When we examined the cells under the cell culture microscope, we found no differences in their spreading and adhesion behaviour compared to control cells. This suggests that other integrins can compensate for the loss of β2 in terms of cell adhesion. Only reduced expression of kindlin-3 led to a reduction in adhesion, although even with expression of 5% of kindlin-3 compared to WT cells, some MCs were still able to adhere.

Although not completely conclusive, our data suggest that integrins may play an additional role in macropinocytosis beyond their role in mediating cell adhesion.

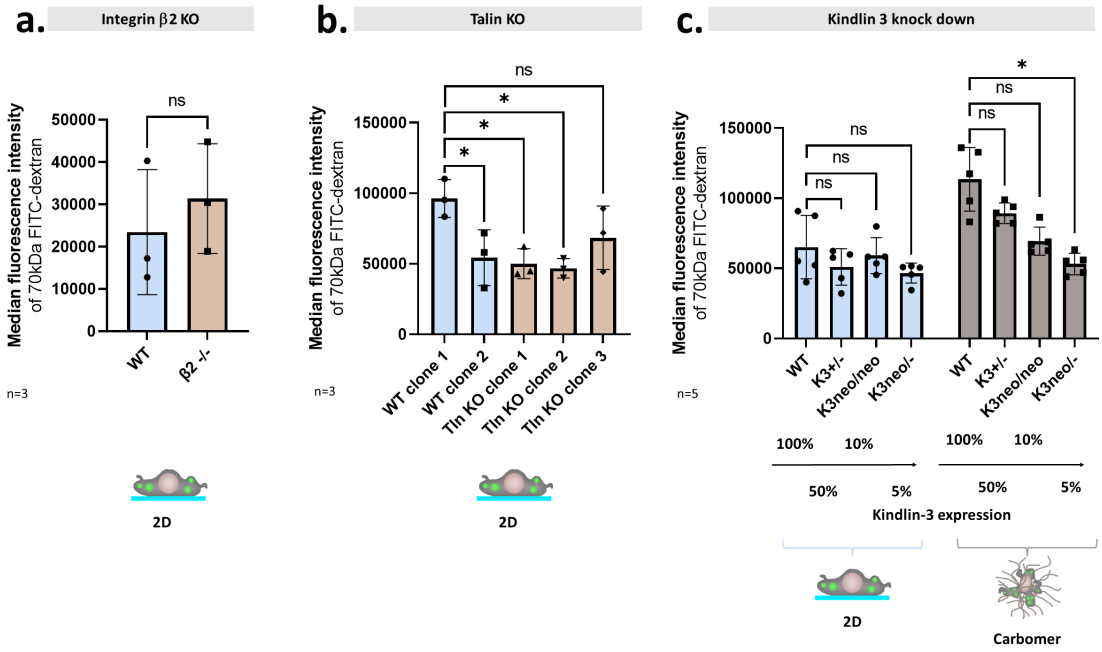

Figure 13: Genetic alteration of cell adhesion: a. Macropinocytosis in Hoxb8-derived macrophages (MCs) with reduced adhesion due to β2 deletion, **b.** Macropinocytosis in MCs derived from different talin knock out (KO) Hoxb8 clones. **c.** Macropinocytosis of Hoxb8-derived MCs expressing different levels of kindlin-3 on 2D surfaces and inside 3D carbomer hydrogels. Error bars represent the standard deviation between all replicates. The number of biological replicates is indicated by n=. Significances were calculated using a paired t-test for **a.** and a repeated measures ANOVA for **b.+c.** and are presented as: ns $p > 0.05$, * $p \leq 0.05$, ** $p \leq 0.01$.

4.2.6 *Macrophages that perform more phagocytosis perform less macropinocytosis*

One of the most important functions of macropinocytosis in the immune system is its ability to sample for pathogens. As BoseDasgupta and Pieters reported that inflammatory signalling leads to a switch from phagocytosis to macropinocytosis for enhanced pathogen clearance [27], we wondered whether the increase in macropinocytosis in 3D environments would also increase pathogen clearance.

To test this, we incubated MCs with either fluorescein isothiocyanate (FITC)-dextran as a macropinocytosis marker alone, TexasRed labelled *E. coli* alone, both together or in combination with ethylisopropyl amiloride (EIPA) to inhibit macropinocytosis.

While in a 2D environment the presence of *E. coli* showed only a slight trend towards decreased fluid uptake, the opposite was true within the carbomer hydrogel where the presence of *E. coli* appeared to increase fluid uptake. Yet, both effects were not statistically significant. In both cases, EIPA treatment decreased dextran uptake (see Figure 14a.). The uptake of *E. coli* was not substantially affected by EIPA treatment either on the 2D surface or inside the 3D carbomer hydrogel, suggesting that uptake was mainly by phagocytosis (see Figure 14b.). Strikingly, *E. coli* uptake was much lower within the carbomer hydrogels. Thus, we did not observe a pathogen-induced increase in macropinocytosis, nor a significant uptake of *E. coli* via macropinocytosis. On the contrary, the increase in macropinocytosis in the 3D hydrogel seemed to reduce the uptake of *E.coli* by phagocytosis.

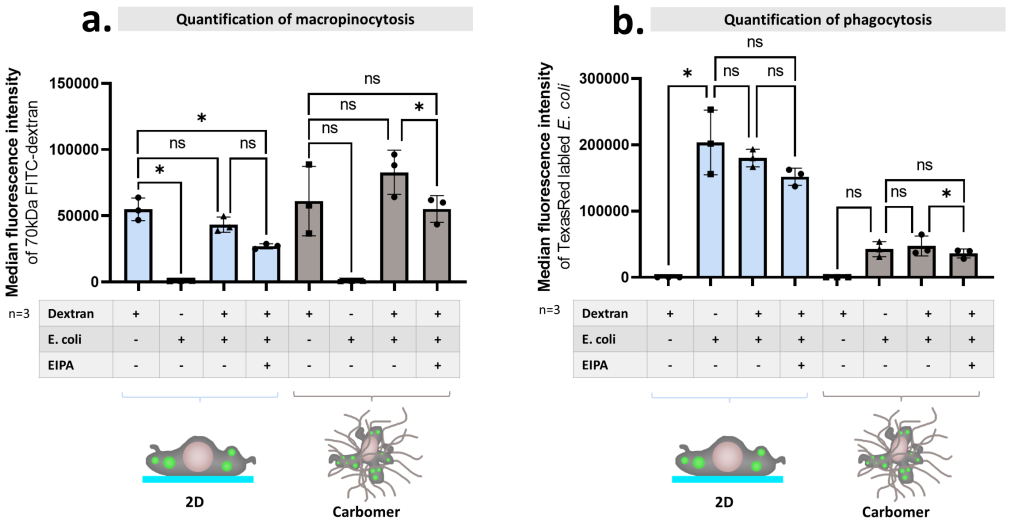

Figure 14: Correlation between macropinocytosis and phagocytosis: a. Quantification of macropinocytosis in Hoxb8-derived macrophages (MCs) using 70 kDa fluorescein isothiocyanate (FITC)-dextran in the presence and absence of TexasRed labelled *E. coli* within wild-type (WT) MCs. Macropinocytosis was inhibited using 55 µM ethylisopropyl amiloride (EIPA). Left side (blue) on 2D surface, right side (grey) in 3D carbomer network. **b.** The corresponding quantification of *E. coli* uptake using the TexasRed signal. Error bars represent the standard deviation between n=3 biological replicates. Significances were calculated using repeated measures ANOVA and are presented as follows: ns $p > 0.05$, * $p \leq 0.05$.

As it has already been described in the literature that impairment of kindlin-3 can lead to decreased phagocytosis [148], we decided to also investigate the relationship between phagocytosis and macropinocytosis in MCs derived from Hoxb8 cells with lower kindlin-3 expression. We used the same assay combining FITC-dextran and TexasRed labelled *E. coli* as before. While in 2D environments *E. coli* will always sediment over time, which could lead to local accumulation

of *E. coli*, MCs in 3D environments only have access to *E. coli* in their direct surroundings. This could explain our observation from the previous experiment that *E. coli* uptake is higher on 2D surfaces. To rule out this possible source of error, we also performed the assay with MCs on collagen hydrogels, where we previously observed an increase in macropinocytosis due to lower adhesion.

Using fluorescence activated cell sorting (FACS) analysis, we observed that fluid uptake was higher for WT MCs in carbomer hydrogels (Figure 14b.) and on collagen (Figure 14c.) compared to 2D (Figure 14a.). In contrast, in K3neo/- with expression of 5% of kindlin-3 compared to WT cells, fluid uptake on carbomer and collagen is barely changed and in all three cases is lower than in WT cells. While the presence of *E. coli* on the 2D surface and on collagen I decreases fluid uptake in WT cells, a slight increase is observed in carbomer. In K3neo/- cells, the presence of *E. coli* has no effect on fluid uptake in all three settings.

The uptake of *E. coli* is increased in all three settings for kindlin-3 knockdowns. While the uptake is much lower inside 3D carbomer hydrogels (Figure 14d.), the rates on 2D (Figure 14e.) and on collagen I (Figure 14f.) are comparable. This shows that the uptake rates of *E. coli* between 2D and Carbomer are in fact not comparable due to the aforementioned problems of accessibility of *E. coli* within carbomer.

The results may indicate that cells with a higher rate of phagocytosis, such as the K3neo/-, perform less macropinocytosis. On the other hand, an increase in macropinocytosis, such as in low adhesion situations and in 3D, seems to have no effect on phagocytosis.

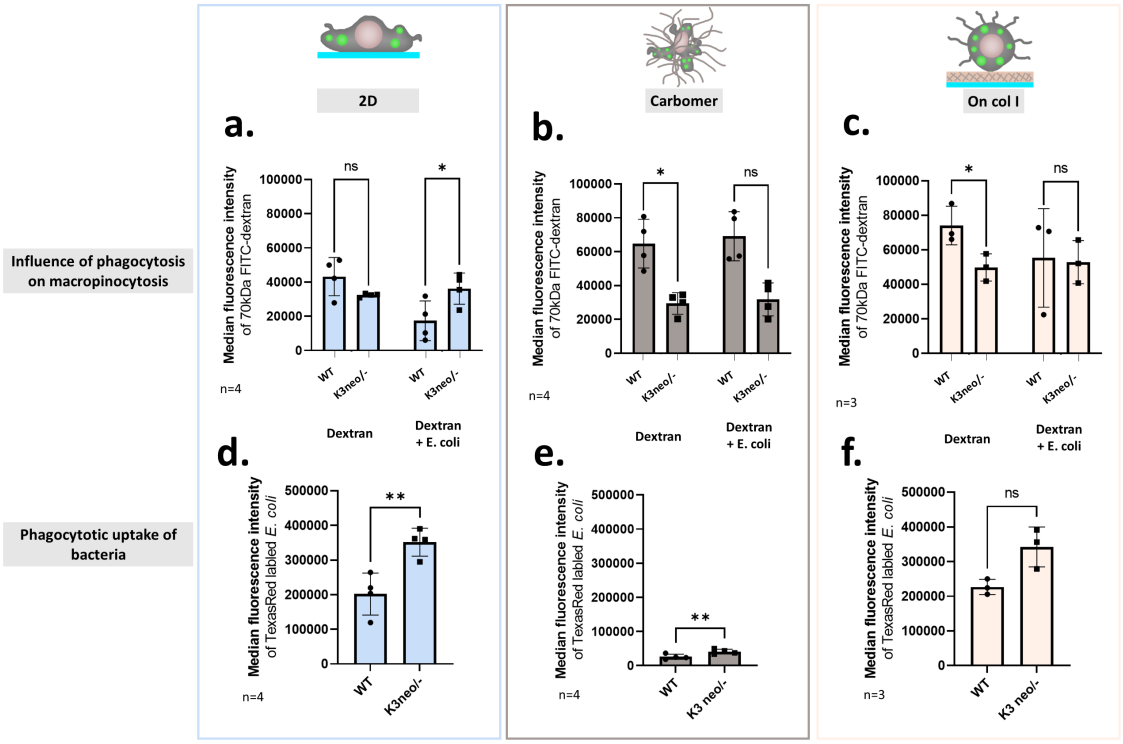

Figure 15: Macropinocytosis and phagocytosis in macrophages with reduced kindlin-3 expression: Investigation of macropinocytotic uptake in cells with reduced kindlin-3 expression in relation to phagocytosis (**a.+b.+c.**) and phagocytotic uptake in the same cells (**d.+e.+f.**) using 70 kDa fluorescein isothiocyanate (FITC)-dextran as a marker for macropinocytosis and TexasRed-labelled *E. coli* as a marker for phagocytosis. The assay was performed with Hoxb8-derived macrophages (MCs) on 2D surface (**a.+d.**) inside carbomer hydrogels (**b.+e.**) and on top of collagen hydrogels (**c.+f.**). Error bars represent the standard deviation between all replicates. The number of biological replicates is indicated by n=. Significances were calculated using a paired t-test and are presented as follows: ns $p > 0.05$, * $p \leq 0.05$, ** $p \leq 0.01$.

4.2.7 *Macropinocytosis of highly adhesive cells requires formin-mediated linear actin, whereas macropinocytosis in less adhesive environments is requires Arp2/3 mediated branched actin networks*

Both phagocytosis and macropinocytosis are actin-dependent processes. We wondered whether the decrease in adhesiveness leading to increased fluid uptake in 3D environments was related to changes in actin dynamics. As we have shown in Figure 3b. and Figure 7d., inhibiting directed actin polymerisation by forcing undirected actin polymerisation with jasplakinolide decreased macropinocytosis in 2D and 3D environments.

There are two ways in which actin can be polymerised. On the one hand, formins generate linear actin filaments. On the other hand, Arp2/3 generates branched actin networks. So far, both formins and Arp2/3 have been implicated in macropinocytosis [110, 116, 214]. At the same time, all of these assays were performed in classical 2D environments. We wanted to understand how actin

network formation is affected by the environment, and whether there are mechanistic differences of actin polymerisation during macropinocytosis in different environments.

To test whether there are differences in the use of formins and Arp2/3, we used two pharmacological inhibitors. Smifh2 is a pharmacological inhibitor of formins and CK666 of Arp2/3. We used these inhibitors in different environments.

First, we tested them in carbomer hydrogels (see Figure 16a.+d.). We seeded Hoxb8-derived wild-type (WT) MCs either on cell culture treated plastic 6-wells as a 2D environment or inside carbomer hydrogels. In both environments we incubated the cells either with Smifh2 or dimethyl sulfoxide (DMSO) as a control to study formin-mediated linear actin polymerisation. In addition we used CK666 or the inactive form CK689 as a control to study Arp2/3-mediated formation of branched actin networks. We again used 70 kDa FITC-dextran as a marker for macropinocytosis and analysed its uptake using fluorescence activated cell sorting (FACS).

While treatment with Smifh2 on 2D surfaces significantly reduced macropinocytosis of FITC-dextran, treatment with the same concentration of Smifh2 in carbomer had no significant effect, but a slight trend towards increased macropinocytosis. On the other hand, when we treated cells with CK666 and its inactive form CK689, we observed no changes in dextran uptake in 2D, but a significant reduction in 3D carbomer hydrogels. This suggests that macropinocytosis on highly adhesive 2D plastic surfaces depends on formin-mediated linear actin polymerisation and that Arp2/3-mediated actin branching does not play a role in this environment. On the other hand, in 3D carbomer hydrogels, formins do not play a role but Arp2/3 mediated actin branching is important.

To investigate whether we would observe similar effects in other 3D environments, we repeated the experiment in 3D collagen I hydrogels (see Figure 16b.+e.). As before, we used lower concentrations of dextran but longer incubation times of 3 h instead of the usual 15 min. Therefore, the cells were exposed to the pharmacological inhibitors for much longer than in the carbomer assay. When we quantified the uptake of our macropinocytosis marker FITC-dextran, we observed that treatment with Smifh2 decreased the uptake of dextran in both 2D and 3D. For Arp2/3, we observed the same effect of decreased macropinocytosis by treatment with CK666 in 2D and 3D. This leaves us with two alternative explanations. On the one hand, it is possible that the actin organisation differs between carbomer and collagen I hydrogels because their physical properties such as pore size and density are different. However, the fact that there are also differences in the 2D control, with CK666 affecting macropinocytosis in 2D after longer incubation, suggests that the more plausible reason for the differences we observed lies in the longer incubation time with the inhibitors. Whereas in carbomer the cells were only preincubated with the inhibitor for 1 h and then were in contact with the inhibitor for further 15 min during dextran uptake, the cells in collagen were pretreated with the inhibitor for 1 h but still in contact with

it for further 3 h during dextran uptake. Therefore, it is possible that the longer incubation time leads to unspecific off-target effects [97, 208].

Since we hypothesised that the decrease in adhesion in carbomer hydrogels is the reason for the increased macropinocytosis, and we had shown that macropinocytosis is also increased when MCs are less adhesive on top of collagen hydrogels, we were also interested to see how actin is polymerised in this environment. We seeded Hoxb8-derived MCs onto hydrogels, treated them with Smifh2 to inhibit formins and CK666 to inhibit Arp2/3 and compared the uptake of our macropinocytosis marker (see Figure 16c.+f.). Similar to the effects in carbomer, we observed a significant decrease in dextran uptake when cells were treated with Smifh2 on 2D plastic surfaces, but no effect of Smifh2 on collagen I hydrogels. When we inhibited Arp2/3 with CK666, we also observed no effect on 2D surfaces, but a decrease in macropinocytosis on collagen hydrogels, which was almost statistically significant with a p-value of 0.0897. The 2D data from this experimental set strengthen the suspicion against the results obtained with longer incubation times inside collagen gels, as they overlap with the results for the 2D controls from the carbomer experiment set. In addition, these data show that formins do not play an important role in macropinocytosis on low adhesive surfaces, whereas Arp2/3 may play a role.

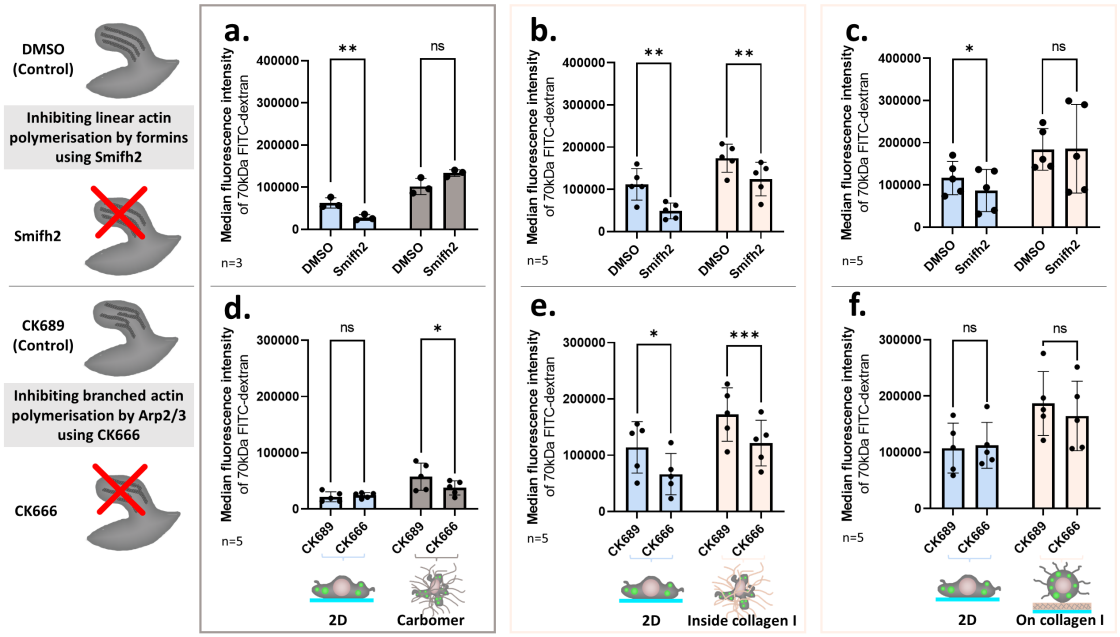

Figure 16: Mechanism of actin polymerisation in different environments: Inhibition of linear actin polymerisation via formins using 60 µM Smifh2 (**a.+b.+c.**) and inhibition of branched actin formation via Arp2/3 using 60 µM CK666 (**d.+e.+f.**) with CK689 as inactive control. **a.+d.** represent the comparison between 2D surface and inside 3D carbomer hydrogels, **b.+e.** inside collagen I hydrogels and **c.+f.** on top of collagen I hydrogels. All experiments were performed with Hoxb8-derived wild-type (WT) macrophages (MCs). Error bars represent the standard deviation between all replicates. The number of biological replicates is indicated by n=. Significances were calculated using a paired t-test and are presented as follows: ns $p > 0.05$, * $p \leq 0.05$, ** $p \leq 0.01$, *** $p \leq 0.001$.

Our results suggest that macropinocytosis is formin mediated on 2D surfaces, whereas it is Arp2/3 dependent in 3D environments. To further investigate this relationship, we used genetic knock out (KO) lines. Arp2/3 can be recruited by either the Wasp complex or the Wave complex. Therefore, we used KOs of Hem1 as part of the Wave complex and KOs of the Wasp complex. Hoxb8 KO lines were provided by the Sixt lab. We used MCs derived from these lines again adhering to 2D surfaces, inside carbomer, inside collagen I and on top of collagen I. We investigated the uptake of 70 kDa-dextran as a marker for macropinocytosis.

We started with the assay inside carbomer hydrogels (see Figure 17a.). As seen before, WT MCs showed an increase in macropinocytosis when seeded inside carbomer hydrogels compared to when adhering to highly adhesive 2D plastic surfaces. In contrast, MC with a KO of Hem1 perform less macropinocytosis inside carbomer hydrogels than on 2D surfaces. While the Wasp KO does not show a decrease in macropinocytosis like the Hem1 KO, it also does not show an increase like the WT cells. Instead, the amount of macropinocytosis is unchanged when comparing Wasp KO MCs on 2D surfaces and inside carbomer hydrogels. These results further suggest that Arp2/3 mediated actin branching is important for macropinocytosis in carbomer hydrogels, as both Arp2/3 recruiting molecules show an effect on macropinocytosis in 3D.

In the next step, we repeated the experiment in collagen I hydrogels with longer incubation time and lower dextran concentration (see Figure 17b.). WT MCs again showed an increase in macropinocytosis in collagen I hydrogels compared to 2D surfaces, although this increase was not statistically significant. Hem1 and Wasp KO MCs showed reduced macropinocytosis when seeded inside collagen I hydrogels compared to 2D surfaces. This highlights the importance of these Arp2/3 recruiters for macropinocytosis in 3D environments.

Finally, we aimed to test if we could observe the same dependence on Hem1 and Wasp in cells adhering to a less adhesive 2D surface (see Figure 17c.). For this, we seeded MCs on collagen I hydrogels. Macropincoytosis in WT cells was increased when seeded on the less adhesive 2D collagen I surface than on the more adhesive plastic surfaces. At the same time, Hem1 KO cells showed no change in their macropinocytosis rate between these two surfaces. Interestingly, macropinocytosis in Wasp KO MCs was also increased on top of collagen I hydrogels, yet to a lower extend. These results suggest that while Hem1 plays a role in macropinocytosis on the lower adhesive surfaces, WASP is not as important.

Taken together, we were able to show that Hem1 plays an important role in macropinocytosis in less adhesive and 3D environments. Wasp, on the other hand, seems to play a role in macropinocytosis in 3D environments, but is not as important in 2D scenarios with lower adhesion. This finding suggests that there are mechanistic differences between the increased macropinocytosis on less adhesive 2D surfaces and less adhesive 3D surfaces.

In conclusion, macropinocytosis in highly adhesive 2D environments is more dependent on formin-mediated linear actin polymerisation, as shown by the effects of Smifh2 in this environment, whereas in less adhesive 2D environments

and in less adhesive 3D environments Arp2/3 is more important. The importance of Arp2/3 is further highlighted by the reduction in macropinocytosis caused by the loss of the Arp2/3 recruiters Hem1 and Wasp. The switch from formin-mediated actin polymerisation to Arp2/3-mediated actin branching could explain why we observed higher macropinocytosis in less adhesive environments and in 3D.

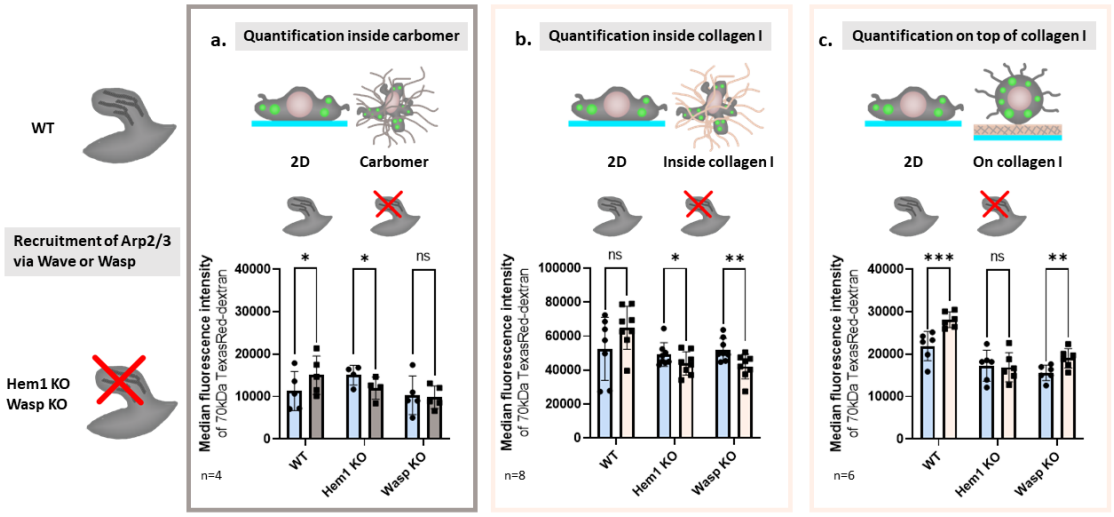

Figure 17: Blocking Arp2/3 recruitment pathways by genetic knock out (KO) of Hem1 and Wasp: Blocking Arp2/3 recruitment via the Wave and Wasp pathway by knocking out Hem1 as part of the Wave complex and the Wasp complex. **a.** Comparison between macrophages (MCs) on 2D and MCs inside 3D carbomer hydrogel. **b.** Comparison between MCs on 2D and MCs inside 3D collagen I hydrogel. **c.** Comparison between MCs on 2D and MCs on top of collagen I hydrogel. All MC were derived either from wild-type (WT) Hoxb8 cells or from Hoxb8 with the respective KO. Error bars represent the standard deviation between all replicates. The number of biological replicates is indicated by n=. Significances were calculated using a paired t-test and are presented as follows: ns $p > 0.05$, * $p \leq 0.05$, ** $p \leq 0.01$, *** $p \leq 0.001$.

4.2.8 *Macrophages that perform macropinocytosis show increased membrane tension*

Actin polymerisation can exert a force on the cell membrane. The influence of membrane tension on macropinocytosis is not fully understood. While earlier publications showed that higher membrane tension inhibits macropinocytosis [86] because cells have to invest more energy to generate membrane ruffles, recent publications correlate higher membrane tension with macropinosome closure [155]. Membrane tension can be measured using the Flipper-TR membrane tension sensor [204]. This sensor allows the measurement of membrane tension by measuring the fluorescence lifetime [204]. The sensor is lipophilic and intercalates into the lipid bilayer of the cell membrane [204]. It has two conformations. Which of these conformations the sensor adopts depends on the tension of the surrounding membrane [204]. While in low tension environments the sensor

adopts a twisted conformation, which is associated with shorter fluorescence lifetimes, in high tension environments it is forced into a planar conformation, which leads to an increase in fluorescence lifetime [204].

Since we have shown that macropinocytosis is increased in environments with lower cell adhesion, we decided to investigate membrane tension again using micropatterned surfaces. We seeded Hoxb8-derived MCs either on unpatterned glass surfaces or on micropatterns with round adhesive spots with a diameter of 1.5 µm at different distances together with the Flipper-TR membrane dye. After 1 h of adhesion, we imaged the cells using a confocal microscope equipped for lifetime measurements. On the micropatterns, we acquired images of cells on the patterns with the smallest distance (5 µm adhesion spot distance) and the largest distance (13.4 µm adhesion spot distance). For analysis, we drew a region of interest (roi) around the cell membrane to analyse the lifetime only in the plasma membrane, ignoring the lifetime of other cell compartments.

Our data demonstrate a clear correlation between macropinocytosis and membrane tension. Cells on unpatterned glass slides showed a homogeneous signal of low membrane tension (green) with only small areas of higher membrane tension (orange). When cells were placed on micropatterns, they began to develop more areas of higher tension, particularly in areas where membrane ruffles were formed (see Figure 18a.). In the lowest adhesion situation, cells form ruffles all around the cell and membrane tension is homogeneously high. This observation was also reflected in the lifetime measurements of the entire cell, where cells on unpatterned surfaces had the lowest lifetimes, while cells with lower adhesion on micropatterned surfaces had higher lifetimes (see Figure 18b.). Thus, we observed a positive correlation between macropinocytosis and membrane tension, where higher macropinocytosis coincided with higher membrane tension.

This observation led to the question of whether macropinocytosis is increased by higher membrane tension or whether the higher membrane tension is the result of increased macropinocytotic activity. To answer this question, we used the macropinocytosis inhibitor ethylisopropyl amiloride (EIPA) and the actin inhibitor jasplakinolide, which forces actin polymerisation. We expected both inhibitors to have the same effect as they prevent macropinocytosis. If higher membrane tension caused the increase in macropinocytosis, we would expect that inhibiting macropinocytosis would have no effect, as high membrane tension would remain even in the absence of macropinocytosis. On the other hand, if macropinocytosis increases membrane tension, we would expect to see a decrease in membrane tension when macropinocytosis is inhibited.

When we imaged dimethyl sulfoxide (DMSO)-treated control cells, we observed a heterogeneous lifetime distribution with higher lifetimes on lamellipodia as well as a stretched cell morphology. Treatment with both jasplakinolide and EIPA resulted in lower adhesion and narrower connections of the adhesive areas to the main cell body (see Figure 18d.). To our surprise, we observed differences in the effects caused by treatment with the actin inhibitor jasplakinolide and the macropinocytosis inhibitor EIPA (see Figure 18c.). Treatment with jasplakinolide

showed a tendency to reduce membrane tension, although the effect is neither consistent nor significant. EIPA, on the other hand, shows a tendency to increase membrane tension, although this trend is also not statistically significant. More repetitions of this experiment are needed to prove that the observed trends are true.

In conclusion, our data indicate that macropinocytosis and membrane tension are positively correlated, leading to higher membrane tension when cells are less adhesive. We could not definitively answer the question whether the higher membrane tension causes more macropinocytosis or whether higher macropinocytosis causes more membrane tension.

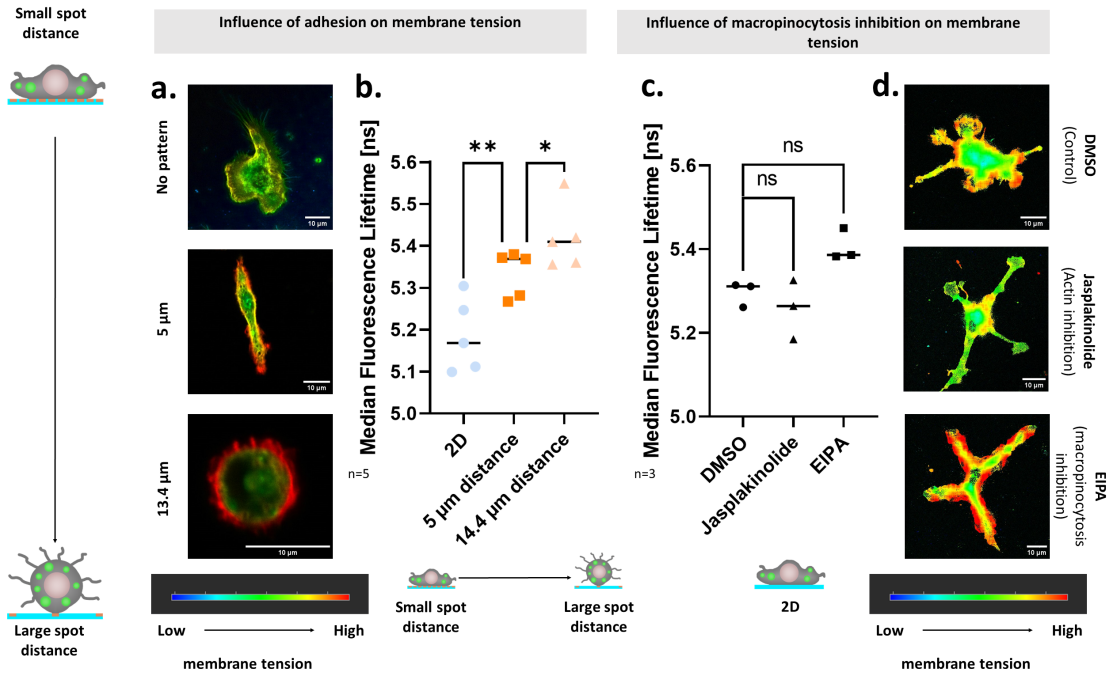

Figure 18: Investigation of the relationship between membrane tension and macropinocytosis: a.+b. Investigation of the influence of cell adhesion on membrane tension. Cells are imaged either on 2D surfaces without micropatterns or on circular 1.5 µm micropatterns with 5 µm or 14.4 µm distance. **a.** Representative images showing membrane tension as a heat map. The lowest membrane tension is shown in blue and the highest in red. **b.** Lifetime in different environments. Higher lifetime correlates with higher membrane tension. **c.+d.** Measurement of membrane tension in macrophages (MCs) treated with 55 µM ethylisopropyl amiloride (EIPA) or 8 µM jasaplakinolide to inhibit macropinocytosis. **c.** Lifetime after 1 h of incubation with the respective inhibitors. **d.** Representative images showing membrane tension of inhibitor-treated cells as a heat map. Experiments were performed using Hoxb8-derived wild-type (WT) MCs. The number of biological replicates is indicated by n=. Significances were calculated using a paired t-test and are presented as follows: ns $p > 0.05$, * $p \leq 0.05$, ** $p \leq 0.01$.

4.2.9 *Macrophages perform less macropinocytosis, when cholesterol is depleted from the cell membrane*

Cholesterol is an important molecule in the organisation of the cell membrane, for example in caveolin-mediated endocytosis [132]. At the same time, high cholesterol levels increase membrane rigidity [39] and reduce fluidity [230]. On the other hand, Biswas et al. showed that reducing cholesterol levels in the cell membrane with methyl-β-cyclodextrin (mβCD) can increase membrane tension [19].

We used different concentrations of mβCD ranging from 1 µM to 10 µM and analysed the fluid uptake on a 2D surface. Fluid uptake was reduced in a dose-dependent manner (see Figure 19a.). Using a concentration of 6 µM on 2D surfaces and inside carbomer hydrogels also showed a strong reduction of the fluid uptake in both environments (see Figure 19b.). This again highlights the importance of membrane organisation in general and membrane tension in the regulation of macropinocytosis.

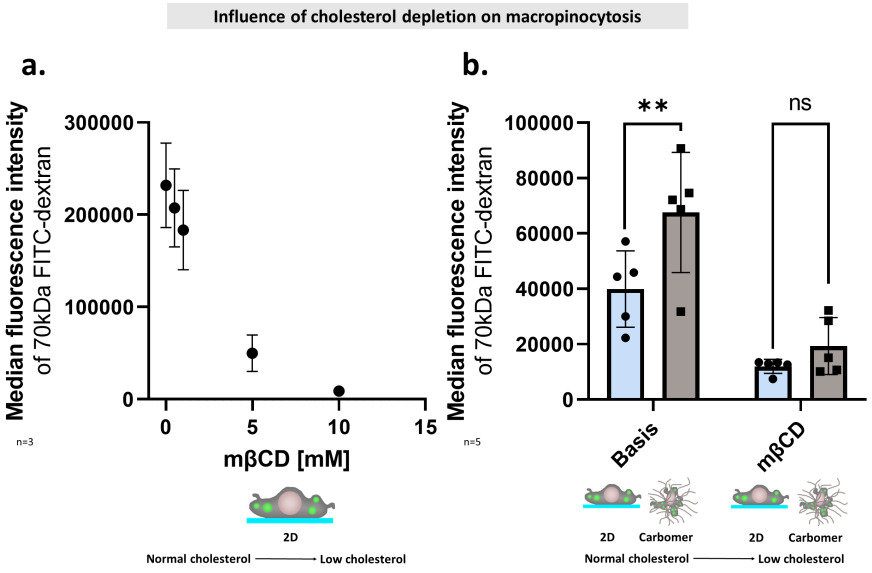

Figure 19: Effect of cholesterol removal on macropinocytosis: a. Cholesterol removal from the cell membrane of Hoxb8-derived wild-type (WT) macrophages (MCs) using methyl-β-cyclodextrin (mβCD) at concentrations ranging from 1 µM to 10 µM. **b.** Cholesterol removal from Hoxb8-derived WT MCs adhering to either a 2D surface or inside a 3D carbomer hydrogel using 6 µM mβCD. Error bars represent the standard deviation between all replicates. The number of biological replicates is indicated by n=. Significances were calculated using a paired t-test and are presented as follows: ns $p > 0.05$, * $p \leq 0.05$, ** $p \leq 0.01$.

5 DISCUSSION

5.1 IDENTIFYING NEW GENES RELATED TO MACROPINOCYTOSIS USING A GENOME WIDE CRISPR-CAS9 SCREEN

In the first part of our project, we used a genome-wide CRISPR screen in macrophages (MCs), which perform consistently high levels of macropinocytosis, to identify genes not previously associated with macropinocytosis.

The results of our genome-wide knock out (KO) screen are of mixed quality. We could demonstrate the ability of our screening system to select for cells with higher or lower rates of macropinocytosis. Using a genetic KO of neurofibromin 1 (NF1), a known negative regulator of macropinocytosis [23,25,79,251], we demonstrated the functionality of our approach to generate genetic KOs in MCs using lentiviral single guide RNA (sgRNA) delivery. We were also able to enrich cells with the desired modifications using fluorescence activated cell sorting (FACS), using the fluorescence signal of 70 kda fluorescein isothiocyanate (FITC)-dextan as a marker for macropinocytosis. When we mixed NF1 KO MCs with wild-type (WT) MCs, we observed an enrichment of cells carrying NF1 mutations in the population with the highest fluorescence and a depletion in the population with the lowest fluorescence (see Figure 3 d.). Thus, our screening system is in principle able to enrich for KOs with alterations in their macropinocytosis rate.

However, our screening results are less convincing. While the sequencing worked well, showing good alignment between the guides within the library and the sequenced reads (see Figure 4 b.), the correlation between the biological replicates is poor (see Figure 4 c.). In addition, the correlation between the different bioinformatic software tools used is low (see Figure 4 d.+e.) and we did not find the known regulators of macropinocytosis such as NF1 [23] or calcium-sensing receptor (CaSR) [37] significantly enriched in the respective populations. The only candidate gene that appears in our screen and that has been associated with macropinocytosis is Atp6v1e1. This gene encodes a subunit of the V-ATPase. Ramirez et al. demonstrated that V-ATPase activity is required for macropinocytosis in tumours with oncogenic Ras mutations [194].

The absence of most of the known regulators of macropinocytosis suggests that the results of our screen are not the most reliable. A possible explanation for this could be the low amount of deoxyribonucleic acid (DNA) isolated from the sorted cells. While sufficient numbers of cells were sorted for all biological replicates, ranging from 10.3×10^6 to 13.8×10^6 cells, corresponding to our expectation of more than 100 cells per guide in the library, the total DNA isolated was only between 8.76 µg and 11.56 µg. This is well below the expected amount of DNA for these cell numbers of 30 µg to 50 µg, suggesting that we lost DNA either

when sorting the cells or when isolating the DNA. If we were indeed losing DNA, this would explain the high variation between biological replicates and the resulting poor performance of the screen, as DNA loss is most likely random. Poor results from a CRISPR screen in the first round of screening with a genome-wide library are actually not uncommon [62]. One way to overcome this problem is to use sub-libraries. After the genome-wide screen, one can employ software tools to select candidates that are most likely to be significantly altered. With these candidates, a sub-library is generated in which the number of sgRNAs per candidate is increased to higher numbers [62]. The screen is then repeated using this sub-library. The advantage of this approach is that the higher number of sgRNAs per candidate makes the screen more robust against non-functional sgRNAs or generating unspecific off-target effects [62]. Therefore, it may be possible to improve our screening results by performing such a secondary screen with a sub-library of candidates in a follow up project.

Although our screening results are probably not the most reliable, we have identified two potential positive regulators of macropinocytosis, Pilra and Adgre1, and one potential negative regulator, Lrch2.

Pilra encodes the immunoglobulin-like type 2 receptor Pilrα (also known as FDF03), which forms an antagonistic receptor pair with Pilrβ. In this receptor pair, Pilrα is inhibitory and Pilrβ is activatory [253]. These genes are mainly expressed by myeloid cells such as granulocytes, monocytes, MCs and monocyte-derived dendritic cells (DCs) [71]. The receptor pair has been implicated in important immune cell functions such as neutrophil infiltration [247]. It acts by recruiting the tyrosine phosphatases SHP-1 and SHP-2 via its intracellular ITAM domain [176]. Pilrα can bind a variety of different ligands such as CD99 and HSV-1 glycoprotein B, recognising a combination of sialic acid and protein motifs [232].

Pilra has been linked to monocyte infiltration into adipose tissue, where monocytes differentiate into MCs. Loss of Pilra leads to increased monocyte infiltration into adipose tissue. In the adipose tissue, monocytes differentiate into F4/80$^+$ macrophages. Mice lacking Pilra are also more likely to develop obesity and changes in liver size due to fibrosis [124]. Pilrα expression can also be increased by lipopolysaccharide (LPS) stimulation of bone marrow (BM)-derived MCs and Raw264.7 MCs [20].

This close association of Pilra with the immune system in general and MCs in particular, together with its known function as an inhibitory receptor, makes Pilra a very interesting candidate to negatively regulate macropinocytosis in immune cells. It also raises the question of whether Pilrβ might play an activating role on the other side, although Pilrb did not appear in our screen in the population with lower macropinocytosis.

It is difficult to predict how Pilra might affect macropinocytosis. The "String" database for protein-protein interactions lists an interaction of Pilra with the C2 domain of phosphatidylinositol-4-phosphate-3-kinase (PIK3) detected by coimmunoprecipitation [8]. PIK3 forms phosphoinositide (PI)(3)P and PI$(3,4)P_2$ by phosphorylating PI at position 3. As PI plays an important role in the initiation

of macropinocytosis and the maturation of macropinosomes (see Figure 2), it is possible that activation of Pilra leads to activation of PIK3, thereby reducing the amount of PI available for the initiation of macropinocytosis.

Adgre1 is better known for the transmembrane protein it encodes, called F4/80. F4/80 (also known as EMR1) is a cell surface marker associated with monocytes and MCs. The potential ligands of F4/80 have not yet been identified [245]. Although it is one of the most widely used surface markers of monocytes and MCs, the function of the protein is surprisingly still unknown. Recently it has been shown that its expression can be induced in colorectal cancer by tumour-associated MCs, which is associated with worse patient outcomes [9]. In addition, expression of F4/80 on antigen presenting cells is required for the production of regulatory T cells [145]. McKnight et al. proposed that F4/80 is related to MC adhesion in tissues due to unspecified structural elements and its expression pattern [165]. This relationship with cell adhesion, combined with our observation that cells with lower adhesion perform more macropinocytosis, may suggest that F4/80 reduces macropinocytosis by increasing cell adhesion. Therefore, loss of F4/80 could lead to lower adhesion and higher macropinocytosis.

Lrch2 belongs to a group of Lrch proteins grouped according to their structural similarity [202]. They all contain a calponin homology domain and varying numbers of leucine-rich repeat domains [202]. As leucine-rich repeats are associated with protein-protein interaction and the calponin homology domain is known to interact with actin, it is likely that the Lrch proteins play a role in protein recruitment to actin [202]. While Lrch4 expression is negatively correlated with pro-inflammatory signals [181] and Lrch3 has been implicated in myosin-mediated actin remodelling [186], little is known about the role of this group of proteins in general and Lrch2 in particular. By characterising chromosomal alterations in low-grade glioma-derived induced pluripotent stem cells, Liu et al. found amplification of Xq23, the location of Lrch2, leading to a higher frequency of these regions in glioma patients compared to healthy patients [150]. Therefore, Lrch2 expression may play a role in glioma formation [150].

RNAi profiling also showed an alteration in HeLa cell division when Lrch2 was depleted in combination with Moesin [73]. The association with Moesin suggests a role for Lrch2 in cell membrane organisation, as Moesin localises to filopodia and membrane protrusions [12].

One might speculate that Lrch2 regulates macropinocytosis by recruiting other proteins to actin filaments, which in turn promote actin polymerisation. One candidate could be Dock8. The "String" database shows an experimentally determined interaction between Lrch2 and Dock8 [7]. Dock8 is a guanine nucleotide exchange factor (GEF) that plays an important role in activating actin polymerisation via small GTPases such as Rac or CDC42 [87,173]. It is therefore possible that Lrch2 recruits Dock8 to pre-existing actin filaments. At these filaments, Dock8 exchanges bound GDP for GTP in small GTPases, which in turn activates them, leading to actin filament extension or branching [87].

In conclusion, our screen has allowed us to identify three new candidates, Pilra, Adgre1 and Lrch2, which have not previously been associated with macropinocytosis. These candidates need to be further validated, first by using more sgRNAs to confirm that the observed effects are not the result of unspecific off-target effects. In addition, it would be important to generate fluorescently tagged variants of the proteins to visualise their localisation specifically in relation to the cell membrane, actin structures and macropinosomes. This would allow their localisation to be followed during macropinosome formation and maturation. To further investigate their involvement in macropinocytosis, it would be important to perform a rescue experiment, in which the protein is re-expressed in cells with a KO background to restore the WT phenotype.

In addition, the screen has helped us to develop and validate important tools such as the generation of KOs using the Hoxb8 cell system and the quantification of macropinocytosis using FACS.

5.2 ANALYSING HOW THE MICROENVIRONMENT REGULATES MACROPINOCYTOSIS

5.2.1 *Increased rates of macropinocytosis inside 3D environments*

In the second part of the project, we investigated whether there are differences between macropinocytosis on 2D surfaces and in more physiological 3D environments, using a variety of different assays ranging from 3D hydrogels to surface modifications and micropatterning.

We were able to show that macropinocytosis by MCs, immature DCs and 4T1 breast cancer cells is increased when they are located in more physiological 3D environments (see Figure 7 + 8). This increase is ethylisopropyl amiloride (EIPA) sensitive. While most other cell types tested also showed an increase in 3D environments, this increase was not sensitive to the macropinocytosis inhibitor EIPA (see Figure 8). There could be two reasons for this observation. One is that these cell types are insensitive to EIPA treatment. There is an ongoing debate whether EIPA is a selective inhibitor of macropinocytosis, as its inhibition of the sodium proton exchanger (NHE) also affects other cellular processes such as water flux and cell migration [229]. Another possible explanation could be that other endocytotic pathways are also upregulated in 3D environments, leading to uptake via these processes. However, as 70 kDa dextran is specifically taken up via macropinocytosis [141], this explanation is rather unlikely.

To identify the underlying mechanism of the increase in macropinocytosis rates in 3D, we used carbomer hydrogels of different densities and pharmacological inhibitors of nuclear tension sensing. Our results show that the increase in macropinocytosis inside 3D hydrogels is not the result of cell confinement, as more dense carbomer hydrogels decreased fluid uptake (see Figure 9a.). This shows that the increase in macropinocytosis is not a response to cell squeezing, and that too much spatial confinement can actually spatially hinder macropinocy-

tosis. Bhattacharjee and Angelini analysed the relationship between pore size, yield stress and carbomer concentration in carbomer hydrogels [18]. For 0.5% hydrogels they observed a yield stress of 1.1 Pa and a pore size of 1.1 µm, while at concentrations of 0.72% the yield stress increased to 6.2 Pa and the pore size decreased to 0.75 µm [18]. At concentrations of 0.6% they observed a yield stress of 2.1 Pa and pore sizes of 1 µm [18]. This shows that higher carbomer concentrations result in higher yield stress and smaller pore sizes.

Correlating their results with our own data suggests that the physical inhibition of macropinocytosis begins at a yield stress higher than 2.1 Pa and pore sizes lower than 1 µm. In particular, observing the strong increase in yield stress with increasing carbomer concentration, it seems plausible that cells are unable to generate enough force to deform the hydrogel at concentrations above 0.6% and therefore have problems to form membrane ruffles. Fischer et al. measured a mean pore size of 6.78 µm for collagen hydrogels with $3\,\mathrm{g\,L^{-1}}$. [69]. As this concentration is comparable to the concentration we used ($3.3\,\mathrm{g\,L^{-1}}$), the pore sizes in our collagen assays are most likely significantly larger than in our carbomer assay. Therefore, spatial confinement within our collagen I hydrogels should be unproblematic. It would be interesting to test whether higher collagen concentrations also limit macropinocytosis, although the smaller pore size would further hinder diffusion, making this experiment technically more challenging.

To further analyse the effect of cell squeezing on macropinocytosis, we inhibited the signal transduction cascade of nuclear squeezing sensitivity. Lomakin et al. showed that the activity of the calcium-sensitive lipase cPLA2 is required for nuclear pore size sensing [153]. Venturini et al. identified the same mechanism using the pharmacological cPLA2 inhibitor pyrrophenone [242]. Therefore, we also used different concentrations of pyrrophenone with MCs on 2D surfaces and inside 3D carbomer hydrogels (see Figure 9b.). In both cases we observed only small insignificant changes. This suggests that nuclear squeezing is not the mechanism triggering higher macropinocytosis in 3D environments. At the same time, it should be noted that cPLA2 inhibition by pyrrphenone is known to have additional effects on cell physiology, such as inhibition of calcium release from the endoplasmic reticulum [260]. This unspecific side effect of pyrrophenone could also influence our measurements and explain the high standard deviation at higher inhibitor concentrations in carbomer.

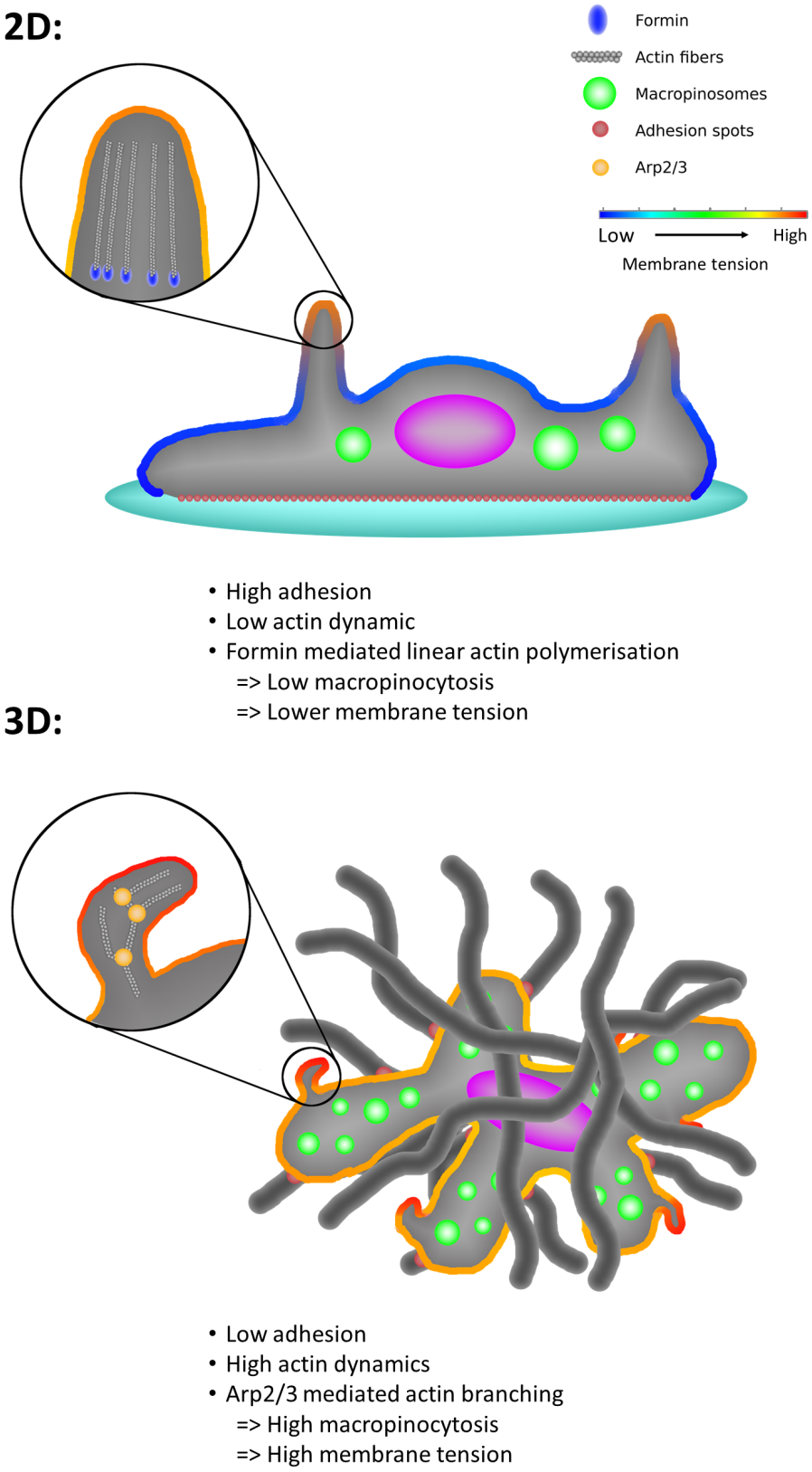

Figure 20: Graphical abstract: Macropinocytosis is increased in 3D environments. This increase is the result of differences in cell adhesion and actin organisation and is associated with changes in membrane tension.

5.2.2 *The increased rate of macropinocytosis in 3D environments is the result of lower cell adhesion*

Since we identified that the increase in macropinocytosis was not the result of confinement (see Figure 9), we next focused on cell adhesion. It has been shown that in migrating cells, confinement decreases cell adhesion and therefore leads to a switch from integrin-mediated to amoeboid migration [149]. As carbomer hydrogels have also been described to be poorly adhesive [52], we hypothesised that reduced adhesion might not only trigger changes in cell migration but also in macropinocytosis. Our data show a clear correlation between adhesion and macropinocytosis (see Figures 10, 11, 12). On micropatterns, we observe higher macropinocytosis when cells have less adhesive area (see Figures 10, 11). We also observed an increase in macropinocytosis when MC were seeded on collagen I or on 3T3 cells, where they have problems adhering (see Figure 12d., e.). Our observation of higher macropinocytosis in situations where cells are less adhesive is consistent with previous observations in *Dictyostelium discoideum*, showing that cells in suspension perform more macropinocytosis than cells adhered to the substrate [185].

Substrate stiffness is also known to affect micropinocytosis. For example it has been shown that 3T3 cells [261] and tumour cells [74] form more ruffles on surfaces with higher stiffness. Freeman et al. also showed that in tumour cells this increased macropinocytotic activity was dependent on the tension-sensitive Ca^{2+} channel Piezo1. These observations are in contrast to our own findings. Carbomer hydrogels and collagen hydrogels have a much lower stiffness than the cell culture treated plastic surfaces we used as 2D surfaces, with carbomer ranging from 17 kPa to 40 kPa [47] and collagen from 0.5 kPa to 27 kPa [196], whereas plastic has a stiffness of about 10^6 kPa. [80]. While within the hydrogels stiffness is likely to be less important than density-related forces, we also observed higher macropinocytosis when seeding MCs on top of 2D collagen hydrogels, where stiffness is lower than on our 2D plastic surfaces (see Figure 12d.). This demonstrates that stiffness does not reduce macropinocytosis in MCs.

As Freeman et al. detected in tumour cells that the increase in macropinocytosis was dependent on the tension-sensitive Ca^{2+} channel Piezo1 [74], we also analysed the role of Piezo1 activity in our carbomer hydrogels, since membrane stretching by confinement could also activate Piezo1 by increasing tension. We used the Piezo1 inhibitor D-GsMTx4 and the activator Yoda-1 in our carbomer hydrogels. None of the inhibitors showed the effects we would expect from the Freeman paper [74]. D-GsMTx4 showed a trend towards increased macropinocytosis on the stiffer 2D surface and slightly decreased it inside the 3D carbomer hydrogel, whereas Yoda-1 treatment showed no effects on the 2D surfaces or inside the carbomer hydrogel (data not shown).

Thus, our data show that while cell adhesion to the substrate plays an important role in macropinocytosis in MCs, stiffness-mediated membrane stretching that activates Piezo1 seems not to be important in this context. In addition, our data

on macropinocytosis in cells seeded on top of collagen hydrogels suggest that substrate stiffness either does not play a role or is even negatively correlated with macropinocytosis, showing more macropinocytosis on less stiff collagen I hydrogels.

We also attempted to modify cell adhesion by altering the expression of the integrin $\beta 2$, talin, which is important for integrin substrate affinity, and kindlin-3, an integrin linker protein. All of these genetic modifications were aimed at reducing adhesion in order to confirm our results showing higher macropinocytosis in less adhesive environments at the genetic level. The $\beta 2$ KO showed the expected increase in macropinocytosis, while the loss of talin actually tended to reduce macropinocytosis (see Figure 13 a.+b.). The reduced expression of kindlin-3 had no effect when cells were seeded on a 2D surface, but showed a clear dose-dependent reduction when seeded inside carbomer hydrogels (see Figure 13 c.).

At the same time, it is important to be aware that integrins are not only involved in cell adhesion, but also in a variety of other cellular processes such as signal transduction [171], cytoskeleton organisation [60], cell migration [95] and cell differentiation [75, 118]. It is therefore plausible that the effects we observe with changes in integrin expression and integrin affinity may not be the result of reduced cell adhesion, but are caused by other effects.

For example, Schwartz et al. were able to show that integrin $\alpha 5\beta 1$ activates NHE, leading to an increase in cellular pH in response to fibronectin-mediated integrin clustering [213]. If our attempts to modulate in integrin affinity by targeting talin and kindlin-3 expression would alter the activity of NHE, this would explain possible effects on macropinocytosis, as pH regulation by NHE plays an important role in the regulation of macropinocytosis [125].

Several publications link integrin function to macropinocytosis. Gu et al. showed that migrating fibroblasts use macropinosomes to recycle integrin $\beta 3$ from the cell rear to the cell front, thereby playing a role in growth factor-induced cell migration [84]. Similarly, Le et al. observed that CYRI-A is required for macropinosome-mediated recycling of $\alpha 5\beta 1$ in HEK293T and Cos-7 cells [136]. In glioblastoma, overexpression of integrin $\alpha 3\beta 1$ was also observed to promote angiogenesis by promoting macropinosome formation and exocytosis of lysosomal contents [17].

There is also an interplay between macropinocytosis and integrins in cell senescence. LY6D can induce macropinocytosis leading to the formation of senescence-inducing vacuoles [179]. This macropinosome formation is abolished when $\beta 1$ is knocked down by siRNA, demonstrating a direct link between integrins and macropinocytosis activity [179].

Sendo et al. revealed a relationship between the $\beta 2$-associated GPI-anchored protein GPI-80 and macropinocytosis [215]. Using a monoclonal antibody against GPI-80, the authors observed an increase in macropinocytosis in human monocytes [215].

Together these data show a link between macropinocytosis and integrins. Our data further support this relationship. Our findings suggest that loss of $\beta 2$ alone could increase macropinocytosis, most likely through reduced adhesion. At the same time, reducing integrin affinity globally by knocking out talin and reducing kindlin-3 expression impairs macropinocytosis, most likely independently of cell adhesion effects, as integrins also have other roles in the cell. It is difficult to determine which integrins are responsible for these changes as there are at least 18 variants of the α subunit and eight variants of the β subunit, generating 24 heterodimers [237].

5.2.3 *Macropinocytosis and phagocytosis*

As it has been shown that stimulation of macropinocytosis by bacterial LPS can increase bacterial uptake and thereby enhance bacterial clearing [27], we performed a combined uptake assay by simultaneously incubating MCs with FITC-dextran as a macropinocytosis marker and TexasRed-labelled *E. coli* for phagocytic uptake. In WT MCs, we observed no changes in *E. coli* uptake in environments where macropinocytosis is higher compared to 2D surfaces where macropinocytosis is lower (see Figure 14). In addition, *E. coli* uptake was not sensitive to EIPA. Therefore, at least in WT cells, no significant uptake of *E. coli* by macropinocytosis was observed.

When we compared the uptake between WT MCs and MCs with lower kindlin-3 expression, we again observed that macropinocytosis was lower in cells with low kindlin-3 expression compared to WT cells (see Figure 15). At the same time, cells with low kindlin-3 expression took up more *E. coli*. This indicates that at least *E. coli* is not cleared by macropinocytosis, but most likely by phagocytosis. Since *E. coli* are 1 µm to 2 µm in length [200], they represent a rather large cargo for macropinosomes. Although macropinosomes can reach sizes of up to 5 µm [144], their average size is in the range of 1.75 µm $\pm$ 0.6 µm [259]. It is therefore possible that *E. coli* is simply too large for most newly formed macropinosomes. Therefore, it seems more likely that macropinocytosis is mainly used to clear pathogen fragments rather than entire pathogens.

Our results may also point to an additional effect. Phagocytosis and macropinocytosis are mechanistically very similar. In both cases, changes in PI phosphorylation play an important role in the regulation of actin [138]. As these two processes are similarly regulated and use the same actin pool, it is possible that they could behave antagonistically. While we did not observe a change in phygocytotic uptake of *E. coli* when macropinocytosis was increased on lower adhesive surfaces, the increased phagocytosis in cells with lower kindlin-3 expression combined with lower macropinocytosis of these cells could be an indication into this direction. But one has to keep in mind that while MCs can only perform phagocytosis in the presence of *E. coli*, they always perform macropinocytosis, even in the absence of FITC-dextran as a macropinocytosis marker. Therefore, the only situation in which cells perform only phagocytosis and no macropinocytosis is

when macropinocytosis is fully blocked by EIPA. When we completely inhibited macropinocytosis with EIPA, we also observed a small reduction in *E. coli* uptake. However, this decrease in uptake could also be the result of a small part of the *E. coli* being taken up by macropinocytosis. When we imaged the cells incubated with FITC-dextran and TexasRed labeled *E. coli*, most *E. coli* did not colocalise with dextran vesicles. However, in a few rare cases *E. coli* did colocalise. Therefore, it cannot be excluded that a few *E. coli* are also taken up by macropinocytosis, while the majority is taken up by phagocytosis.

An alternative explanation for the reduced uptake of *E. coli* could be that EIPA may also affect phagocytosis. While it is generally accepted that EIPA does not affect phagocytosis, there are some publications claiming that EIPA interferes with phagocytosis and other actin-related processes [94, 100, 131, 178].

5.2.4 *Actin organisation during macropinocytosis differs between highly adhesive 2D environments and lower adhesive environments*

Macropinocytosis is highly dependent on actin-mediated membrane ruffling [144]. There are two ways in which actin can be polymerised. On the one hand, formins can mediate the formation of linear actin filaments [81]. On the other hand, Arp2/3 mediates the formation of branched actin networks [190]. In general, it is thought that formin-mediated linear actin is more important for filopodia formation, whereas branched actin is important for more complex structural changes, such as in the case of macropinocytosis [36]. At the same time, both processes have been implicated in macropinocytosis [110, 116, 214]. We wondered whether the increase in macropinocytosis we observed in 3D environments was the result of changes in actin dynamics. We therefore used the pharmacological inhibitors Smifh2 to target formins and CK666 to target Arp2/3. Using these inhibitors, we observed a decrease in macropinocytosis in 2D environments by using the formin inhibitor Smifh2, while there was no change in 3D environments (see Figure 16). On the other hand, we observed unchanged or slightly increased macropinocytosis rates using the Arp2/3 inhibitor CK666 in 2D, while macropinocytosis was decreased in 3D. We observed similar effects using KOs of the Arp2/3 recruiters Wasp and Wave (see Figure 17). Together, our findings suggest that macropinocytosis is preferentially mediated by formins in 2D, whereas it is preferentially mediated by Arp2/3 in 3D.

These observations may also explain an interesting observation by Condon et al. who observed that LPS-stimulated macropinocytosis in MCs is mediated by f-actin-rich filopodia on the top of the cells [51]. They termed this process "tent pole ruffling". As they performed their experiments with MCs adhering to a 2D surface, this observation is in line with our own findings, as these filopodia are most likely generated by fomin-mediated actin polymerisation. There is also evidence that formins do not play a role in macropinocytosis in 3D environments. Vargas et al. studied macropinocytosis in immature DCs migrating in polydimethylsiloxane (PDMS) microchannels [239]. They observed no change

in macropinocytosis when cells were treated with Smifh2 or when the formin mDia1 was knocked out [239]. On the other hand, loss of formins rendered DCs insensitive to the LPS-induced reduction in macropinocytosis that they observed in non-inhibitor-treated controls and WT cells [239]. At the same time, the authors observed a reduction of macropinocytosis in immature Arp2/3 KO DCs within microchannels [239].

We also tried to perform experiments with immature Hem1 and Wasp KOs DCs derived from the Hoxb8 lines, which we had previously used for our experiments with MCs. Hem1 KO DCs showed much less macropinocytosis in 2D and 3D, whereas the Wasp KO DCs showed an increase in macropinocytosis in both environments. Contrary to our expectations, both lines showed an increase from 2D to 3D (data not shown). As mentioned earlier, we encountered technical challenges with the immature DCs, as it was very difficult to identify the right time point where there were not too many spontaneously mature DCs in the cell culture. Therefore, we cannot be sure whether our observations in MCs may also apply to immature DCs, as suggested by the data of Vargas et al. [239].

Previous publications showed that the environment can influence actin polymerisation. Davidson and Wood showed that MCs in *Drosophila* embryos use Arp2/3 mediated actin polymerisation for phagocytosis in an unconfined environment, but switch to fomin mediated actin polymerisation when spatially confined [55]. This may again suggest that macropinocytosis and phagocytosis are antagonistic: while macropinocytosis uses formins in 2D environments, it switches to Arp2/3 in 3D. Antagonistically, phagocytosis may use Arp2/3 in 2D and may switches to formins in more confined situations.

5.2.5 *Macropinocytosis and membrane tension*

Finally, we investigated how membrane tension affects macropinocytosis. Since actin is directly linked to the cell membrane by membrane-to-cortex attachment, the force generated by actin can be transmitted to the cell membrane [58]. We therefore wondered how the change in actin polymerisation affects membrane tension. There are two views on the relationship between macropinocytosis and membrane tension. Traditionally, it is thought that macropinocytosis requires lower membrane tension because cells in this situation need to generate less force to form membrane protrusions. More recent reports show that higher membrane tension can induce macropinocytosis [146].

We used our micropatterns to measure membrane tension, as we had demonstrated that less adhesive cells perform more macropinocytosis. We observed a negative correlation between adhesive area and membrane tension (see Figure 18). Cells with a high adhesive area on unpatterned surfaces showed the lowest membrane tension, whereas cells confined to a single 1.5 µm adhesive spot showed the highest membrane tension. Focusing on membrane tension on a single cell, we also observed higher membrane tension in areas where the cell tends to show higher membrane dynamics. In the 2D cells, these areas are the

lamellipodia, whereas in the more 3D cells with low adhesion, the entire cell membrane showed high activity and tension.

Our data therefore support the observations of Lin and Liu, who observed higher membrane tension in stretched myotubes [146], and the computational model of Lutton et al. [155], which predicts that higher membrane tension is required to close macropinomes. However, as we observed higher membrane tension specifically in the areas of higher macropinocytosis, we wondered whether the high membrane tension actually causes macropinocytosis, or whether the higher membrane tension is rather the result of increased actin dynamics in the case of higher macropinocytosis.

To answer this question, we performed inhibitor experiments. As we had previously shown, both jasplakinolide and EIPA are effective in reducing fluid uptake (see Figures 3b., 7c., d.). To our surprise, we observed completely opposite effects on membrane tension with these two inhibitors (see Figure 18). Jasplakinolide treatment decreased membrane tension, whereas EIPA increased membrane tension. This demonstrates that although the effect on fluid uptake is comparable, the mode of action of the two inhibitors is completely different. Since jasplakinolide is known to force actin polymerisation and stabilise existing F-actin filaments [34], it appears that the loss of controlled actin polymerisation and depolymerisation reduces membrane tension. This suggests that not only controlled actin polymerisation but also depolymerisation is required for the proper function of macropinocytosis.

It also indicates that actin activity and subsequent increased macropinocytosis activity may indeed be the reason for the increased membrane tension, in contrast to the findings of Lutton et al. [155] who argued that the higher membrane tension increased macropinocytosis. However, if this is true, the question remains why EIPA increases membrane tension. EIPA is also thought to interfere with actin polymerisation by lowering the intracellular pH and thereby preventing Rac1 and Cdc42 signalling [125]. As the NHE is also closely related to intracellular water homeostasis [229], a possible explanation for the different behaviour of EIPA could be additional effects on intracellular water homeostasis by EIPA treatment. Roffay et al. investigated the correlation between cell volume and membrane tension in EIPA-treated cells when the cells were treated with hypotonic or hypertonic solutions [205]. They observed a complete decoupling of membrane tension and cell volume when EIPA treated cells were additionally treated with hypotonic solution [205]. In contrast, they show a normal response to hypertonic solutions with a coupled loss of cell volume and membrane tension [205]. The explanation for this behavior is that EIPA-treated cells have a higher initial volume [205]. This leads to an almost complete unfolding of the cell membrane already in the isotonic environment [205]. When these cells are treated with hypotonic solution, there is little residual membrane left to unfold, limiting the potential increase in membrane tension [205].

If this is true, higher membrane tension would be the result of increased fluid influx due to EIPA treatment, leading to an increase in volume. This model would

also provide an additional explanation for the effect of EIPA on macropinocytosis. The lack of residual membrane combined with the high membrane tension could prevent cells from forming ruffles because the energy demand is too high and no membrane is available for ruffling.

Actin dynamics and membrane tension are known to be linked through the membrane cortex complex [220]. The cortex is a structure consisting of actin filaments and myosin II [220]. These parts are all interconnected and can generate forces. The actin filaments in the cortex can be linked directly to membrane proteins or indirectly to the membrane via membrane-to-cortex proteins [220]. This allows the force generated by the cortex to be transmitted onto the cell membrane [220].

However, the cortex is not only important for the generation of forces by membrane tension, but also for the transmission of forces. De Belly et al. showed that local force transmission on the cell membrane by tether pulling only changes the membrane tension locally, while there are no global changes across the entire cell membrane [58]. Only when the actin cortex was disrupted by latrunculin B in combination with osmotic shock, the authors were able to observe global changes in membrane tension [58]. This demonstrates that the actin cortex dampens external forces applied to the cell membrane. At the same time, they observed global changes in membrane tension when they induced the formation of protusions locally with photoinducible Rac1 [58]. This observation shows that the local force generated by actin polymerisation is transmitted through the cortex, leading to global changes in membrane tension [58].

This model can be easily transferred to our model of macropinocytosis. In a low adhesive environment, cells can form more Arp2/3-mediated membrane ruffles, leading to increased fluid uptake via macropinocytosis. This increased ruffling activity should lead to a global increase in membrane tension according to the model proposed by De Belly et al. [58]. This supports our argument that increased macropinocytosis induces increased membrane tension.

In summary, we have shown that macropinocytosis is increased in more physiological 3D environments compared to cells adhering to highly adhesive 2D surfaces. We were able to show that this increase is not the result of cell confinement, but of reduced adhesiveness in 3D environments. This reduced adhesiveness induces a switch from fomin-mediated linear actin polymerisation to Arp2/3-mediated actin branching. This switch results in increased membrane dynamics. The interaction of actin with the cell membrane via membrane-cortex attachment increases membrane tension both locally and globally. The increase in macropinocytosis and membrane tension is closely linked to actin dynamics and can be disrupted by perturbing actin dynamics and further increasing membrane tension.

Since the main function of macropinocytosis is to sample the environment for pathogens, the question arises how immune cells can benefit from increased macropinocytosis when they are less adhesive. We propose that there are certain situations *in vivo* in which cells experience, at least in part, lower adhesion. One

of these situations could be in the subcapsular sinus of the lymph nodes. At this location, subcapsular sinus MCs and resident subcapsular sinus DCs have to sample the incoming lymph fluid for pathogens. They perform this sampling by extending protrusions through the epithelial layer into the lymph fluid [102, 154]. We propose that these protrusions extending into the lymphatic fluid are less adhesive, thereby increasing their sampling capacity via macropinocytosis.

A similar situation could occur in the intestine. MCs and DCs in the intestine can form transepithelial dendrites through the intestinal epithelium to sample the intestinal lumen for pathogens [38, 48, 68]. Our *in vitro* observations thus may explain phenotypes observed *in vivo*. To the best of our knowledge, macropinocytosis has not been quantified in these situations. It would therefore be interesting to combine macropinocytosis and membrane tension measurements *in vivo*. If our hypothesis is correct, we would expect to observe higher rates of macropinocytosis when protrusions enter the lumen, accompanied by an increase in membrane tension. Unfortunately, *in vivo* imaging of macropinocytosis and membrane tension is challenging.

5.3 CONCLUSIONS

In conclusion, we were able to perform a genome-wide CRISPR KO screen for macropinocytosis. With this screen, we identified three novel candidate genes not previously implicated in macropinocytosis. Adgre1 and Pilra are potential candidates for negative regulation of macropinocytosis while Lrch2 could be a potential positive regulator. It will be interesting to validate these candidates and elucidate the mechanism by which they may regulate macropinocytosis.

In the second part of the project, we demonstrated that macropinocytosis is increased when immune cells are located in 3D environments. This effect is not due to confinement but is caused by reduced cell adhesion in 3D environments. The increase in macropinocytosis is associated with a switch from formin-mediated actin polymerisation on the 2D surface to Arp2/3-mediated actin branching inside 3D environments. Finally, we demonstrated that increased actin dynamics, which facilitate the formation of more membrane ruffles, increase membrane tension locally and globally.

Our results highlight the necessity of taking the environment into account when studying macropinocytosis as we were able to show that there are mechanistic differences between macropinocytosis in more physiological 3D environments and less physiological highly adhesive 2D surfaces. This may have implications for research in the field of cancer treatment, as macropinocytosis is a major feeding mechanism for growing tumours, and immune surveillance, as antigen-presenting cells use macropinocytosis to sample their environment.

Our results may also explain how immune cells can increase their sampling efficiency in specific physiological situations. For example, in the intestine and lymph nodes DCs and MCs are known to extend protrusions through epithelial layers to sample for pathogens and antigens. In these situations, the protrusions

extending into the fluid-filled space could be less adhesive, which according to our model, could increase the sampling rate by macropinocytosis.

So far, we have observed the effect of increased macropinocytosis in 3D environments in MCs, immature DCs and 4T1 breast cancer cells. As we used MC to unravel the mechanistic details, it will be interesting to investigate the mechanism we have uncovered in other cell types to see if these are general mechanisms or MC-specific effects.

BIBLIOGRAPHY

[1] Atp6v1e1 atpase h+ transporting v1 subunit e1 [homo sapiens (human)]. https://www.ncbi.nlm.nih.gov/gene/529#gene-expression. Accessed: 2023-10-27.

[2] Caveolin-mediated endocytosis of virus by host. https://viralzone.expasy.org/976. Accessed: 2023-10-11.

[3] Clathrin-mediated endocytosis of virus by host. https://viralzone.expasy.org/957. Accessed: 2023-10-11.

[4] Mark3 gene - microtubule affinity regulating kinase 3. https://www.genecards.org/cgi-bin/carddisp.pl?gene=MARK3&keywords=Mark3. Accessed: 2023-10-27.

[5] Q14246 · agre1_human. https://www.uniprot.org/uniprotkb/Q14246/entry#function. Accessed: 2023-10-27.

[6] Q8td57 · dyh3_human. https://www.uniprot.org/uniprotkb/Q8TD57/entry#function. Accessed: 2023-10-27.

[7] String analysis lrch2. https://string-db.org/cgi/network?taskId=b5DWym7dFRWF&sessionId=bescgcTY5EwH. Accessed: 2023-11-18.

[8] String analysis pilra. https://string-db.org/cgi/network?taskId=bRtO8UVn933J&sessionId=bescgcTY5EwH. Accessed: 2023-11-18.

[9] R. Akter, K. Kim, H. Y. Kwon, Y. Kim, Y. W. Eom, H.-m. Cho, and M.-Y. Cho. Emr1/adgre1 expression in cancer cells upregulated by tumor-associated macrophages is related to poor prognosis in colorectal cancer. *Biomedicines*, 10(12):3121, 2022.

[10] K. M. O. Alblazi and C. H. Siar. Cellular protrusions-lamellipodia, filopodia, invadopodia and podosomes-and their roles in progression of orofacial tumours: current understanding. *Asian Pacific Journal of Cancer Prevention*, 16(6):2187–2191, 2015.

[11] P. Aleksandrowicz, A. Marzi, N. Biedenkopf, N. Beimforde, S. Becker, T. Hoenen, H. Feldmann, and H.-J. Schnittler. Ebola virus enters host cells by macropinocytosis and clathrin-mediated endocytosis. *The Journal of Infectious Diseases*, 204(suppl_3):S957–S967, 2011.

[12] M. R. Amieva and H. Furthmayr. Subcellular localization of moesin in dynamic filopodia, retraction fibers, and other structures involved in substrate

exploration, attachment, and cell-cell contacts. *Experimental Cell Research*, 219(1):180–196, 1995.

[13] J. V. V. Arafiles, H. Hirose, M. Akishiba, S. Tsuji, M. Imanishi, and S. Futaki. Stimulating macropinocytosis for intracellular nucleic acid and protein delivery: A combined strategy with membrane-lytic peptides to facilitate endosomal escape. *Bioconjugate Chemistry*, 31(3):547–553, 2020.

[14] J. V. V. Arafiles, H. Hirose, Y. Hirai, M. Kuriyama, M. M. Sakyiamah, W. Nomura, K. Sonomura, M. Imanishi, A. Otaka, H. Tamamura, et al. Discovery of a macropinocytosis-inducing peptide potentiated by medium-mediated intramolecular disulfide formation. *Angewandte Chemie*, 133(21):12035–12043, 2021.

[15] P. Aravamudhan, K. Raghunathan, J. Konopka-Anstadt, A. Pathak, D. M. Sutherland, B. D. Carter, and T. S. Dermody. Reovirus uses macropinocytosis-mediated entry and fast axonal transport to infect neurons. *PLOS Pathogens*, 16(2):e1008380, 2020.

[16] J. Babitt, B. Trigatti, A. Rigotti, E. J. Smart, R. W. Anderson, S. Xu, and M. Krieger. Murine sr-bi, a high density lipoprotein receptor that mediates selective lipid uptake, is n-glycosylated and fatty acylated and colocalizes with plasma membrane caveolae. *Journal of Biological Chemistry*, 272(20):13242–13249, 1997.

[17] E. Bae, P. Huang, G. Müller-Greven, D. Hambardzumyan, A. E. Sloan, A. S. Nowacki, N. Marko, C. R. Carlin, and C. L. Gladson. Integrin $\alpha 3\beta 1$ promotes vessel formation of glioblastoma-associated endothelial cells through calcium-mediated macropinocytosis and lysosomal exocytosis. *Nature Communications*, 13(1):4268, 2022.

[18] T. Bhattacharjee and T. E. Angelini. 3d t cell motility in jammed microgels. *Journal of Physics D: Applied Physics*, 52(2):024006, 2018.

[19] A. Biswas, P. Kashyap, S. Datta, T. Sengupta, and B. Sinha. Cholesterol depletion by mβcd enhances cell membrane tension and its variations-reducing integrity. *Biophysical Journal*, 116(8):1456–1468, 2019.

[20] S. Biswas, M. Adrian, K. Evdokimov, K. Schledzewski, J. Weber, M. Winkler, S. Goerdt, and C. Géraud. Counter-regulation of the ligand-receptor pair leda-1/pianp and pilrα during the lps-mediated immune response of murine macrophages. *Biochemical and Biophysical Research Communications*, 464(4):1078–1083, 2015.

[21] V. Bitsikas, I. R. Corrêa Jr, and B. J. Nichols. Clathrin-independent pathways do not contribute significantly to endocytic flux. *eLife*, 3:e03970, 2014.

[22] E. Blanchard, S. Belouzard, L. Goueslain, T. Wakita, J. Dubuisson, C. Wychowski, and Y. Rouillé. Hepatitis c virus entry depends on clathrin-mediated endocytosis. *Journal of Virology*, 80(14):6964–6972, 2006.

[23] G. Bloomfield, D. Traynor, S. P. Sander, D. M. Veltman, J. A. Pachebat, and R. R. Kay. Neurofibromin controls macropinocytosis and phagocytosis in *Dictyostelium*. *eLife*, 4:e04940, 2015.

[24] P. Bohley and P. Seglen. Proteases and proteolysis in the lysosome. *Experientia*, 48:151–157, 1992.

[25] G. Bollag, D. W. Clapp, S. Shih, F. Adler, Y. Y. Zhang, P. Thompson, B. J. Lange, M. H. Freedman, F. McCormick, T. Jacks, et al. Loss of nf1 results in activation of the ras signaling pathway and leads to aberrant growth in haematopoietic cells. *Nature Genetics*, 12(2):144–148, 1996.

[26] C. Bollensdorff, T. Zimmer, and K. Benndorf. Amiloride derivatives are potent blockers of k atp channels. *Naunyn-Schmiedeberg's Archives of Pharmacology*, 364:351–358, 2001.

[27] S. BoseDasgupta and J. Pieters. Inflammatory stimuli reprogram macrophage phagocytosis to macropinocytosis for the rapid elimination of pathogens. *PLOS Pathogens*, 10(1):e1003879, 2014.

[28] J. Boumelha, P. Romero-Clavijo, S. de Carné, M. Molina-Arcas, and J. Downward. In vivo crispr screening identifies mediators of immune evasion in kras-mutant lung cancer. *Cancer Research*, 82(12_Supplement):1352–1352, 2022.

[29] N. Briand, I. Dugail, and S. Le Lay. Cavin proteins: New players in the caveolae field. *Biochimie*, 93(1):71–77, 2011.

[30] E. K. Brinkman, T. Chen, M. Amendola, and B. Van Steensel. Easy quantitative assessment of genome editing by sequence trace decomposition. *Nucleic Acids Research*, 42(22):e168–e168, 2014.

[31] S. Brode and P. A. Macary. Cross-presentation: dendritic cells and macrophages bite off more than they can chew! *Immunology*, 112(3):345–351, 2004.

[32] U. Brunk, J. Schellens, and B. Westermark. Influence of epidermal growth factor (egf) on ruffling activity, pinocytosis and proliferation of cultivated human glia cells. *Experimental Cell Research*, 103(2):295–302, 1976.

[33] K. L. Bryant, J. D. Mancias, A. C. Kimmelman, and C. J. Der. Kras: feeding pancreatic cancer proliferation. *Trends in Biochemical Sciences*, 39(2):91–100, 2014.

[34] M. R. Bubb, A. Senderowicz, E. A. Sausville, K. Duncan, and E. D. Korn. Jasplakinolide, a cytotoxic natural product, induces actin polymerization and competitively inhibits the binding of phalloidin to f-actin. *Journal of Biological Chemistry*, 269(21):14869–14871, 1994.

[35] J. T. Bulcha, Y. Wang, H. Ma, P. W. Tai, and G. Gao. Viral vector platforms within the gene therapy landscape. *Signal Transduction and Targeted Therapy*, 6(1):53, 2021.

[36] S. Buracco, S. Claydon, and R. Insall. Control of actin dynamics during cell motility. *F1000Research*, 8, 2019.

[37] J. Canton, D. Schlam, C. Breuer, M. Gütschow, M. Glogauer, and S. Grinstein. Calcium-sensing receptors signal constitutive macropinocytosis and facilitate the uptake of nod2 ligands in macrophages. *Nature Communications*, 7(1):11284, 2016.

[38] V. Cerovic, C. C. Bain, A. M. Mowat, and S. W. Milling. Intestinal macrophages and dendritic cells: what's the difference? *Trends in Immunology*, 35(6):270–277, 2014.

[39] S. Chakraborty, M. Doktorova, T. R. Molugu, F. A. Heberle, H. L. Scott, B. Dzikovski, M. Nagao, L.-R. Stingaciu, R. F. Standaert, F. N. Barrera, et al. How cholesterol stiffens unsaturated lipid membranes. *Proceedings of the National Academy of Sciences*, 117(36):21896–21905, 2020.

[40] Y.-Y. Chang, J. Enninga, and V. Stévenin. New methods to decrypt emerging macropinosome functions during the host–pathogen crosstalk. *Cellular Microbiology*, 23(7):e13342, 2021.

[41] Y.-Y. Chang, V. Stévenin, M. Duchateau, Q. Giai Gianetto, V. Hourdel, C. D. Rodrigues, M. Matondo, N. Reiling, and J. Enninga. Shigella hijacks the exocyst to cluster macropinosomes for efficient vacuolar escape. *PLOS Pathogens*, 16(8):e1008822, 2020.

[42] G. Charras and E. Sahai. Physical influences of the extracellular environment on cell migration. *Nature Reviews Molecular Cell Biology*, 15(12):813–824, 2014.

[43] C. Chaudhury, S. Mehnaz, J. M. Robinson, W. L. Hayton, D. K. Pearl, D. C. Roopenian, and C. L. Anderson. The major histocompatibility complex–related fc receptor for igg (fcrn) binds albumin and prolongs its lifespan. *Journal of Experimental Medicine*, 197(3):315–322, 2003.

[44] A. Chavez, J. Scheiman, S. Vora, B. W. Pruitt, M. Tuttle, E. PR Iyer, S. Lin, S. Kiani, C. D. Guzman, D. J. Wiegand, et al. Highly efficient cas9-mediated transcriptional programming. *Nature Methods*, 12(4):326–328, 2015.

[45] T. Chaya, R. Tsutsumi, L. R. Varner, Y. Maeda, S. Yoshida, and T. Furukawa. Cul3-klhl18 ubiquitin ligase modulates rod transducin translocation during light-dark adaptation. *The EMBO Journal*, 38(23):e101409, 2019.

[46] G. Chen, L. Han, S. Tan, X. Jia, H. Wu, Y. Quan, Q. Zhang, B. Yu, Z. Hu, K. Xia, et al. Loss-of-function of kmt5b leads to neurodevelopmental disorder and impairs neuronal development and neurogenesis. *Journal of Genetics and Genomics*, 49(9):881–890, 2022.

[47] Z. Chen, D. Zhao, B. Liu, G. Nian, X. Li, J. Yin, S. Qu, and W. Yang. 3d printing of multifunctional hydrogels. *Advanced Functional Materials*, 29(20):1900971, 2019.

[48] M. Chieppa, M. Rescigno, A. Y. Huang, and R. N. Germain. Dynamic imaging of dendritic cell extension into the small bowel lumen in response to epithelial cell tlr engagement. *Journal of Experimental Medicine*, 203(13):2841–2852, 2006.

[49] J. Chu and M. Ng. Infectious entry of west nile virus occurs through a clathrin-mediated endocytic pathway. *Journal of Virology*, 78(19):10543–10555, 2004.

[50] C. Commisso, S. M. Davidson, R. G. Soydaner-Azeloglu, S. J. Parker, J. J. Kamphorst, S. Hackett, E. Grabocka, M. Nofal, J. A. Drebin, C. B. Thompson, et al. Macropinocytosis of protein is an amino acid supply route in ras-transformed cells. *Nature*, 497(7451):633–637, 2013.

[51] N. D. Condon, J. M. Heddleston, T.-L. Chew, L. Luo, P. S. McPherson, M. S. Ioannou, L. Hodgson, J. L. Stow, and A. A. Wall. Macropinosome formation by tent pole ruffling in macrophages. *Journal of Cell Biology*, 217(11):3873–3885, 2018.

[52] T. Czerwinski, L. Bischof, D. Böhringer, S. Kara, E. Wittmann, A. Winterl, R. Gerum, G. Nusser, M. Wiesinger, S. Budday, et al. Immune cells employ traction forces to overcome steric hindrance in 3d biopolymer networks. *BioRxiv*, pages 2023–04, 2023.

[53] J. Daecke, O. T. Fackler, M. T. Dittmar, and H.-G. Kräusslich. Involvement of clathrin-mediated endocytosis in human immunodeficiency virus type 1 entry. *Journal of Virology*, 79(3):1581–1594, 2005.

[54] J. A. Daniel, N. Chau, M. K. Abdel-Hamid, L. Hu, L. von Kleist, A. Whiting, S. Krishnan, P. Maamary, S. R. Joseph, F. Simpson, et al. Phenothiazine-derived antipsychotic drugs inhibit dynamin and clathrin-mediated endocytosis. *Traffic*, 16(6):635–654, 2015.

[55] A. J. Davidson and W. Wood. Macrophages use distinct actin regulators to switch engulfment strategies and ensure phagocytic plasticity in vivo. *Cell Reports*, 31(8):107692, 2020.

[56] S. M. Davidson, O. Jonas, M. A. Keibler, H. W. Hou, A. Luengo, J. R. Mayers, J. Wyckoff, A. M. Del Rosario, M. Whitman, C. R. Chin, et al. Direct evidence for cancer-cell-autonomous extracellular protein catabolism in pancreatic tumors. *Nature Medicine*, 23(2):235–241, 2017.

[57] P. F. Davies and R. Ross. Mediation of pinocytosis in cultured arterial smooth muscle and endothelial cells by platelet-derived growth factor. *Journal of Cell Biology*, 79(3):663–671, 1978.

[58] H. De Belly, S. Yan, H. B. da Rocha, S. Ichbiah, J. P. Town, P. J. Zager, D. C. Estrada, K. Meyer, H. Turlier, C. Bustamante, et al. Cell protrusions and contractions generate long-range membrane tension propagation. *Cell*, 2023.

[59] H. Delanoe-Ayari, R. Al Kurdi, M. Vallade, D. Gulino-Debrac, and D. Riveline. Membrane and acto-myosin tension promote clustering of adhesion proteins. *Proceedings of the National Academy of Sciences*, 101(8):2229–2234, 2004.

[60] K. A. DeMali, K. Wennerberg, and K. Burridge. Integrin signaling to the actin cytoskeleton. *Current Opinion in Cell Biology*, 15(5):572–582, 2003.

[61] H.-X. Deng, Y. Shi, Y. Yang, K. B. Ahmeti, N. Miller, C. Huang, L. Cheng, H. Zhai, S. Deng, K. Nuytemans, et al. Identification of tmem230 mutations in familial parkinson's disease. *Nature Genetics*, 48(7):733–739, 2016.

[62] J. G. Doench. Am i ready for crispr? a user's guide to genetic screens. *Nature Reviews Genetics*, 19(2):67–80, 2018.

[63] J. A. Dubland and G. A. Francis. Lysosomal acid lipase: at the crossroads of normal and atherogenic cholesterol metabolism. *Frontiers in Cell and Developmental Biology*, 3:3, 2015.

[64] Y. Egami and N. Araki. Dynamic changes in the spatiotemporal localization of rab21 in live raw264 cells during macropinocytosis. *PLOS ONE*, 4(8):e6689, 2009.

[65] Y. Egami, T. Taguchi, M. Maekawa, H. Arai, and N. Araki. Small gtpases and phosphoinositides in the regulatory mechanisms of macropinosome formation and maturation. *Frontiers in Physiology*, 5:374, 2014.

[66] C. J. Empig and M. A. Goldsmith. Association of the caveola vesicular system with cellular entry by filoviruses. *Journal of Virology*, 76(10):5266–5270, 2002.

[67] Y.-L. Fan, N.-Y. Zhang, D.-Y. Hou, Y. Hao, R. Zheng, J. Yang, Z. Fan, H.-W. An, and H. Wang. Programmable peptides activated macropinocytosis for direct cytosolic delivery. *Advanced Healthcare Materials*, page 2301162, 2023.

[68] J. Farache, I. Koren, I. Milo, I. Gurevich, K.-W. Kim, E. Zigmond, G. C. Furtado, S. A. Lira, and G. Shakhar. Luminal bacteria recruit cd103+ dendritic cells into the intestinal epithelium to sample bacterial antigens for presentation. *Immunity*, 38(3):581–595, 2013.

[69] T. Fischer, A. Hayn, and C. T. Mierke. Fast and reliable advanced two-step pore-size analysis of biomimetic 3d extracellular matrix scaffolds. *Scientific Reports*, 9(1):8352, 2019.

[70] R. S. Flannagan, V. Jaumouillé, and S. Grinstein. The cell biology of phagocytosis. *Annual Review of Pathology: Mechanisms of Disease*, 7:61–98, 2012.

[71] N. Fournier, L. Chalus, I. Durand, E. Garcia, J. J. Pin, T. Churakova, S. Patel, C. Zlot, D. Gorman, S. Zurawski, J. Abrams, E. E. Bates, and P. Garrone. Fdf03, a novel inhibitory receptor of the immunoglobulin superfamily, is expressed by human dendritic and myeloid cells. *Journal of immunology (Baltimore, Md. : 1950)*, 165(3):1197–1209, 2000.

[72] N. Fournier, L. Chalus, I. Durand, E. Garcia, J.-J. Pin, T. Churakova, S. Patel, C. Zlot, D. Gorman, S. Zurawski, et al. Fdf03, a novel inhibitory receptor of the immunoglobulin superfamily, is expressed by human dendritic and myeloid cells. *The Journal of Immunology*, 165(3):1197–1209, 2000.

[73] H. Foussard, P. Ferrer, P. Valenti, C. Polesello, S. Carreno, and F. Payre. Lrch proteins: a novel family of cytoskeletal regulators. *PLOS ONE*, 5(8):e12257, 2010.

[74] S. Freeman, R. Cai, X. Chen, and X. Huang. Automechanical gating of piezo1 triggers the fusogenic steps in macropinocytosis. *Research Square*, 2022.

[75] J. E. Frith, R. J. Mills, J. E. Hudson, and J. J. Cooper-White. Tailored integrin–extracellular matrix interactions to direct human mesenchymal stem cell differentiation. *Stem Cells and Development*, 21(13):2442–2456, 2012.

[76] M. Gabi, A. Larmagnac, P. Schulte, and J. Vörös. Electrically controlling cell adhesion, growth and migration. *Colloids and Surfaces B: Biointerfaces*, 79(2):365–371, 2010.

[77] K. M. Galenkamp, C. M. Galapate, Y. Zhang, and C. Commisso. Automated imaging and analysis for the quantification of fluorescently labeled macropinosomes. *Journal of Visualized Experiments*, (174):e62828, 2021.

[78] B. E. Garcia-Perez, R. Mondragon-Flores, and J. Luna-Herrera. Internalization of mycobacterium tuberculosis by macropinocytosis in non-phagocytic cells. *Microbial Pathogenesis*, 35(2):49–55, 2003.

[79] P. Ghoshal, B. Singla, H. Lin, M. Cherian-Shaw, R. Tritz, C. A. Padgett, F. Hudson, H. Zhang, B. K. Stansfield, and G. Csányi. Loss of gtpase activating protein neurofibromin stimulates paracrine cell communication via macropinocytosis. *Redox Biology*, 27:101224, 2019.

[80] P. M. Gilbert, K. L. Havenstrite, K. E. Magnusson, A. Sacco, N. A. Leonardi, P. Kraft, N. K. Nguyen, S. Thrun, M. P. Lutolf, and H. M. Blau. Substrate elasticity regulates skeletal muscle stem cell self-renewal in culture. *Science*, 329(5995):1078–1081, 2010.

[81] B. L. Goode and M. J. Eck. Mechanism and function of formins in the control of actin assembly. *Annual Review of Biochemistry*, 76:593–627, 2007.

[82] S. Greenberg and S. Grinstein. Phagocytosis and innate immunity. *Current Opinion in Immunology*, 14(1):136–145, 2002.

[83] N. Groulx, F. Boudreault, S. N. Orlov, and R. Grygorczyk. Membrane reserves and hypotonic cell swelling. *The Journal of Membrane Biology*, 214:43–56, 2006.

[84] Z. Gu, E. H. Noss, V. W. Hsu, and M. B. Brenner. Integrins traffic rapidly via circular dorsal ruffles and macropinocytosis during stimulated cell migration. *Journal of Cell Biology*, 193(1):61–70, 2011.

[85] C. Gundu, V. K. Arruri, P. Yadav, U. Navik, A. Kumar, V. S. Amalkar, A. Vikram, and R. R. Gaddam. Dynamin-independent mechanisms of endocytosis and receptor trafficking. *Cells*, 11(16):2557, 2022.

[86] U. Hacker, R. Albrecht, and M. Maniak. Fluid-phase uptake by macropinocytosis in dictyostelium. *Journal of Cell Science*, 110(2):105–112, 1997.

[87] Y. Harada, Y. Tanaka, M. Terasawa, M. Pieczyk, K. Habiro, T. Katakai, K. Hanawa-Suetsugu, M. Kukimoto-Niino, T. Nishizaki, M. Shirouzu, et al. Dock8 is a cdc42 activator critical for interstitial dendritic cell migration during immune responses. *Blood*, 119(19):4451–4461, 2012.

[88] J. R. Henley, E. W. Krueger, B. J. Oswald, and M. A. McNiven. Dynamin-mediated internalization of caveolae. *Journal of Cell Biology*, 141(1):85–99, 1998.

[89] B. Hernaez and C. Alonso. Dynamin-and clathrin-dependent endocytosis in african swine fever virus entry. *Journal of Virology*, 84(4):2100–2109, 2010.

[90] M. M. Hill, M. Bastiani, R. Luetterforst, M. Kirkham, A. Kirkham, S. J. Nixon, P. Walser, D. Abankwa, V. M. Oorschot, S. Martin, et al. Ptrf-cavin, a conserved cytoplasmic protein required for caveola formation and function. *Cell*, 132(1):113–124, 2008.

[91] E. Hoijman, H.-M. Häkkinen, Q. Tolosa-Ramon, S. Jimenez-Delgado, C. Wyatt, M. Miret-Cuesta, M. Irimia, A. Callan-Jones, S. Wieser, and V. Ruprecht. Cooperative epithelial phagocytosis enables error correction in the early embryo. *Nature*, 590(7847):618–623, 2021.

[92] G. Honda, N. Saito, T. Fujimori, H. Hashimura, M. J. Nakamura, A. Nakajima, and S. Sawai. Microtopographical guidance of macropinocytic signaling patches. *Proceedings of the National Academy of Sciences*, 118(50):e2110281118, 2021.

[93] M. Hörning and T. Shibata. Three-dimensional cell geometry controls excitable membrane signaling in *Dictyostelium* cells. *Biophysical Journal*, 116(2):372–382, 2019.

[94] D. Humphreys, V. Singh, and V. Koronakis. Inhibition of wave regulatory complex activation by a bacterial virulence effector counteracts pathogen phagocytosis. *Cell reports*, 17(3):697–707, 2016.

[95] A. Huttenlocher and A. R. Horwitz. Integrins in cell migration. *Cold Spring Harbor Perspectives in Biology*, 3(9):a005074, 2011.

[96] D. S. Hwang, S. B. Sim, and H. J. Cha. Cell adhesion biomaterial based on mussel adhesive protein fused with rgd peptide. *Biomaterials*, 28(28):4039–4046, 2007.

[97] M. Innocenti. Investigating mammalian formins with smifh2 fifteen years in: Novel targets and unexpected biology. *International Journal of Molecular Sciences*, 24(10):9058, 2023.

[98] R. Insall, A. Müller-Taubenberger, L. Machesky, J. Köhler, E. Simmeth, S. J. Atkinson, I. Weber, and G. Gerisch. Dynamics of the dictyostelium arp2/3 complex in endocytosis, cytokinesis, and chemotaxis. *Cytoskeleton*, 50(3):115–128, 2001.

[99] M. Isshiki, J. Ando, R. Korenaga, H. Kogo, T. Fujimoto, T. Fujita, and A. Kamiya. Endothelial ca2+ waves preferentially originate at specific loci in caveolin-rich cell edges. *Proceedings of the National Academy of Sciences*, 95(9):5009–5014, 1998.

[100] A. I. Ivanov. *Pharmacological Inhibition of Endocytic Pathways: Is It Specific Enough to Be Useful?*, pages 15–33. Humana Press, Totowa, NJ, 2008.

[101] A. I. Ivanov, A. Nusrat, and C. A. Parkos. Endocytosis of epithelial apical junctional proteins by a clathrin-mediated pathway into a unique storage compartment. *Molecular Biology of the Cell*, 15(1):176–188, 2004.

[102] S. Jalkanen and M. Salmi. Lymphatic endothelial cells of the lymph node. *Nature Reviews Immunology*, 20(9):566–578, 2020.

[103] H.-K. Jang, B. Song, G.-H. Hwang, and S. Bae. Current trends in gene recovery mediated by the crispr-cas system. *Experimental & Molecular Medicine*, 52(7):1016–1027, 2020.

[104] V. Jayashankar and A. L. Edinger. Macropinocytosis confers resistance to therapies targeting cancer anabolism. *Nature Communications*, 11(1):1121, 2020.

[105] H.-H. Jeong, S. Y. Kim, M. W. Rousseaux, H. Y. Zoghbi, and Z. Liu. Crisprcloud: a secure cloud-based pipeline for crispr pooled screen deconvolution. *Bioinformatics*, 33(18):2963–2965, 2017.

[106] J. Jiang, A. L. Kolpak, and Z.-Z. Bao. Myosin iib isoform plays an essential role in the formation of two distinct types of macropinosomes. *Cytoskeleton*, 67(1):32–42, 2010.

[107] X. Jiang, Y. Xu, H. Ren, J. Jiang, M. Wudu, Q. Wang, J. Guan, H. Su, Y. Zhang, B. Zhang, et al. Klhl18 inhibits the proliferation, migration, and invasion of non-small cell lung cancer by inhibiting pi3k/pd-l1 axis activity. *Cell & Bioscience*, 10(1):1–15, 2020.

[108] M. Jinek, K. Chylinski, I. Fonfara, M. Hauer, J. A. Doudna, and E. Charpentier. A programmable dual-rna–guided dna endonuclease in adaptive bacterial immunity. *Science*, 337(6096):816–821, 2012.

[109] J. Joung, S. Konermann, J. S. Gootenberg, O. O. Abudayyeh, R. J. Platt, M. D. Brigham, N. E. Sanjana, and F. Zhang. Genome-scale crispr-cas9 knockout and transcriptional activation screening. *Nature Protocols*, 12(4):828–863, 2017.

[110] A. Junemann, V. Filić, M. Winterhoff, B. Nordholz, C. Litschko, H. Schwellenbach, T. Stephan, I. Weber, and J. Faix. A diaphanous-related formin links ras signaling directly to actin assembly in macropinocytosis and phagocytosis. *Proceedings of the National Academy of Sciences*, 113(47):E7464–E7473, 2016.

[111] I. Jutras and M. Desjardins. Phagocytosis: at the crossroads of innate and adaptive immunity. *Annual Review of Cell and Developmental Biology*, 21:511–527, 2005.

[112] Y. Kagawa, S. Matsumoto, Y. Kamioka, K. Mimori, Y. Naito, T. Ishii, D. Okuzaki, N. Nishida, S. Maeda, A. Naito, et al. Cell cycle-dependent rho gtpase activity dynamically regulates cancer cell motility and invasion in vivo. *PLOS ONE*, 8(12):e83629, 2013.

[113] M. Kaksonen and A. Roux. Mechanisms of clathrin-mediated endocytosis. *Nature Reviews Molecular Cell Biology*, 19(5):313–326, 2018.

[114] M. Kaksonen and A. Roux. Mechanisms of clathrin-mediated endocytosis. *Nature Reviews Molecular Cell Biology*, 19(5):313–326, 2018.

[115] R. Kawamura, M. Mishima, S. Ryu, Y. Arai, M. Okose, Y. R. Silberberg, S. R. Rao, and C. Nakamura. Controlled cell adhesion using a biocompatible anchor for membrane-conjugated bovine serum albumin/bovine serum albumin mixed layer. *Langmuir*, 29(21):6429–6433, 2013.

[116] R. R. Kay. Macropinocytosis: biology and mechanisms. *Cells & Development*, 168:203713, 2021.

[117] A. Kendirli, C. de la Rosa, K. F. Lämmle, K. Eglseer, I. J. Bauer, V. Kavaka, S. Winklmeier, L. Zhuo, C. Wichmann, L. A. Gerdes, et al. A genome-wide in vivo crispr screen identifies essential regulators of t cell migration to the cns in a multiple sclerosis model. *Nature Neuroscience*, pages 1–13, 2023.

[118] B. G. Keselowsky, D. M. Collard, and A. J. García. Integrin binding specificity regulates biomaterial surface chemistry effects on cell differentiation. *Proceedings of the National Academy of Sciences*, 102(17):5953–5957, 2005.

[119] M. R. Ketterer, J. Q. Shao, D. B. Hornick, B. Buscher, V. K. Bandi, and M. A. Apicella. Infection of primary human bronchial epithelial cells by haemophilus influenzae: macropinocytosis as a mechanism of airway epithelial cell entry. *Infection and Immunity*, 67(8):4161–4170, 1999.

[120] J. T. Kim, C. Am Kim, K. Zhang, C. H. Jang, and H. J. Choi. Effect of polymer–surfactant interaction on its turbulent drag reduction. *Colloids and Surfaces A: Physicochemical and Engineering Aspects*, 391(1-3):125–129, 2011.

[121] S. M. Kim, T. T. Nguyen, A. Ravi, P. Kubiniok, B. T. Finicle, V. Jayashankar, L. Malacrida, J. Hou, J. Robertson, D. Gao, et al. Pten deficiency and ampk activation promote nutrient scavenging and anabolism in prostate cancer cells. *Cancer Discovery*, 8(7):866–883, 2018.

[122] K. Kitamura, N. Iguchi, Y. Kaneko, H. Tanaka, and Y. Nishimune. Characterization of a novel postacrosomal perinuclear theca-specific protein, cypt1. *Biology of Reproduction*, 71(6):1927–1935, 2004.

[123] S. Klapproth, F. A. Moretti, M. Zeiler, R. Ruppert, U. Breithaupt, S. Mueller, R. Haas, M. Mann, M. Sperandio, R. Fässler, et al. Minimal amounts of kindlin-3 suffice for basal platelet and leukocyte functions in mice. *Blood*, 126(24):2592–2600, 2015.

[124] M. Kohyama, S. Matsuoka, K. Shida, F. Sugihara, T. Aoshi, K. Kishida, K. J. Ishii, and H. Arase. Monocyte infiltration into obese and fibrilized tissues is regulated by pilrα. *European Journal of Immunology*, 46(5):1214–1223, 2016.

[125] M. Koivusalo, C. Welch, H. Hayashi, C. C. Scott, M. Kim, T. Alexander, N. Touret, K. M. Hahn, and S. Grinstein. Amiloride inhibits macropinocytosis by lowering submembranous ph and preventing rac1 and cdc42 signaling. *Journal of Cell Biology*, 188(4):547–563, 2010.

[126] Y.-i. KOYAMA, K. Norose-Toyoda, S. HIRANO, M. KOBAYASHI, T. EBIHARA, I. SOMEKI, H. FUJISAKI, and S. IRIE. Type i collagen is a nonadhesive extracellular matrix for macrophages. *Archives of Histology and Cytology*, 63(1):71–79, 2000.

[127] H. Kress, E. H. Stelzer, D. Holzer, F. Buss, G. Griffiths, and A. Rohrbach. Filopodia act as phagocytic tentacles and pull with discrete steps and a load-dependent velocity. *Proceedings of the National Academy of Sciences*, 104(28):11633–11638, 2007.

[128] S. Krishna, W. Palm, Y. Lee, W. Yang, U. Bandyopadhyay, H. Xu, O. Florey, C. B. Thompson, and M. Overholtzer. Pikfyve regulates vacuole maturation and nutrient recovery following engulfment. *Developmental Cell*, 38(5):536–547, 2016.

[129] J. Kroll, M. J. Ruiz-Fernandez, M. B. Braun, J. Merrin, and J. Renkawitz. Quantifying the probing and selection of microenvironmental pores by motile immune cells. *Current Protocols*, 2(4):e407, 2022.

[130] M. Kuriyama, H. Hirose, T. Masuda, M. Shudou, J. V. V. Arafiles, M. Imanishi, M. Maekawa, Y. Hara, and S. Futaki. Piezo1 activation using yoda1 inhibits macropinocytosis in a431 human epidermoid carcinoma cells. *Scientific Reports*, 12(1):6322, 2022.

[131] A. Lagana, J. Vadnais, P. Le, T. Nguyen, R. Laprade, I. Nabi, and J. Noel. Regulation of the formation of tumor cell pseudopodia by the na+/h+ exchanger nhe1. *Journal of Cell Science*, 113(20):3649–3662, 2000.

[132] P. Lajoie and I. Nabi. Regulation of raft-dependent endocytosis. *Journal of Cellular and Molecular Medicine*, 11(4):644–653, 2007.

[133] T. Lämmermann, B. L. Bader, S. J. Monkley, T. Worbs, R. Wedlich-Söldner, K. Hirsch, M. Keller, R. Förster, D. R. Critchley, R. Fässler, et al. Rapid leukocyte migration by integrin-independent flowing and squeezing. *Nature*, 453(7191):51–55, 2008.

[134] P. Lanzerstorfer, U. Müller, K. Gordiyenko, J. Weghuber, and C. M. Niemeyer. Highly modular protein micropatterning sheds light on the role of clathrin-mediated endocytosis for the quantitative analysis of protein-protein interactions in live cells. *Biomolecules*, 10(4):540, 2020.

[135] D. Laundon, B. T. Larson, K. McDonald, N. King, and P. Burkhardt. The architecture of cell differentiation in choanoflagellates and sponge choanocytes. *PLoS biology*, 17(4):e3000226, 2019.

[136] A. H. Le, T. Yelland, N. R. Paul, L. Fort, S. Nikolaou, S. Ismail, and L. M. Machesky. Cyri-a limits invasive migration through macropinosome formation and integrin uptake regulation. *Journal of Cell Biology*, 220(9):e202012114, 2021.

[137] A. Leithner, J. Renkawitz, I. De Vries, R. Hauschild, H. Häcker, and M. Sixt. Fast and efficient genetic engineering of hematopoietic precursor cells for the study of dendritic cell migration. *European Journal of Immunology*, 48(6):1074–1077, 2018.

[138] R. Levin, S. Grinstein, and D. Schlam. Phosphoinositides in phagocytosis and macropinocytosis. *Biochimica et Biophysica Acta (BBA) - Molecular and Cell Biology of Lipids*, 1851(6):805–823, 2015.

[139] W. Lewis. Pinocytosis. *John Hopkins Hosp. Bull.*, 1931.

[140] W. H. Lewis. Pinocytosis by malignant cells. *The American Journal of Cancer*, 29(4):666–679, 1937.

[141] L. Li, T. Wan, M. Wan, B. Liu, R. Cheng, and R. Zhang. The effect of the size of fluorescent dextran on its endocytic pathway. *Cell Biology International*, 39(5):531–539, 2015.

[142] W. Li, J. Köster, H. Xu, C.-H. Chen, T. Xiao, J. S. Liu, M. Brown, and X. S. Liu. Quality control, modeling, and visualization of crispr screens with mageck-vispr. *Genome Biology*, 16:1–13, 2015.

[143] W. Li, H. Xu, T. Xiao, L. Cong, M. I. Love, F. Zhang, R. A. Irizarry, J. S. Liu, M. Brown, and X. S. Liu. Mageck enables robust identification of essential genes from genome-scale crispr/cas9 knockout screens. *Genome Biology*, 15(12):1–12, 2014.

[144] J. P. Lim and P. A. Gleeson. Macropinocytosis: an endocytic pathway for internalising large gulps. *Immunology and cell biology*, 89(8):836–843, 2011.

[145] H.-H. Lin, D. E. Faunce, M. Stacey, A. Terajewicz, T. Nakamura, J. Zhang-Hoover, M. Kerley, M. L. Mucenski, S. Gordon, and J. Stein-Streilein. The macrophage f4/80 receptor is required for the induction of antigen-specific efferent regulatory t cells in peripheral tolerance. *Journal of Experimental Medicine*, 201(10):1615–1625, 2005.

[146] S.-S. Lin and Y.-W. Liu. Mechanical stretch induces mtor recruitment and activation at the phosphatidic acid-enriched macropinosome in muscle cell. *Frontiers in Cell and Developmental Biology*, 7:78, 2019.

[147] H. Liu, M. Sun, Z. Liu, C. Kong, W. Kong, J. Ye, J. Gong, D. C. Huang, and F. Qian. Kras-enhanced macropinocytosis and reduced fcrn-mediated recycling sensitize pancreatic cancer to albumin-conjugated drugs. *Journal of Controlled Release*, 296:40–53, 2019.

[148] H. Liu, L. Zhu, T. Dudiki, B. Gabanic, L. Good, E. A. Podrez, O. A. Cherepanova, J. Qin, and T. V. Byzova. Macrophage migration and phagocytosis are controlled by kindlin-3's link to the cytoskeleton. *The Journal of Immunology*, 204(7):1954–1967, 2020.

[149] Y.-J. Liu, M. Le Berre, F. Lautenschlaeger, P. Maiuri, A. Callan-Jones, M. Heuzé, T. Takaki, R. Voituriez, and M. Piel. Confinement and low adhesion induce fast amoeboid migration of slow mesenchymal cells. *Cell*, 160(4):659–672, 2015.

[150] Z. Liu, P. Che, J. J. Mercado, J. R. Hackney, G. K. Friedman, C. Zhang, Z. You, X. Zhao, Q. Ding, K. Kim, et al. Characterization of ipscs derived from low grade gliomas revealed early regional chromosomal amplifications during gliomagenesis. *Journal of Neuro-Oncology*, 141:289–301, 2019.

[151] Z. Liu and P. A. Roche. Macropinocytosis in phagocytes: regulation of mhc class-ii-restricted antigen presentation in dendritic cells. *Frontiers in Physiology*, 6:1, 2015.

[152] J. Loh, M.-C. Chuang, S.-S. Lin, J. Joseph, Y.-A. Su, T.-L. Hsieh, Y.-C. Chang, A. P. Liu, and Y.-W. Liu. An acute decrease in plasma membrane tension induces macropinocytosis via pld2 activation. *Journal of Cell Science*, 132(17):jcs232579, 2019.

[153] A. Lomakin, C. Cattin, D. Cuvelier, Z. Alraies, M. Molina, G. Nader, N. Srivastava, P. Sáez, J. Garcia-Arcos, I. Zhitnyak, et al. The nucleus acts as a ruler tailoring cell responses to spatial constraints. *Science*, 370(6514):eaba2894, 2020.

[154] D. A. P. Louie and S. Liao. Lymph node subcapsular sinus macrophages as the frontline of lymphatic immune defense. *Frontiers in Immunology*, 10:347, 2019.

[155] J. E. Lutton, H. L. Coker, P. Paschke, C. J. Munn, J. S. King, T. Bretschneider, and R. R. Kay. Formation and closure of macropinocytic cups in *Dictyostelium*. *Current Biology*, 33(15):3083–3096, 2023.

[156] M. Mallat, J. L. Marín-Teva, and C. Chéret. Phagocytosis in the developing cns: more than clearing the corpses. *Current Opinion in Neurobiology*, 15(1):101–107, 2005.

[157] K. Mandal, I. Wang, E. Vitiello, L. A. C. Orellana, and M. Balland. Cell dipole behaviour revealed by ecm sub-cellular geometry. *Nature Communications*, 5(1):5749, 2014.

[158] A. R. Mantegazza, J. G. Magalhaes, S. Amigorena, and M. S. Marks. Presentation of phagocytosed antigens by mhc class i and ii. *Traffic*, 14(2):135–152, 2013.

[159] E. Maréchal. Primary endosymbiosis: emergence of the primary chloroplast and the chromatophore, two independent events. *Plastids: Methods and Protocols*, pages 3–16, 2018.

[160] C. Mark, T. Czerwinski, S. Roessner, A. Mainka, F. Hörsch, L. Heublein, A. Winterl, S. Sanokowski, S. Richter, N. Bauer, et al. Cryopreservation impairs 3-d migration and cytotoxicity of natural killer cells. *Nature Communications*, 11(1):5224, 2020.

[161] W. F. Martin, A. G. Tielens, M. Mentel, S. G. Garg, and S. B. Gould. The physiology of phagocytosis in the context of mitochondrial origin. *Microbiology and Molecular Biology Reviews*, 81(3):10–1128, 2017.

[162] M. E. Maxson, H. Sarantis, A. Volchuk, J. H. Brumell, and S. Grinstein. Rab5 regulates macropinocytosis by recruiting the inositol 5-phosphatases ocrl and inpp5b that hydrolyse ptdins (4, 5) p2. *Journal of Cell Science*, 134(7):jcs252411, 2021.

[163] R. C. May and L. M. Machesky. Phagocytosis and the actin cytoskeleton. *Journal of Cell Science*, 114(6):1061–1077, 2001.

[164] S. Mayor and R. E. Pagano. Pathways of clathrin-independent endocytosis. *Nature Reviews Molecular Cell Biology*, 8(8):603–612, 2007.

[165] A. J. McKnight, A. J. Macfarlane, P. Dri, L. Turley, A. C. Willis, and S. Gordon. Molecular cloning of f4/80, a murine macrophage-restricted cell surface glycoprotein with homology to the g-protein-linked transmembrane 7 hormone receptor family. *Journal of Biological Chemistry*, 271(1):486–489, 1996.

[166] H. T. McMahon and E. Boucrot. Molecular mechanism and physiological functions of clathrin-mediated endocytosis. *Nature Reviews Molecular Cell Biology*, 12(8):517–533, 2011.

[167] F. Y. McWhorter, T. Wang, P. Nguyen, T. Chung, and W. F. Liu. Modulation of macrophage phenotype by cell shape. *Proceedings of the National Academy of Sciences*, 110(43):17253–17258, 2013.

[168] O. Meier, K. Boucke, S. V. Hammer, S. Keller, R. P. Stidwill, S. Hemmi, and U. F. Greber. Adenovirus triggers macropinocytosis and endosomal leakage together with its clathrin-mediated uptake. *Journal of Cell Biology*, 158(6):1119–1131, 2002.

[169] I. Mendel, N. Yacov, Y. Salem, O. Propheta-Meiran, E. Ishai, and E. Breitbart. Identification of motile sperm domain–containing protein 2 as regulator of human monocyte migration. *The Journal of Immunology*, 198(5):2125–2132, 2017.

[170] J. Mercer and A. Helenius. Gulping rather than sipping: macropinocytosis as a way of virus entry. *Current Opinion in Microbiology*, 15(4):490–499, 2012.

[171] J. E. Meredith Jr, S. Winitz, J. M. Lewis, S. Hess, X.-D. Ren, M. W. Renshaw, and M. A. Schwartz. The regulation of growth and intracellular signaling by integrins. *Endocrine Reviews*, 17(3):207–220, 1996.

[172] A. Millius, N. Watanabe, and O. D. Weiner. Diffusion, capture and recycling of scar/wave and arp2/3 complexes observed in cells by single-molecule imaging. *Journal of Cell Science*, 125(5):1165–1176, 2012.

[173] Y. Miyamoto, T. Torii, K. Kawahara, A. Tanoue, and J. Yamauchi. Dock8 interacts with nck1 in mediating schwann cell precursor migration. *Biochemistry and Biophysics Reports*, 6:113–123, 2016.

[174] A. Mogilner and G. Oster. Force generation by actin polymerization ii: the elastic ratchet and tethered filaments. *Biophysical Journal*, 84(3):1591–1605, 2003.

[175] H. D. Moreau, C. Blanch-Mercader, R. Attia, M. Maurin, Z. Alraies, D. Sanseau, O. Malbec, M.-G. Delgado, P. Bousso, J.-F. Joanny, et al. Macropinocytosis overcomes directional bias in dendritic cells due to hydraulic resistance and facilitates space exploration. *Developmental Cell*, 49(2):171–188, 2019.

[176] D. D. Mousseau, D. Banville, D. L'Abbé, P. Bouchard, and S.-H. Shen. Pilrα, a novel immunoreceptor tyrosine-based inhibitory motif-bearing protein, recruits shp-1 upon tyrosine phosphorylation and is paired with the truncated counterpart pilrβ. *Journal of Biological Chemistry*, 275(6):4467–4474, 2000.

[177] N. Mulherkar, M. Raaben, J. C. de la Torre, S. P. Whelan, and K. Chandran. The ebola virus glycoprotein mediates entry via a non-classical dynamin-dependent macropinocytic pathway. *Virology*, 419(2):72–83, 2011.

[178] G. Nagao, K. Ishii, K. Hirota, K. Makino, and H. Terada. Role of lipid rafts in phagocytic uptake of polystyrene latex microspheres by macrophages. *Anticancer Research*, 30(8):3167–3176, 2010.

[179] K. Nakagawa, T. Nagano, R. Katasho, T. Iwasaki, and S. Kamada. Integrin β1 transduces the signal for ly6d-induced macropinocytosis and mediates senescence-inducing stress-evoked vacuole formation via fak. *FEBS Letters*, 596(21):2768–2780, 2022.

[180] T. K. Neklesa and R. W. Davis. A genome-wide screen for regulators of torc1 in response to amino acid starvation reveals a conserved npr2/3 complex. *PLOS Genetics*, 5(6):e1000515, 2009.

[181] A. C. Ng, J. M. Eisenberg, R. J. Heath, A. Huett, C. M. Robinson, G. J. Nau, and R. J. Xavier. Human leucine-rich repeat proteins: a genome-wide bioinformatic categorization and functional analysis in innate immunity. *Proceedings of the National Academy of Sciences*, 108(supplement_1):4631–4638, 2011.

[182] B. Nichols. Caveosomes and endocytosis of lipid rafts. *Journal of Cell Science*, 116(23):4707–4714, 2003.

[183] K. Noguchi, M. Obuki, H. Sumi, M. Klussmann, K. Morimoto, S. Nakai, T. Hashimoto, D. Fujiwara, I. Fujii, E. Yuba, et al. Macropinocytosis-inducible extracellular vesicles modified with antimicrobial protein cap18-derived cell-penetrating peptides for efficient intracellular delivery. *Molecular Pharmaceutics*, 18(9):3290–3301, 2021.

[184] C. C. Norbury, L. J. Hewlett, A. R. Prescott, N. Shastri, and C. Watts. Class i mhc presentation of exogenous soluble antigen via macropinocytosis in bone marrow macrophages. *Immunity*, 3(6):783–791, 1995.

[185] K. D. Novak, M. D. Peterson, M. C. Reedy, and M. A. Titus. *Dictyostelium* myosin i double mutants exhibit conditional defects in pinocytosis. *Journal of Cell Biology*, 131(5):1205–1221, 1995.

[186] T. O'Loughlin, T. A. Masters, and F. Buss. The myo6 interactome reveals adaptor complexes coordinating early endosome and cytoskeletal dynamics. *EMBO Reports*, 19(4):e44884, 2018.

[187] Y. Ophinni, S. Miki, Y. Hayashi, and M. Kameoka. Multiplexed tat-targeting crispr-cas9 protects t cells from acute hiv-1 infection with inhibition of viral escape. *Viruses*, 12(11):1223, 2020.

[188] R. G. Parton and M. A. Del Pozo. Caveolae as plasma membrane sensors, protectors and organizers. *Nature Reviews Molecular Cell Biology*, 14(2):98–112, 2013.

[189] R. G. Parton, M. Hanzal-Bayer, and J. F. Hancock. Biogenesis of caveolae: a structural model for caveolin-induced domain formation. *Journal of Cell Science*, 119(5):787–796, 2006.

[190] T. D. Pollard. Regulation of actin filament assembly by arp2/3 complex and formins. *Annual Review of Biophysics and Biomolecular Structure*, 36:451–477, 2007.

[191] B. Pontes, P. Monzo, L. Gole, A.-L. Le Roux, A. J. Kosmalska, Z. Y. Tam, W. Luo, S. Kan, V. Viasnoff, P. Roca-Cusachs, et al. Membrane tension controls adhesion positioning at the leading edge of cells. *Journal of Cell Biology*, 216(9):2959–2977, 2017.

[192] S. Porter. The rise of predators. *Geology*, 39(6):607–608, 2011.

[193] R. Ramachandran. Vesicle scission: dynamin. In *Seminars in cell & developmental biology*, volume 22, pages 10–17. Elsevier, 2011.

[194] C. Ramirez, A. D. Hauser, E. A. Vucic, and D. Bar-Sagi. Plasma membrane v-atpase controls oncogenic ras-induced macropinocytosis. *Nature*, 576(7787):477–481, 2019.

[195] A. Ramos, C. E. Koch, Y. Liu, R. D. Hellinger, T. Kyung, K. L. Abbott, J. Fröse, D. Goulet, K. S. Gordon, R. C. Larson, et al. Leukemia-intrinsic determinants of car-t response revealed by iterative in vivo genome-wide crispr screening. *BioRxiv*, pages 2022–02, 2022.

[196] C. Raub, A. Putnam, B. Tromberg, and S. George. Predicting bulk mechanical properties of cellularized collagen gels using multiphoton microscopy. *Acta Biomaterialia*, 6(12):4657–4665, 2010.

[197] B. Razani, T. P. Combs, X. B. Wang, P. G. Frank, D. S. Park, R. G. Russell, M. Li, B. Tang, L. A. Jelicks, P. E. Scherer, et al. Caveolin-1-deficient mice are lean, resistant to diet-induced obesity, and show hypertriglyceridemia with adipocyte abnormalities. *Journal of Biological Chemistry*, 277(10):8635–8647, 2002.

[198] M. V. Recouvreux and C. Commisso. Macropinocytosis: a metabolic adaptation to nutrient stress in cancer. *Frontiers in Endocrinology*, 8:261, 2017.

[199] V. Redecke, R. Wu, J. Zhou, D. Finkelstein, V. Chaturvedi, A. A. High, and H. Häcker. Hematopoietic progenitor cell lines with myeloid and lymphoid potential. *Nature Methods*, 10(8):795–803, 2013.

[200] M. Riley. Correlates of smallest sizes for microorganisms. In *Size limits of very small microorganisms: proceedings of a workshop*, volume 3, page 21. National Academies Press Washington, DC, 1999.

[201] L. Rink, A. Kruse, and H. Haase. *Immunologie für Einsteiger*. Springer, 2012.

[202] T. Rivière, A. Bader, K. Pogoda, B. Walzog, and D. Maier-Begandt. Structure and emerging functions of lrch proteins in leukocyte biology. *Frontiers in Cell and Developmental Biology*, 8:584134, 2020.

[203] J. Robert-Paganin, O. Pylypenko, C. Kikuti, H. L. Sweeney, and A. Houdusse. Force generation by myosin motors: a structural perspective. *Chemical Reviews*, 120(1):5–35, 2019.

[204] C. Roffay, J. M. García-Arcos, P. Chapuis, J. López-Andarias, F. Schneider, A. Colom, C. Tomba, I. D. Meglio, V. Dunsing, S. Matile, et al. Technical insights into fluorescence lifetime microscopy of mechanosensitive flipper probes. *BioRxiv*, pages 2022–09, 2022.

[205] C. Roffay, G. Molinard, K. Kim, M. Urbanska, V. Andrade, V. Barbarasa, P. Nowak, V. Mercier, J. García-Calvo, S. Matile, et al. Passive coupling of membrane tension and cell volume during active response of cells to osmosis. *Proceedings of the National Academy of Sciences*, 118(47):e2103228118, 2021.

[206] J. S. Rossman, G. P. Leser, and R. A. Lamb. Filamentous influenza virus enters cells via macropinocytosis. *Journal of Virology*, 86(20):10950–10960, 2012.

[207] K. G. Rothberg, J. E. Heuser, W. C. Donzell, Y.-S. Ying, J. R. Glenney, and R. G. Anderson. Caveolin, a protein component of caveolae membrane coats. *Cell*, 68(4):673–682, 1992.

[208] J. D. Rotty, C. Wu, and J. E. Bear. New insights into the regulation and cellular functions of the arp2/3 complex. *Nature Reviews Molecular Cell Biology*, 14(1):7–12, 2013.

[209] L. Sagan. On the origin of mitosing cells. *Journal of Theoretical Biology*, 14(3):225–IN6, 1967.

[210] F. Sallusto, M. Cella, C. Danieli, and A. Lanzavecchia. Dendritic cells use macropinocytosis and the mannose receptor to concentrate macromolecules in the major histocompatibility complex class ii compartment: downregulation by cytokines and bacterial products. *Journal of Experimental Medicine*, 182(2):389–400, 1995.

[211] K. O. Schink, K. W. Tan, H. Spangenberg, D. Martorana, M. Sneeggen, V. Stévenin, J. Enninga, C. Campsteijn, C. Raiborg, and H. Stenmark. The phosphoinositide coincidence detector phafin2 promotes macropinocytosis by coordinating actin organisation at forming macropinosomes. *Nature Communications*, 12(1):6577, 2021.

[212] W. Schubert, P. G. Frank, B. Razani, D. S. Park, C.-W. Chow, and M. P. Lisanti. Caveolae-deficient endothelial cells show defects in the uptake and transport of albumin in vivo. *Journal of Biological Chemistry*, 276(52):48619–48622, 2001.

[213] M. A. Schwartz, C. Lechene, and D. E. Ingber. Insoluble fibronectin activates the na/h antiporter by clustering and immobilizing integrin alpha 5 beta 1, independent of cell shape. *Proceedings of the National Academy of Sciences*, 88(17):7849–7853, 1991.

[214] D. J. Seastone, E. Harris, L. A. Temesvari, J. E. Bear, C. L. Saxe, and J. Cardelli. The wasp-like protein scar regulates macropinocytosis, phagocytosis and endosomal membrane flow in *Dictyostelium*. *Journal of Cell Science*, 114(14):2673–2683, 2001.

[215] D. Sendo, Y. Takeda, T. Watanabe, F. Sendo, and Y. Araki. A monoclonal antibody to gpi-80, a novel β2 integrin associated glycosylphosphatidylinositol anchored protein, selectively enhances macropinocytosis in human monocytes. *Bulletin of the Yamagata University. Medical science: Yamagata medical journal*, 23(1):69–82, 2005.

[216] O. Shalem, N. E. Sanjana, E. Hartenian, X. Shi, D. A. Scott, T. S. Mikkelsen, D. Heckl, B. L. Ebert, D. E. Root, J. G. Doench, et al. Genome-scale crispr-cas9 knockout screening in human cells. *Science*, 343(6166):84–87, 2014.

[217] P. Sharma, S. Ghavami, G. L. Stelmack, K. D. McNeill, M. M. Mutawe, T. Klonisch, H. Unruh, and A. J. Halayko. β-dystroglycan binds caveolin-1 in smooth muscle: a functional role in caveolae distribution and ca2+ release. *Journal of Cell Science*, 123(18):3061–3070, 2010.

[218] T. Shemesh, A. D. Bershadsky, and M. M. Kozlov. Physical model for self-organization of actin cytoskeleton and adhesion complexes at the cell front. *Biophysical Journal*, 102(8):1746–1756, 2012.

[219] W. Shi, D. Ma, Y. Cao, L. Hu, S. Liu, D. Yan, S. Zhang, G. Zhang, Z. Wang, J. Wu, et al. Sphk2/s1p promotes metastasis of triple-negative breast cancer through the pak1/limk1/cofilin1 signaling pathway. *Frontiers in Molecular Biosciences*, 8:598218, 2021.

[220] E. Sitarska and A. Diz-Muñoz. Pay attention to membrane tension: Mechanobiology of the cell surface. *Current Opinion in Cell Biology*, 66:11–18, 2020.

[221] M. Sixt and T. Lämmermann. In vitro analysis of chemotactic leukocyte migration in 3d environments. *Cell Migration: Developmental Methods and Protocols*, pages 149–165, 2011.

[222] B. A. Smith, S. B. Padrick, L. K. Doolittle, K. Daugherty-Clarke, I. R. Corrêa Jr, M.-Q. Xu, B. L. Goode, M. K. Rosen, and J. Gelles. Three-color single molecule imaging shows wasp detachment from arp2/3 complex triggers actin filament branch formation. *eLife*, 2:e01008, 2013.

[223] J. SOARES, D. G. FREITAS, P. S. LOURENÇO, J. FARIAS, and B. PONTES. Mechanobiology of the cell surface: Probing its remodeling dynamics using membrane tether pulling assays with optical tweezers. *Biocell*, 46(9):2009–2013, 2022.

[224] B. Song, S. Yang, G.-H. Hwang, J. Yu, and S. Bae. Analysis of nhej-based dna repair after crispr-mediated dna cleavage. *International Journal of Molecular Sciences*, 22(12):6397, 2021.

[225] P. N. Spahn, T. Bath, R. J. Weiss, J. Kim, J. D. Esko, N. E. Lewis, and O. Harismendy. Pinapl-py: A comprehensive web-application for the analysis of crispr/cas9 screens. *Scientific Reports*, 7(1):15854, 2017.

[226] E. Stang, J. Kartenbeck, and R. G. Parton. Major histocompatibility complex class i molecules mediate association of sv40 with caveolae. *Molecular Biology of the Cell*, 8(1):47–57, 1997.

[227] R. M. Steinman, S. E. Brodie, and Z. A. Cohn. Membrane flow during pinocytosis. a stereologic analysis. *Journal of Cell Biology*, 68(3):665–687, 1976.

[228] V. Stévenin, Y.-Y. Chang, Y. Le Toquin, M. Duchateau, Q. G. Gianetto, C. H. Luk, A. Salles, V. Sohst, M. Matondo, N. Reiling, et al. Dynamic growth and shrinkage of the salmonella-containing vacuole determines the intracellular pathogen niche. *Cell Reports*, 29(12):3958–3973, 2019.

[229] K. M. Stroka, H. Jiang, S.-H. Chen, Z. Tong, D. Wirtz, S. X. Sun, and K. Konstantopoulos. Water permeation drives tumor cell migration in confined microenvironments. *Cell*, 157(3):611–623, 2014.

[230] W. K. Subczynski, M. Pasenkiewicz-Gierula, J. Widomska, L. Mainali, and M. Raguz. High cholesterol/low cholesterol: effects in biological membranes: a review. *Cell Biochemistry and Biophysics*, 75:369–385, 2017.

[231] S. Suetsugu, D. Yamazaki, S. Kurisu, and T. Takenawa. Differential roles of wave1 and wave2 in dorsal and peripheral ruffle formation for fibroblast cell migration. *Developmental Cell*, 5(4):595–609, 2003.

[232] Y. Sun, K. Senger, T. K. Baginski, A. Mazloom, Y. Chinn, H. Pantua, K. Hamidzadeh, S. R. Ramani, E. Luis, I. Tom, et al. Evolutionarily conserved paired immunoglobulin-like receptor α (pilrα) domain mediates its interaction with diverse sialylated ligands. *Journal of Biological Chemistry*, 287(19):15837–15850, 2012.

[233] Z. Sun, J. Huang, L. Su, J. Li, F. Qi, H. Su, Y. Chen, Q. Zhang, Q. Zhang, Z. Li, et al. Arf6-mediated macropinocytosis-enhanced suicide gene therapy of c16tab-condensed tat/pdna nanoparticles in ovarian cancer. *Nanoscale*, 13(34):14538–14551, 2021.

[234] J. A. Swanson. Shaping cups into phagosomes and macropinosomes. *Nature Reviews Molecular Cell Biology*, 9(8):639–649, 2008.

[235] J. A. Swanson and N. Araki. Roles for 3'phosphoinositides in macropinocytosis. In *Macropinocytosis: Functions and Mechanisms*, pages 119–141. Springer, 2022.

[236] J. A. Swanson and C. Watts. Macropinocytosis. *Trends in Cell Biology*, 5(11):424–428, 1995.

[237] Y. Takada, X. Ye, and S. Simon. The integrins. *Genome Biology*, 8:1–9, 2007.

[238] A. I. Tauber. Metchnikoff and the phagocytosis theory. *Nature Reviews Molecular Cell Biology*, 4(11):897–901, 2003.

[239] P. Vargas, P. Maiuri, M. Bretou, P. J. Sáez, P. Pierobon, M. Maurin, M. Chabaud, D. Lankar, D. Obino, E. Terriac, et al. Innate control of actin nucleation determines two distinct migration behaviours in dendritic cells. *Nature Cell Biology*, 18(1):43–53, 2016.

[240] D. M. Veltman. Drink or drive: competition between macropinocytosis and cell migration. *Biochemical Society Transactions*, 2015.

[241] D. M. Veltman, T. D. Williams, G. Bloomfield, B.-C. Chen, E. Betzig, R. H. Insall, and R. R. Kay. A plasma membrane template for macropinocytic cups. *eLife*, 5:e20085, 2016.

[242] V. Venturini, F. Pezzano, F. Catala Castro, H.-M. Häkkinen, S. Jiménez-Delgado, M. Colomer-Rosell, M. Marro, Q. Tolosa-Ramon, S. Paz-López, M. A. Valverde, et al. The nucleus measures shape changes for cellular proprioception to control dynamic cell behavior. *Science*, 370(6514):eaba2644, 2020.

[243] A. von Delwig, E. Bailey, D. M. Gibbs, and J. H. Robinson. The route of bacterial uptake by macrophages influences the repertoire of epitopes presented to cd4 t cells. *European Journal of Immunology*, 32(12):3714–3719, 2002.

[244] A. von Delwig, C. M. Hilkens, D. M. Altmann, R. Holmdahl, J. D. Isaacs, C. V. Harding, H. Robertson, N. McKie, and J. H. Robinson. Inhibition of macropinocytosis blocks antigen presentation of type ii collagen in vitro and in vivo in hla-dr1 transgenic mice. *Arthritis Research & Therapy*, 8:1–11, 2006.

[245] L. A. Waddell, L. Lefevre, S. J. Bush, A. Raper, R. Young, Z. M. Lisowski, M. E. McCulloch, C. Muriuki, K. A. Sauter, E. L. Clark, et al. Adgre1 (emr1, f4/80) is a rapidly-evolving gene expressed in mammalian monocyte-macrophages. *Frontiers in Immunology*, 9:2246, 2018.

[246] A. A. Wall, L. Luo, Y. Hung, S. J. Tong, N. D. Condon, A. Blumenthal, M. J. Sweet, and J. L. Stow. Small gtpase rab8a-recruited phosphatidylinositol 3-kinase γ regulates signaling and cytokine outputs from endosomal toll-like receptors. *Journal of Biological Chemistry*, 292(11):4411–4422, 2017.

[247] J. Wang, I. Shiratori, J. Uehori, M. Ikawa, and H. Arase. Neutrophil infiltration during inflammation is regulated by pilrα via modulation of integrin activation. *Nature Immunology*, 14(1):34–40, 2013.

[248] T. P. Welliver and J. A. Swanson. A growth factor signaling cascade confined to circular ruffles in macrophages. *Biology Open*, 1(8):754–760, 2012.

[249] H. J. Wensley, W. S. Smith, S. E. Holmes, S. U. Flavell, and D. J. Flavell. The effect of small molecule pharmacological agents on the triterpenoid saponin induced endolysosomal escape of saporin and a saporin-based immunotoxin in target human lymphoma cells. *Biomedicines*, 9(3):300, 2021.

[250] M. A. West, M. S. Bretscher, and C. Watts. Distinct endocytotic pathways in epidermal growth factor-stimulated human carcinoma a431 cells. *Journal of Cell Biology*, 109(6):2731–2739, 1989.

[251] T. D. Williams and R. R. Kay. The physiological regulation of macropinocytosis during *Dictyostelium* growth and development. *Journal of Cell Science*, 131(6):jcs213736, 2018.

[252] C. D. Williamson and J. G. Donaldson. Arf6, jip3, and dynein shape and mediate macropinocytosis. *Molecular Biology of the Cell*, 30(12):1477–1489, 2019.

[253] M. D. Wilson, J. Cheung, D. W. Martindale, S. W. Scherer, and B. F. Koop. Comparative analysis of the paired immunoglobulin-like receptor (pilr) locus in six mammalian genomes: duplication, conversion, and the birth of new genes. *Physiological Genomics*, 27(3):201–218, 2006.

[254] N. S. Wilson, D. El-Sukkari, and J. A. Villadangos. Dendritic cells constitutively present self antigens in their immature state in vivo and regulate antigen presentation by controlling the rates of mhc class ii synthesis and endocytosis. *Blood*, 103(6):2187–2195, 2004.

[255] A. Wittinghofer and H. Waldmann. Ras—a molecular switch involved in tumor formation. *Angewandte Chemie International Edition*, 39(23):4192–4214, 2000.

[256] A. Wittrup, S. Sandgren, J. Lilja, C. Bratt, N. Gustavsson, M. Mörgelin, and M. Belting. Identification of proteins released by mammalian cells that mediate dna internalization through proteoglycan-dependent macropinocytosis. *Journal of Biological Chemistry*, 282(38):27897–27904, 2007.

[257] Z. Wu, H. Yang, and P. Colosi. Effect of genome size on aav vector packaging. *Molecular Therapy*, 18(1):80–86, 2010.

[258] Y. Xing, Z. Wen, W. Gao, Z. Lin, J. Zhong, and Y. Jiu. Multifaceted functions of host cell caveolae/caveolin-1 in virus infections. *Viruses*, 12(5):487, 2020.

[259] S. Yoshida, A. D. Hoppe, N. Araki, and J. A. Swanson. Sequential signaling in plasma-membrane domains during macropinosome formation in macrophages. *Journal of Cell Science*, 122(18):3250–3261, 2009.

[260] B. Yun, H. Lee, H. Ewing, M. H. Gelb, and C. C. Leslie. Off-target effect of the cpla2α inhibitor pyrrophenone: Inhibition of calcium release from the

endoplasmic reticulum. *Biochemical and Biophysical Research Communications*, 479(1):61–66, 2016.

[261] Y. Zeng, T. Lai, C. G. Koh, P. R. LeDuc, and K.-H. Chiam. Investigating circular dorsal ruffles through varying substrate stiffness and mathematical modeling. *Biophysical Journal*, 101(9):2122–2130, 2011.

[262] M. K. Zenni, P. C. Giardina, H. A. Harvey, J. Shao, M. R. Ketterer, D. M. Lubaroff, R. D. Williams, and M. A. Apicella. Macropinocytosis as a mechanism of entry into primary human urethral epithelial cells by neisseria gonorrhoeae. *Infection and Immunity*, 68(3):1696–1699, 2000.

[263] Y.-Y. Zhang, R. Liang, S.-J. Wang, Z.-W. Ye, T.-Y. Wang, M. Chen, J. Liu, L. Na, Y.-L. Yang, Y.-B. Yang, et al. Sars-cov-2 hijacks macropinocytosis to facilitate its entry and promote viral spike–mediated cell-to-cell fusion. *Journal of Biological Chemistry*, 298(11), 2022.

[264] J. Zhu, Y. Xu, Z. Li, S. Liu, W. Fu, and Y. Wei. Interleukin-36β exacerbates dss-induce acute colitis via inhibiting foxp3+ regulatory t cell response and increasing th2 cell response. *International Immunopharmacology*, 108:108762, 2022.

[265] Y.-Z. Zhu, Q.-Q. Xu, D.-G. Wu, H. Ren, P. Zhao, W.-G. Lao, Y. Wang, Q.-Y. Tao, X.-J. Qian, Y.-H. Wei, et al. Japanese encephalitis virus enters rat neuroblastoma cells via a ph-dependent, dynamin and caveola-mediated endocytosis pathway. *Journal of Virology*, 86(24):13407–13422, 2012.

A

CONTRIBUTIONS

The experimental design and general project planning was carried out by Malte Benjamin Braun in close cooperation with Professor Jörg Renkawitz. The original project idea for the genome-wide CRISPR KO screen and the investigation of macropinocytosis in 3D environments was developed by Professor Jörg Renkawitz.

All cell culture work was performed by Malte Benjamin Braun with some support from Katarzyna Stefanowski.

The genome-wide library for the CRISPR screen was designed and generated by Arek Kendirli from the Kerschensteiner lab [117]. Library amplification, isolation, and virus production were performed by Malte Benjamin Braun. Establishment of the staining protocol for FACS-based quantification of macropinocytosis and validation of the protocol were performed by Malte Benjamin Braun. Hoxb8 cells expressing Cas9 for the CRISPR screen were provided by the Schmidt-Supprian lab. Viral infection of Hoxb8 cells with the lentiviral library, differentiation into MCs and staining with the macropinocytosis marker were performed by Malte Benjamin Braun. FACS sorting of cells by fluorescence was performed by Dr. Lisa Richter and Pardis Khosravani from the "Core Facility Flow Cytometry" at the Biomedical Center Munich (BMC). DNA isolation, amplification and quality control were performed by Malte Benjamin Braun. Next-generation sequencing (NGS) was performed by Dr. Stefan Krebs from the Blum lab. Bioinfomatic analysis of the screening data was performed by Malte Benjamin Braun using CRISPRCloud2, MaGECK and PinAPL-Py. CRISPRCloud2 was developed and provided by the Liu lab [105], MaGECK by the Liu lab [143] and PinAPL-Py by the Harismendy lab [225].

All experiments shown in the second project, which compares fluid uptake by macropinocytosis in 3D environments with 2D environments, were performed by Malte Benjamin Braun. The 2-photon images used in Figure 7 were acquired by PD Dr. Petra Kameritsch. The images were used for representative purposes only and no data from these experiments are presented in this work. Micropatterned surfaces and fully polyethylene glycol (PEG)-coated surfaces were prepared by Dr. Julien Polleux. Hoxb8 cell lines with Hem1 and Wasp KO were provided and generated by the Sixt lab. β2 KO, talin KO and kindlin-3 knockdowns were provided by Thomas Bromberger from the Moser lab.

B

ACKNOWLEDGMENTS

This PhD has been a long journey. Sometimes filled with joy, excitement and happiness, at other points frustrating, depressing and disheartening.

I have to thank a lot of people who have joined me for this great journey. My friends and family who have supported me over the entire time bearing my mods when there were stressful periods, trying to lift me up when it seemed like nothing was working, and joining me in my scientific excitement when it finally did.

This is especially true for my great lab mates Janina Kroll, Mauricio Ruiz, Madeleine Schmitt, Kasia Stefanowski, Artur Kuznetcov and Johanna Schmid. Without your continuous support, your great scientific input and your support in all areas, I would not have been able to complete this endeavour . This is is also true for my great supervisor Jörg Renkawitz, who not only entrusted me with the responsibility for this exciting research project, but also somehow never lost faith in my ability to complete this project successfully, and supported me with his great ideas and scientific knowledge. In addition, his door was always open when there were any problems, even beyond the purely PhD related stuff.

I also have to thank our two formal group members Petra Kameritsch and Rifat Ara Reza. Petra Kameritsch took the great pictures of macrophages performing macropinocytosis in 3D environments at the 2-photon microscope and then took the effort to quantify this imaging data. Without Rifat Ara Reza's great master thesis on macropinocytosis in macrophages confined under agarose gel, we probably would not have focused on the 3D project at all. So she laid the foundation on which I was able to build this project.

I also have to thank all our great collaborators. Julien Polleux, who generated the micropattern for us. Arek Kendirli, who prepared the CRISPR library we used in our screen and who also helped me a lot with everything around the screen. Stefan Krebs for performed the NGS for us. Thomas Bromberger and Markus Moser, who provided us with the integrin KO cells and thus enabled us to investigate this part of cell adhesion in macropinocytosis.

This project would also not have been possible without the support of our in-house core facilities here at the BMC. Steffen Dietzel, Andreas Thomae and Mariano Gonzalez Pisfil from the "Core facility Bioimaging" helped me a lot with all the microscopic work that was was necessary for this project. Lisa Richter and Pardis Khosravani helped me with all the flow related questions and performed the sorting for my genome-wide screen.

I would also like to thank my TAC members Markus Sperandio, Veit Hornung and Annette Müller-Taubenberger for their advice and input during our TAC

meeting. In particular, I have to thank Annette Müller-Taubenberger for joining the TAC shortly before the end of this project.

Special thanks also go to Verena Kochan, the coordinator of our IRTG914 graduate school, who organised many interesting and fun events and excursions for us and always had an open door when there were organizational questions or problems with the PhD.

C

LIST OF PUBLICATIONS

Kroll, J., Ruiz-Fernandez, M. J., Braun, M. B., Merrin, J., & Renkawitz, J. (2022). Quantifying the Probing and Selection of Microenvironmental Pores by Motile Immune Cells. *Current Protocols*, 2(4), e407.

LMU LUDWIG-MAXIMILIANS-UNIVERSITÄT MÜNCHEN

Dean's Office Medical Faculty
Faculty of Medicine

Affidavit

Braun, Malte Benjamin

Surname, first name

Großhaderner Str. 9, 82152 Planegg

Address

I hereby declare, that the submitted thesis entitled

Spatio-temporal dynamics and molecular principles of macropinocytosis in immune cells

is my own work. I have only used the sources indicated and have not made unauthorised use of services of a third party. Where the work of others has been quoted or reproduced, the source is always given.

I further declare that the dissertation presented here has not been submitted in the same or similar form to any other institution for the purpose of obtaining an academic degree.

München 13.08.2024

Place, Date

Malte Benjamin Braun

Signature doctoral candidate

LMU LUDWIG-MAXIMILIANS-UNIVERSITÄT MÜNCHEN

Dean's Office Medical Faculty
Doctoral Office

Confirmation of congruency between printed and electronic version of the doctoral thesis

Doctoral candidate: Malte Benjamin Braun

Address: Großhaderner Str. 9, 82152 Planegg

I hereby declare that the electronic version of the submitted thesis, entitled

Spatio-temporal dynamics and molecular principles of macropinocytosis in immune cells

is congruent with the printed version both in content and format.

München 13.08.2024
Place, Date

Malte Benjamin Braun
Signature doctoral candidate